

A Reference Equation of State for the Thermodynamic Properties of Ethane for Temperatures from the Melting Line to 675 K and Pressures up to 900 MPa

D. Bücker^{a)} and W. Wagner^{b)}

Lehrstuhl für Thermodynamik, Ruhr-Universität Bochum, D-44780 Bochum, Germany

(Received 22 April 2004; revised manuscript received 9 November 2004; accepted 29 November 2004; published online 31 January 2006)

A new formulation for the thermodynamic properties of the fluid phase of ethane in the form of a fundamental equation explicit in the Helmholtz energy is presented. The functional form of the residual part was developed using state-of-the-art linear and nonlinear optimization algorithms. It contains 44 coefficients which were fitted to selected data for the thermal and calorific properties of ethane both in the single-phase region and on the liquid–vapor phase boundary. This work provides information on the available experimental data for the thermodynamic properties of ethane and presents all details of the new formulation. The new equation of state describes the $p\rho T$ surface of ethane with an uncertainty in density of less than 0.02%–0.03% (coverage factor $k=2$ corresponding to a level of confidence of about 95%) from the melting line up to temperatures of 520 K and pressures of 30 MPa. In the gaseous and supercritical region, high precision speed of sound data are represented generally within less than 0.015%. Other reliable data sets are represented within their experimental uncertainties. The primary data, to which the equation was fitted, cover the fluid region from the melting line to temperatures of 675 K and pressures of 900 MPa. Beyond this range the equation shows reasonable extrapolation behavior up to very high temperatures and pressures. In addition to the equation of state, independent equations for the vapor pressure, the saturated-liquid and saturated-vapor densities, and the melting pressure are given. Tables of thermodynamic properties calculated from the new formulation are listed in the Appendix. © 2006 American Institute of Physics. [DOI: 10.1063/1.1859286]

Key words: calorific properties; density; ethane; equation of state; fundamental equation; property tables; thermal properties; thermodynamic properties; vapor–liquid phase boundary.

Contents

1. Introduction	209	2.7.2. Heat Capacities.....	214
1.1. Background.....	209	2.7.3. Enthalpy of Vaporization.....	215
1.2. Previous Equations of State.....	209	3. Experimental Data for the Single-Phase Region...	215
1.3. Notes on the Values of Temperature Used in This Article.....	210	3.1. Thermal Properties.....	215
2. Phase Equilibria of Ethane.....	210	3.1.1. $p\rho T$ Data.....	215
2.1. Triple Point.....	210	3.1.2. Virial Coefficients.....	217
2.2. Critical Point.....	211	3.2. Speeds of Sound.....	218
2.3. Melting Pressure.....	211	3.3. Isochoric Heat Capacities.....	219
2.4. Vapor Pressure.....	211	3.4. Isobaric Heat Capacities.....	220
2.5. Saturated-Liquid Density.....	211	3.4.1. Experimental Results for the Real Fluid.....	220
2.6. Saturated-Vapor Density.....	213	3.4.2. Results for the Ideal-Gas State.....	221
2.7. Caloric Data on the Vapor–Liquid Phase Boundary.....	214	3.5. Enthalpy Differences and Throttling Coefficients.....	221
2.7.1. Speed of Sound.....	214	4. The New Equation of State.....	222
		4.1. The Equation for the Helmholtz Energy of the Ideal Gas.....	223
		4.2. The Equation for the Residual Part of the Helmholtz Energy.....	224
		4.2.1. Fitting Procedures.....	224
		4.2.2. Selected Database.....	225
		4.2.3. The Equation for the Residual Part α^r	225
		5. Comparison of the New Equation of State with	

^{a)}Current address: E.ON Energy Projects GmbH., Denisstr. 2, D-80335 München, Germany.

^{b)}Author to whom correspondence should be addressed; electronic mail: wagner@thermo.ruhr-uni-bochum.de

© 2006 American Institute of Physics.

Experimental Data.....	226	that were assigned to group 1	219
5.1. The Vapor–Liquid Phase Boundary.....	226	16. Summary of the data sets for the speed of sound that were assigned to groups 2 and 3.....	219
5.1.1. Thermal Properties.....	226	17. Summary of the data sets for the isochoric heat capacity that were assigned to group 1	220
5.1.2. Caloric Properties.....	227	18. Summary of the data sets for the isochoric heat capacity that were assigned to groups 2 and 3....	220
5.2. Single-Phase Region.....	228	19. Summary of the data sets for the isobaric heat capacity that were assigned to group 1	221
5.2.1. $p\rho T$ Data.....	228	20. Summary of the data sets for the isobaric heat capacity that were assigned to groups 2 and 3....	222
5.2.2. Virial Coefficients.....	230	21. Summary of the data sets for the isobaric heat capacity in the ideal-gas state	222
5.2.3. Speed of Sound.....	231	22. Summary of the data sets for the enthalpy h , the Joule–Thomson coefficient μ , and the isothermal throttling coefficient δ_T	223
5.2.4. Isochoric Heat Capacity.....	232	23. Relations of thermodynamic properties to the ideal-gas part α° , Eq. (4.6), and the residual part α^r , Eq. (4.8), of the dimensionless Helmholtz energy and their derivatives.....	223
5.2.5. Isobaric Heat Capacity.....	232	24. Coefficients for the correlation equations for the ideal-gas isobaric heat capacity and the ideal-gas part of the Helmholtz energy, Eqs. (4.5) and (4.6).	224
5.2.6. Enthalpy Differences and Throttling Coefficients.....	233	25. The ideal-gas part α° , Eq. (4.6), of the dimensionless Helmholtz free energy and its derivatives.....	224
5.3. Critical Region.....	233	26. Summary of the selected data that were used in the linear and nonlinear optimization algorithms..	225
5.3.1. Thermal Properties.....	234	27. Coefficients and exponents of Eq. (4.8).....	226
5.3.2. Caloric Properties.....	234	28. The residual part α^r , Eq. (4.8), of the dimensionless Helmholtz energy and its derivatives.....	227
5.4. Extrapolation Behavior.....	235	29. Thermodynamic properties of ethane on the vapor–liquid phase boundary as a function of temperature.....	238
5.4.1. High Pressures and High Temperatures.....	235	30. Thermodynamic properties of ethane in the single-phase region.....	243
6. Estimated Uncertainty of Calculated Properties.....	236		
7. Recommendations for Improving the Basis of the Experimental Data.....	236		
8. Acknowledgments.....	237		
9. Appendix: Tables of Thermodynamic Properties of Ethane.....	237		
10. References.....	264		

List of Tables

1. Information on selected equations of state for ethane.....	209
2. Available data for the triple-point temperature of ethane.....	211
3. Available data for the critical point of ethane	212
4. Summary of the data sets for the melting pressure of ethane.....	212
5. Summary of the data sets for the vapor pressure of ethane.....	213
6. Summary of the data sets for the saturated-liquid density of ethane.....	213
7. Summary of the data sets for the saturated-vapor density of ethane.....	214
8. Summary of the data sets for the speed of sound on the vapor–liquid phase boundary of ethane...	214
9. Summary of the data sets for the heat capacity along the saturated-liquid line of ethane.....	215
10. Summary of the data sets for the enthalpy of vaporization of ethane.....	215
11. Summary of the $p\rho T$ data sets that were assigned to group 1	216
12. Summary of the $p\rho T$ data sets that were assigned to groups 2 and 3.....	216
13. Summary of the data sets for the second and third virial coefficients of ethane.....	218
14. Data for the second virial coefficients B calculated by Klimeck (2000) from a square-well potential.....	218
15. Summary of the data sets for the speed of sound	

List of Figures

1. Percentage deviations $100\Delta p_m/p_m = 100(p_{m,\text{exp}} - p_{m,\text{calc}})/p_{m,\text{exp}}$ of experimental data for the melting pressure p_m from values calculated from the melting-pressure equation, Eq. (2.3).....	213
2. Absolute deviations and percentage deviations $100\Delta p_s/p_s = 100(p_{s,\text{exp}} - p_{s,\text{calc}})/p_{s,\text{exp}}$ of experimental data for the vapor pressure p_s from values calculated from the vapor-pressure equation, Eq. (2.4).	213
3. Percentage deviations $100\Delta \rho'/\rho' = 100(\rho'_{\text{exp}} - \rho'_{\text{calc}})/\rho'_{\text{exp}}$ of experimental data for the saturated-liquid density ρ' from values calculated from the equation for the saturated-liquid density, Eq. (2.5).	214

4. Percentage deviations $100\Delta\rho''/\rho'' = 100(\rho''_{\text{exp}} - \rho''_{\text{calc}})/\rho''_{\text{exp}}$ of the selected data for the saturated-vapor density ρ'' from values calculated from the equation for the saturated-vapor density, Eq. (2.6).....	214
5. Distribution of the experimental $p\rho T$ data used to develop the residual part of the equation of state, Eq. (4.1), in a p - T diagram.....	217
6. Distribution of the experimental data for the speed of sound used to develop the residual part of the equation of state, Eq. (4.1), in a p - T diagram.....	219
7. Distribution of the experimental data for the isochoric heat capacity used to develop the residual part of the equation of state, Eq. (4.1), in a p - T diagram.....	220
8. Distribution of the experimental data for the isobaric heat capacity used to develop the residual part of the equation of state, Eq. (4.1), in a p - T diagram.....	221
9. Absolute and percentage deviations [$100\Delta y_m/y_m = 100(y_{m,\text{exp}} - y_{m,\text{calc}})/y_{m,\text{exp}}$ with $y = p_s, \rho', \rho''$] of the selected thermal data at saturation from values calculated from Eq. (4.1). Values calculated from the ancillary equations, Eqs. (2.4)–(2.6), and from the equation of state of Friend <i>et al.</i> (1991) are plotted for comparison.....	227
10. Percentage deviations [$100\Delta y_m/y_m = 100(y_{m,\text{exp}} - y_{m,\text{calc}})/y_{m,\text{exp}}$ with $y = w', c_\sigma$] of experimental data for the speed of sound in the saturated liquid and for the heat capacity along the saturated-liquid line from values calculated from the equation of state, Eq. (4.1). Values calculated from the equation of state of Friend <i>et al.</i> (1991) are plotted for comparison.....	228
11. Representation of the speed of sound on the phase boundary near the critical point. The plotted curves correspond to values calculated from the equation of state, Eq. (4.1), and from the equation of state of Friend <i>et al.</i> (1991).....	228
12. Percentage density deviations of highly accurate $p\rho T$ data (95–210 K) from values calculated from the equation of state, Eq. (4.1). Values calculated from the equation of state of Friend <i>et al.</i> (1991) are plotted for comparison.....	228
13. Percentage density deviations of highly accurate $p\rho T$ data (240–520 K) from values calculated from the equation of state, Eq. (4.1). Values calculated from the equation of state of Friend <i>et al.</i> (1991) are plotted for comparison.....	229
14. Percentage density deviations of $p\rho T$ data (120–350 K) assigned to groups 1 and 2 from values calculated from the equation of state, Eq. (4.1). Values calculated from the equation of state of Friend <i>et al.</i> (1991) are plotted for comparison.....	229
15. Percentage density deviations of $p\rho T$ data (373–623 K) assigned to groups 1 and 2 from values calculated from the equation of state, Eq. (4.1). Values calculated from the equation of state of Friend <i>et al.</i> (1991) are plotted for comparison.....	229
16. Percentage density deviations of $p\rho T$ data in the high-pressure region from values calculated from the equation of state, Eq. (4.1). Values calculated from the equation of state of Friend <i>et al.</i> (1991) are plotted for comparison. Note that the range of validity of the equation of state of Friend <i>et al.</i> (1991) is restricted to pressures up to 70 MPa and temperatures up to 625 K.....	230
17. Representation of data for the second virial coefficient at temperatures up to 650 K. The plotted lines correspond to values calculated from the equation of state, Eq. (4.1), and from the equation of state of Friend <i>et al.</i> (1991).....	230
18. Representation of data for the third virial coefficient at temperatures up to 650 K. The plotted lines correspond to values calculated from the equation of state, Eq. (4.1), and from the equation of state of Friend <i>et al.</i> (1991).....	231
19. Percentage deviations of highly accurate speed of sound data for densities up to about half the critical density from values calculated from the equation of state, Eq. (4.1). Values calculated from the equation of state of Friend <i>et al.</i> (1991) are plotted for comparison.....	231
20. Percentage deviations of speed of sound data in the liquid and supercritical region from values calculated from the equation of state, Eq. (4.1). Values calculated from the equation of state of Friend <i>et al.</i> (1991) are plotted for comparison.....	232
21. Percentage deviations of group 1 isochoric heat capacity data from values calculated from the equation of state, Eq. (4.1). Values calculated from the equation of state of Friend <i>et al.</i> (1991) are plotted for comparison.....	232
22. Percentage deviations of isobaric heat capacity data assigned to groups 1 and 2 from values calculated from the equation of state, Eq. (4.1). Values calculated from the equation of state of Friend <i>et al.</i> (1991) are plotted for comparison.....	232
23. Percentage deviations of experimental enthalpy differences from values calculated from the equation of state, Eq. (4.1). Deviations between isobaric enthalpy differences for $\Delta T = 1$ K, calculated from the equation of state of Friend <i>et al.</i> (1991) and Eq. (4.1) are plotted for comparison..	233
24. Percentage deviations of experimental data for the Joule–Thomson coefficient from values calculated from the equation of state, Eq. (4.1). Values calculated from the equation of state of Friend <i>et al.</i> (1991) are plotted for comparison.....	233

25. Representation of experimental data for the isothermal throttling coefficient. The plotted lines correspond to values calculated from the equation of state, Eq. (4.1), and from the equation of Friend *et al.* (1991). 234
26. Percentage pressure deviations of highly accurate $p\rho T$ data in the extended critical region from values calculated from the equation of state, Eq. (4.1). Values calculated from the equation of Friend *et al.* (1991) are plotted for comparison. 234
27. Representation of the isochoric heat capacity on the critical isochore. The plotted lines correspond to values calculated from the equation of state, Eq. (4.1), and from the equation of Friend *et al.* (1991). 235
28. Representation of the speed of sound on isotherms in the extended critical region. The plotted lines correspond to values calculated from the equation of state, Eq. (4.1), and from the equation of Friend *et al.* (1991). 235
29. Representation of data calculated from the reference equation of state for nitrogen [Span *et al.* (2000)] and transferred to ethane by a simple corresponding states approach. The plotted lines correspond to values calculated from the equation of state, Eq. (4.1), and from the equation of Friend *et al.* (1991). 235
30. "Ideal curves" in a double logarithmic p/p_c vs. T/T_c diagram. The curves correspond to values calculated from the equation of state, Eq. (4.1), and from the equation of Friend *et al.* (1991). The area marked in gray corresponds to the region where Eq. (4.1) was fitted to experimental data. 236
31. Tolerance diagram for densities calculated from the equation of state, Eq. (4.1). In the extended critical region the uncertainty in pressure is given. 236
32. Tolerance diagram for speeds of sound calculated from the equation of state, Eq. (4.1). 236
33. Tolerance diagram for isobaric and isochoric heat capacities calculated from the equation of state, Eq. (4.1). 237

Nomenclature

Latin symbols

<i>a</i>	specific Helmholtz energy
<i>B</i>	second virial coefficient
<i>c</i>	density exponent
<i>c_p</i>	specific isobaric heat capacity
<i>c_v</i>	specific isochoric heat capacity
<i>c_σ</i>	specific heat capacity along the saturated-liquid line
<i>C</i>	third virial coefficient
<i>d</i>	density exponent

<i>g</i>	specific Gibbs energy
<i>h</i>	specific enthalpy
<i>i,j</i>	serial numbers
<i>M</i>	molar mass
<i>n</i>	adjustable coefficient
<i>p</i>	pressure
<i>R</i>	specific gas constant
<i>R_m</i>	molar gas constant
<i>s</i>	specific entropy
<i>t</i>	temperature exponent
<i>T</i>	thermodynamic temperature, ITS-90
<i>u</i>	specific internal energy
<i>v</i>	specific volume
<i>w</i>	speed of sound
<i>y</i>	any thermodynamic property
<i>Z</i>	compression factor [$Z=p/(\rho RT)$]

Greek symbols

α	dimensionless Helmholtz energy [$\alpha=a/(RT)$]
$\beta, \varepsilon, \gamma, \eta, \theta$	adjustable parameters
δ	reduced density ($\delta=\rho/\rho_c$)
δ_T	isothermal throttling coefficient [$\delta_T=(\partial h/\partial p)_T$]
Δ	difference in any quantity
ϑ	transformed temperature ($\vartheta=1-T/T_c$)
μ	Joule-Thomson coefficient [$\mu=(\partial T/\partial p)_h$]
ρ	mass density
τ	inverse reduced temperature ($\tau=T_c/T$)

Superscripts

^o	ideal-gas state
^r	residual contribution
[']	saturated-liquid state
["]	saturated-vapor state

Subscripts

0	at some reference state
90	based on ITS-90
b	at the normal boiling point
c	at the critical point
calc	calculated
exp	experimental
<i>h</i>	isenthalpic
<i>i,j</i>	indices
m	denotes a state on the melting curve
<i>p</i>	isobaric
s	denotes a state on the vapor-pressure curve
<i>s</i>	isentropic
σ	along the saturated-liquid line
t	at the triple point
<i>T</i>	isothermal
<i>v</i>	isochoric

Physical Constants and Characteristic Properties of Ethane

Molar mass	$M = 30.069\ 04\ \text{g mol}^{-1}$	[Coplen (2001)]
Universal gas constant	$R_m = 8.314\ 472\ \text{J mol}^{-1}\ \text{K}^{-1}$	[Mohr and Taylor (1999)]
Specific gas constant	$R = 0.276\ 512\ 72\ \text{kJ kg}^{-1}\ \text{K}^{-1}$	
Critical point		
Temperature	$T_c = 305.322\ \text{K}$	[Funke <i>et al.</i> (2002b)]
Pressure	$p_c = 4.8722\ \text{MPa}$	[Funke <i>et al.</i> (2002b)]
Density	$\rho_c = 206.18\ \text{kg m}^{-3}$	[Funke <i>et al.</i> (2002b)]
Triple point		
Temperature	$T_t = 90.368\ \text{K}$	[Funke <i>et al.</i> (2002b)]
Pressure	$p_t = 1.14\ \text{Pa}$	[Sec. 2.1]
Reference state		
Temperature	$T_0 = 298.15\ \text{K}$	
Pressure	$p_0 = 0.101\ 325\ \text{MPa}$	
Specific enthalpy	$h_0 = 0\ \text{kJ kg}^{-1}$	
Specific entropy	$s_0 = 0\ \text{kJ kg}^{-1}\ \text{K}^{-1}$	

1. Introduction

1.1. Background

As the second member of the alkane series and one of the major components of natural gas, ethane is important both for industrial and scientific applications. An accurate knowledge of the thermodynamic properties of ethane is of vital interest as much to the power and the chemical industry as to scientists in a broad variety of research fields. Numerous experimental studies of the thermodynamic properties of ethane have been carried out over the last century, and today high precision data of its thermal and caloric properties are available for a wide range of temperatures and pressures. This work is part of an international collaboration between the Ruhr University in Bochum and the National Institute of Standards and Technology in Bolder to characterize the properties of ethane (this work), propane (Lemmon, McLinden, and Wagner to be published in *J. Phys. Chem. Ref. Data*), and the butanes (Bücker and Wagner, accepted for publication in *J. Phys. Chem. Ref. Data*, **35**, 2006).

Over the last few decades, a lot of work has been done by the National Institute of Standards and Technology to collect information on the thermodynamic properties of ethane. Comprehensive tables were published by Goodwin *et al.* (1976) and equations of state were developed by Younglove and Ely (1987) and Friend *et al.* (1991). Since the publication of the latter equation, the thermodynamic surface of ethane has been redefined by highly accurate measurements of the thermal and acoustic properties. Moreover, correlation

techniques have improved considerably. Particularly, sophisticated procedures for the optimization of the functional form [Setzmann and Wagner (1989), Tegeler *et al.* (1997)] were developed that provide powerful tools for the development of accurate empirical equations of state.

1.2. Previous Equations of State

A number of correlation equations are available for the thermodynamic properties of ethane. However, none of these equations meets current demands on accuracy. Table 1 summarizes selected equations of state for ethane that cover large parts of the fluid region and that are commonly used in industrial or scientific applications.

Teja and Singh (1977) fitted the coefficients of a Bender-type equation of state. This was the first accurate equation that could describe the homogeneous fluid region of ethane including the vapor–liquid phase equilibrium. The coefficients were refitted later by Büchner *et al.* (1981) to account for more recent data sets.

A higher accuracy and hence a new reference for the thermodynamic properties of ethane was attained in the work of Younglove and Ely (1987) by fitting the coefficients of an equation of state of the modified Benedict–Webb–Rubin (MBWR) type. In the same year, the first equation with a functional form specially designed for the description of the properties of ethane was published by Sychev *et al.* (1987). The equation had been developed in Russia in 1982. Although the tables in the work of Sychev *et al.* were widely

TABLE 1. Information on selected equations of state for ethane

Authors	Year	Temperature range/K	Upper pressure limit/MPa	Structure of the equation	Number of coefficients
Span & Wagner	2003a, b	90–623	52	Helmholtz energy	12
Friend <i>et al.</i>	1991	90–625	70	Helmholtz energy	32
Sychev <i>et al.</i>	1987	90–700	80	Compression factor	50
Younglove & Ely	1987	90–600	70	Pressure explicit	32
Büchner <i>et al.</i>	1981	90–573	100	Pressure explicit	20
Teja & Singh	1977	185–1000	81	Pressure explicit	20

used, the equation itself never was of great importance since the MBWR-type equation of Younglove and Ely is superior both with respect to the functional form and the data used to fit the coefficients.

Till now, the reference for the thermodynamic properties of ethane has been an equation developed at NIST by Friend *et al.* (1991). The functional form of this equation was originally developed by Schmidt and Wagner (1985) for the description of the thermodynamic properties of oxygen. The data used in the fit include thermal properties in the single-phase region and on the vapor–liquid phase boundary, second virial coefficients, speeds of sound in the homogenous region and on the phase boundary, isochoric and isobaric heat capacities, and heat capacities along the saturated-liquid line. The correlation function for the ideal-gas part was fitted to data reported by Chao *et al.* (1973).

A simultaneously optimized functional form was introduced by Span and Wagner (2003a, 2003b) for simple non-polar fluids, including ethane. The rather short functional form was developed for a broad range of substances. The aim was not to reach the highest possible accuracy for each substance but rather to establish a new class of equations which are numerically very stable and which can easily be adopted to physically similar substances even when only restricted data sets are available. These equations are strictly designed for technical applications and do not compete with highly accurate reference equations of state. Data from the recent high precision measurements of the thermal properties by Funke *et al.* (2002a, 2002b) and Claus *et al.* (2003) were not available when the simultaneously optimized equations were set up.

Each of the aforementioned equations has several of the following disadvantages:

- (1) State-of-the-art data for the thermodynamic properties of ethane are not represented within their experimental uncertainty.
- (2) Unreasonable behavior is observed in regions with a poor data situation.
- (3) Extrapolation to temperatures and pressures outside the range of validity yields unreasonable results.
- (4) Data in the extended critical region are not described within their accuracy.
- (5) The temperature values do not correspond to the current International Temperature Scale of 1990 (ITS-90).

In this paper, a new equation of state for ethane is presented to overcome these shortcomings. The thermodynamic surface of ethane in the range covered by reliable experimental data is described within the experimental uncertainties. The new equation was developed using current fitting procedures and state-of-the-art linear and nonlinear optimization algorithms.

1.3. Notes on the Values of Temperature Used in This Article

- (1) All correlation equations presented in this article refer to the ITS-90.

- (2) No distinction is made between the thermodynamic temperature T and the temperature T_{90} of the currently valid International Temperature Scale of 1990 (ITS-90), see Preston-Thomas (1990).
- (3) Temperature values of available experimental data referring to older temperature scales were converted to ITS-90. The conversion from the IPTS-68 temperature scale to ITS-90 temperatures was carried out based on conversion equations given by Rusby (1991). Data corresponding to the IPTS-48 temperature scale were converted to IPTS-68 according to the procedure given by Bedford and Kirby (1969).
- (4) Values calculated from literature equations that are used in the corresponding figures for comparison purposes were, if necessary, converted from their original temperature scale to ITS-90 values.

2. Phase Equilibria of Ethane

Ancillary equations, which accurately describe the phase equilibria, are an important precondition for the development of a wide-range equation of state. Additionally, they serve as a helpful tool for users who are interested in phase equilibria only. To establish the experimental basis for these equations, the available experimental information on the triple point, the critical point, the melting pressure, the vapor pressure, the saturated liquid and vapor densities, and on calorific properties on the vapor–liquid phase boundary have been reviewed. Simple correlation equations are given for the thermal properties.

To provide the reader with an assessment of the quality and importance of the different experimental data, all data sets have been divided into three groups. The assignment considers the critically assessed uncertainty of the data, the size of the data set, the covered temperature range, and the data situation of the corresponding property in the relevant region. Data that are of no significance in regions where highly accurate experimental data are available may gain importance in regions where the data situation is poor. Group 1 includes all the data used for the development of the corresponding correlation equation. Group 2 contains reliable data sets suitable for comparisons. These data are inferior in quality to the group 1 data with respect to at least one of the aspects mentioned above. Data sets that are very small or that show great uncertainties are assigned to group 3 and are not taken under further consideration here. However, an assignment to this group does not imply a devaluation of the data. The ranking is determined by the quality relative to the best available reference data rather than by any kind of absolute level of quality, and data that do not contribute to the level of accuracy aspired to here may be very useful for other purposes.

2.1. Triple Point

The temperature of the gas-liquid-solid triple point of ethane has been determined by different authors since 1930. Table 2 shows selected values of the triple-point temperature

TABLE 2. Available data for the triple-point temperature of ethane

Authors	T_t/K
Funke <i>et al.</i> (2002b)	90.368 ± 0.005
Pavese (1978)	90.361 ± 0.001^a
Atake & Chihara (1976)	90.350 ± 0.002
Roder (1976a)	90.342 ± 0.05
Straty & Tsumura (1976a)	90.357 ± 0.005
Eggers (1975)	90.279 ± 0.02
Burnett & Muller (1970)	89.829 ± 0.03
Clusius & Weigand (1940)	90.36 ± 0.03
Witt & Kemp (1937)	89.88 ± 0.1
Wiebe <i>et al.</i> (1930)	89.53 ± 0.1

^aUncertainty implicitly set to 0.005 K by Bedford *et al.* (1984).

as reported in literature. Some of the older values differ greatly from the more recent and more reliable values. In addition to the inferior measurement techniques, this disagreement is owed to a total of three different solid phases with transitions between them occurring closely beneath the temperature of the gas-liquid-solid triple point. The value reported by Funke *et al.* (2002b) was selected in this work:

$$T_t = (90.368 \pm 0.005) \text{ K.} \quad (2.1a)$$

No experimental values for the pressure at the triple point are available. Therefore, the triple-point pressure was taken as

$$p_t = 1.14 \text{ Pa,} \quad (2.1b)$$

which was calculated by inserting the temperature for the triple point as given in Eq. (2.1a) into the vapor-pressure equation, Eq. (2.4).

2.2. Critical Point

Values for the critical parameters of ethane reported in literature are compiled in Table 3. The parameters reported by Funke *et al.* (2002b) were determined by evaluation of their accurate measurements of the thermal properties on the vapor-liquid phase boundary. These data are consistent with the precise density measurements in the homogeneous region as published by Funke *et al.* (2002a) and were used as the critical parameters in this work:

$$T_c = (305.322 \pm 0.01) \text{ K,} \quad (2.2a)$$

$$p_c = (4.8722 \pm 0.0011) \text{ MPa,} \quad (2.2b)$$

$$\rho_c = (206.18 \pm 0.15) \text{ kg m}^{-3}. \quad (2.2c)$$

2.3. Melting Pressure

Table 4 gives a summary of the available data sets for the melting pressure of ethane. In this work, the melting pressure is used only as the limit of the range of validity of the fundamental equation. Three of the referred articles only give a graphical presentation of their results. These data were not considered for the development of the correlation equation because the other data sets, namely the ones published by Straty and Tsumura (1976a) and by Schutte *et al.* (1979), give reliable information on the melting pressure up to 1026

MPa. Based on the data reported by Straty and Tsumura (1976a) and Schutte *et al.* (1979), a simple correlation equation was formulated for the melting pressure of ethane:

$$\frac{p_m}{p_t} = 1 + n_1 \left[\frac{T}{T_t} - 1 \right] + n_2 \left[\left(\frac{T}{T_t} \right)^{2.55} - 1 \right], \quad (2.3)$$

with $p_t = 1.14 \text{ Pa}$, $T_t = 90.368 \text{ K}$, $n_1 = 2.236\,26315 \times 10^8$, and $n_2 = 1.052\,623\,74 \times 10^8$. The upper temperature limit of Eq. (2.3) is $T = 195 \text{ K}$. Figure 1 compares measured melting pressures with values calculated from Eq. (2.3). The equation represents all p_m data used in the fit to within 0.7%.

2.4. Vapor Pressure

The earliest measurements of the vapor pressure of ethane were reported more than 100 years ago. Since then, this important fluid property has been continually investigated. The available 26 data sets are summarized in Table 5. The vapor pressures reported by Douslin and Harrison (1973) and by Funke *et al.* (2002b) are consistent within 0.01% and were assigned to group 1. The data set published by Funke *et al.* (2002b) describes the entire vapor-pressure curve with very low uncertainties, ranging from 0.006% near the critical point to 0.02% in vapor pressure at $T = 195 \text{ K}$. At temperatures below 190 K, enlarged relative uncertainties arise from an absolute contribution of 2–20 Pa to the relative uncertainty. Nevertheless, these data are still substantially more accurate than the other data sets for which similar effects are encountered. Data that deviate from the aforementioned reference data by no more than (0.2% + 50 Pa) are assigned to group 2.

The vapor-pressure equation of Funke *et al.* (2002b) is also used here to describe the vapor-pressure curve

$$\ln \left(\frac{p_s}{p_c} \right) = \frac{T_c}{T} (n_1 \vartheta + n_2 \vartheta^{1.5} + n_3 \vartheta^{2.5} + n_4 \vartheta^{3.5} + n_5 \vartheta^4), \quad (2.4)$$

with $\vartheta = 1 - T/T_c$, $T_c = 305.322 \text{ K}$, $p_c = 4.8722 \text{ MPa}$, $n_1 = -6.486\,475\,77$, $n_2 = 1.470\,100\,78$, $n_3 = -1.662\,611\,22$, $n_4 = 3.578\,983\,78$, and $n_5 = -4.791\,057\,05$. Comparisons of the group 1 and group 2 data with values calculated from Eq. (2.4) are given in Fig. 2. The diagram is divided into two parts. On the left hand side, absolute deviations are shown for temperatures below 170 K, while on the right hand side, percentage deviations are shown for higher temperatures.

2.5. Saturated-Liquid Density

The 20 available data sets for the saturated-liquid density of ethane are compiled in Table 6. Only the data measured by Funke *et al.* (2002b) were assigned to group 1. The reported uncertainties of the data are less than 0.016% in density at temperatures from the triple point to 303 K. In the vicinity of the critical point, the reported uncertainties increase, but do not exceed 0.4%. Group 2 data deviate from these reference values by no more than 0.2% in general.

TABLE 3. Available data for the critical point of ethane. Uncertainties are given where the original articles contain such estimates

Authors	Method	T_c /K	p_c /MPa	ρ_c /(kg m ⁻³)
Funke <i>et al.</i> (2002b)	A	305.322±0.01	4.8722±0.0011	206.18±0.15
Ambrose & Tsonopoulos (1995)	B	305.32±0.04	4.872±0.01	206.6±3
Colgate <i>et al.</i> (1992)	C	305.362	4.879	
Friend <i>et al.</i> (1991)	B	305.32±0.04	4.8718±0.005	206.6±3
Brunner (1988)	D	305.38±0.1	4.877±0.005	
Brunner (1987)	D	305.6	4.889	
Younglove & Ely (1987)	B	305.33	4.87143	206.7
Morrison & Kincaid (1984)	D	305.385±0.001		200.9
Sychev <i>et al.</i> (1987)	B	305.32±0.02	4.8714±0.005	204.46
Bulavin & Shimanskii (1979)	E	305.339		205.8±4
Burton & Balzarini (1974)	D	305.221±0.03		206.2±0.3
Strumpf <i>et al.</i> (1974)	D	305.36		205.5
Douslin & Harrison (1973)	F	305.322	4.8718	206.6
Bulavin <i>et al.</i> (1971)	E	305.342		206.2
Khazanova & Sominskaya (1971)	D	305.33	4.88	203.9
Miniovich & Sorina (1971)	E	305.34±0.005	4.8749±0.000 05	205.8±0.7
Chaskin <i>et al.</i> (1970)	E	305.49±0.01		205.1±0.6
Sliwinski (1969)	E	305.326		
Tsiklis & Prokhorov (1967)	D	305.28		203
Khodeeva (1966)	D	305.6		203.5
Kay (1964)	D	305.4	4.93	
Tanneberger (1959)	E	305.39		
Kay & Albert (1956)	D	305.1	4.876	
Palmer (1954)	D	305.45		
Schmidt & Thomas (1954)	D	305.32	5.044	
Kay & Brice (1953)	D	305.1	4.876	
Whiteway & Mason (1953)	D	305.3		215
Kay & Nevens (1952)	D	305.24	4.875	201.9
Murray & Mason (1952)	D	305.36		
Atack & Schneider (1950)	D	305.5		
Lu <i>et al.</i> (1941)	D	305.2	4.92	
Mason <i>et al.</i> (1940)	D	305.36		
Beattie <i>et al.</i> (1939a)	F	305.4	4.884	203.0±2
Kay (1938)	D	305.4	4.91	220
Sage <i>et al.</i> (1937)	F	305.7	4.951	212
Prins (1915)	D	305.47	4.877	
Cardoso & Bell (1912)	D	305.25	4.950	
Kuenen & Robson (1902a)	D	305.05	4.907	207
Olszewski (1895)	D	307	5.09	
Dewar (1884)	D	308	4.58	
Hainlen (1894)	D	307.6	5.1	

Methods used to determine the critical parameters:

- A Evaluation of measurements of the saturated-vapor and saturated-liquid densities in the critical region.
- B Equation of state/evaluation of published data.
- C Evaluation of speed of sound measurements on the phase boundary.
- D Disappearance of the meniscus.
- E Other methods or no method indicated.
- F Evaluation of $p\rho T$ measurements.

The equation given by Funke *et al.* (2002b) for the saturated-liquid density

$$\ln\left(\frac{\rho'}{\rho_c}\right) = (n_1 \vartheta^{0.329} + n_2 \vartheta^{4/6} + n_3 \vartheta^{8/6} + n_4 \vartheta^{19/6}), \quad (2.5)$$

with $\vartheta = 1 - T/T_c$, $T_c = 305.322$ K, $\rho_c = 206.18$ kg m⁻³, $n_1 = 1.561\,380\,26$, $n_2 = -0.381\,552\,776$, $n_3 = 0.078\,537\,2040$, $n_4 = 0.037\,031\,5089$, was adopted for this work. Figure 3 shows comparisons of values calculated with Eq. (2.5) to the experimental data assigned to groups 1 and 2.

TABLE 4. Summary of the data sets for the melting pressure of ethane

Authors	Number of data	Pressure range/MPa	Group
van der Putten <i>et al.</i> (1985)	12 ^a	650–1200	—
Wieldraaijer <i>et al.</i> (1983)	8 ^a	2500–4700	—
Geijsel <i>et al.</i> (1979)	6 ^a	500–2500	—
Schutte <i>et al.</i> (1979)	7	213–1026	1
Straty & Tsumura (1976a)	16	0.3–33	1
Clusius & Weigand (1940)	7	0.6–4.3	3

^aData presented in graphs only.

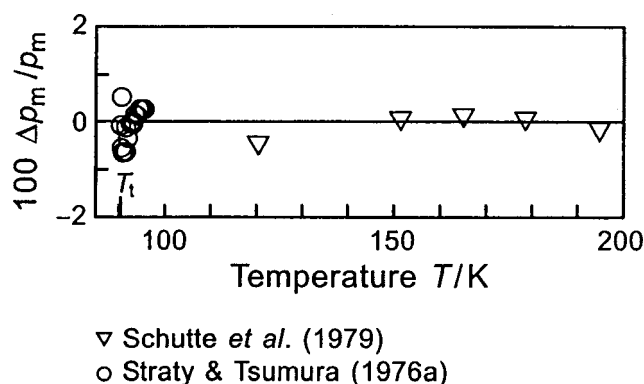


FIG. 1. Percentage deviations $100\Delta p_m/p_m = 100(p_{m,\text{exp}} - p_{m,\text{calc}})/p_{m,\text{exp}}$ of experimental data for the melting pressure p_m from values calculated from the melting-pressure equation, Eq. (2.3).

2.6. Saturated-Vapor Density

Accurate measurement of the saturated-vapor density is difficult as compared to the other thermal properties on the vapor–liquid phase boundary. Consequently, appreciably fewer data are available for this property than for the vapor pressure or the saturated-liquid density. The seven available data sets are summarized in Table 7. Again, the data reported by Funke *et al.* (2002b) were the only values assigned to group 1. The other data sets are of substantially inferior quality. The uncertainties of the saturated-vapor densities re-

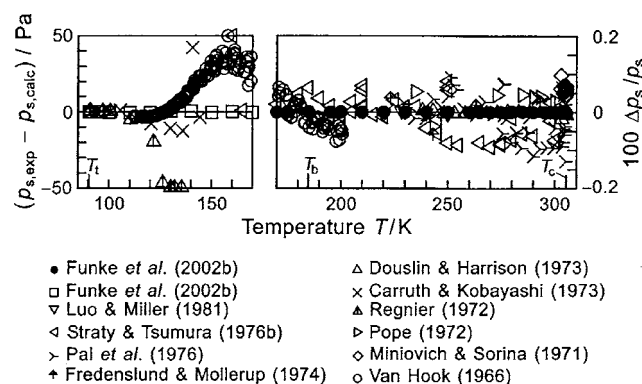


FIG. 2. Absolute deviations and percentage deviations $100\Delta p_s/p_s = 100(p_{s,\text{exp}} - p_{s,\text{calc}})/p_{s,\text{exp}}$ of experimental data for the vapor pressure p_s from values calculated from the vapor-pressure equation, Eq. (2.4).

ported by Funke *et al.* (2002b) are generally less than 0.017% at temperatures from 240 to 303 K. In the vicinity of the critical point, the uncertainties increase up to 0.8% at $T = 305.3$ K. Towards lower temperatures, uncertainties increase up to 0.07% at $T = 185$ K. Below this temperature, no experimental determination of saturated-vapor densities has been achieved yet. Therefore, Funke *et al.* (2002b) determined reliable densities from a virial equation of state with relative uncertainties comparable to those of their experimental vapor-pressure data.

Based on these data, Funke *et al.* (2002b) set up a correlation equation for the saturated-vapor density of ethane

$$\ln\left(\frac{\rho''}{\rho_c}\right) = \frac{T_c}{T}(n_1 \vartheta^{0.346} + n_2 \vartheta^{5/6} + n_3 \vartheta + n_4 \vartheta^2 + n_5 \vartheta^3 + n_6 \vartheta^5), \quad (2.6)$$

TABLE 5. Summary of the data sets for the vapor pressure of ethane

Authors	Number of data	Temperature range/K	Group
Funke <i>et al.</i> (2002b)	44	90–305	1
Holcomb <i>et al.</i> (1995)	6	242–299	3
Brown <i>et al.</i> (1988)	8	207–270	3
Barclay <i>et al.</i> (1982)	7	198–278	3
Luo & Miller (1981)	5	220–250	2
Ohgaki & Katayama (1977)	5	283–298	3
Pal <i>et al.</i> (1976)	50	214–305	2
Straty & Tsumura (1976b)	44	160–300	2
Fredenslund & Mollerup (1974)	5	223–293	2
Gugnoni <i>et al.</i> (1974)	4	241–283	3
Carruth & Kobayashi (1973)	11	91–144	2
Douslin & Harrison (1973)	18	238–305	1 ^a
Kahre (1973)	5	267–300	3
Pope (1972)	9	198–305	2
Regnier (1972)	21	89–135	2
Chui & Canfield (1971)	2	115–162	3
Miniovich & Sorina (1971)	15	302–305	2
Djordjevich & Budenholzer (1970)	6	127–256	3
Van Hook (1966)	182	112–201	2
Tickner & Lossing (1951)	13	89–130	3
Beattie <i>et al.</i> (1935)	2	273–298	3
Loomis & Walters (1926)	34	135–200	3
Porter (1926)	20	184–289	3
Maass & Wright (1921)	7	172–201	3
Burrell & Robertson (1915)	19	113–184	3
Kuenen & Robson (1902b)	15	194–274	3

^aAlthough the data were assigned to group 1, they were not used to develop the new correlation equations because the entire phase boundary is covered by the highly accurate and very consistent data of Funke *et al.* (2002b).

TABLE 6. Summary of the data sets for the saturated-liquid density of ethane

Authors	Number of data	Temperature range/K	Group
Funke <i>et al.</i> (2002b)	42	91–305	1
Pestak <i>et al.</i> (1987)	39	299–305	3
Shinsaka <i>et al.</i> (1985)	20	113–205	3
Luo & Miller (1981)	5	220–250	2
Orrit & Laupretre (1978)	43	103–232	2
Haynes & Hiza (1977)	22	100–270	2
McClune (1976)	17	93–173	2
Pal <i>et al.</i> (1976)	11	216–304	3
Gugnoni <i>et al.</i> (1974)	4	241–283	3
Douslin & Harrison (1973)	13	248–305	3
Kahre (1973)	10	267–300	3
Chui & Canfield (1971)	2	116–161	2
Khazanova & Sominskaya (1971)	7	302–305	3
Miniovich & Sorina (1971)	8	303–305	2
Tomlinson (1971)	7	283–302	3
Sliwinski (1969)	11	283–305	2
Klosek & McKinley (1968)	8	94–183	2
Leadbetter <i>et al.</i> (1964)	18	127–183	3
Mason <i>et al.</i> (1940)	33	296–305	3
Maass & Wright (1921)	10	165–200	3

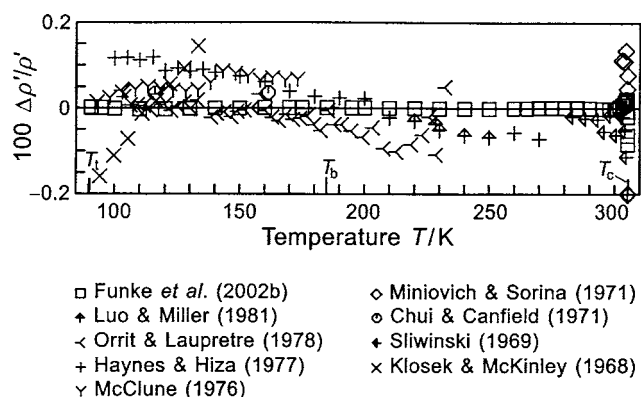


Fig. 3. Percentage deviations $100\Delta\rho'/\rho'=100(\rho'_{exp}-\rho'_{calc})/\rho'_{exp}$ of experimental data for the saturated-liquid density ρ' from values calculated from the equation for the saturated-liquid density, Eq. (2.5).

with $\vartheta=1-T/T_c$, $T_c=305.322$ K, $\rho_c=206.18$ kg m⁻³, $n_1=-1.898\,791\,45$, $n_2=-3.654\,592\,62$, $n_3=0.850\,562\,745$, $n_4=0.363\,965\,487$, $n_5=-1.500\,059\,43$, and $n_6=-2.266\,903\,89$, which was adopted for this work. Comparisons of the available data and saturated-vapor densities calculated from Eq. (2.6) are shown in Fig. 4. The inconsistencies between the reference data reported by Funke *et al.* (2002b) and the older data are well appreciable.

2.7. Caloric Data on the Vapor–Liquid Phase Boundary

No ancillary equations have been developed for the caloric properties on the vapor–liquid phase boundary, but the group 1 data were included in the development of the new equation of state.

2.7.1. Speed of Sound

Four data sets are available for the speed of sound in saturated liquid ethane. Poole and Aziz (1972) and Colgate *et al.* (1992) used resonators while Vangeel (1976) and Tsumura and Straty (1977) performed measurements using pulse-echo techniques. The only available experimental speeds of sound in the saturated vapor were reported by Colgate *et al.* (1992). The relevant information on all data sets is given in Table 8.

The measurements by Colgate *et al.* (1992) were carried out in the immediate vicinity of the critical point. The objec-

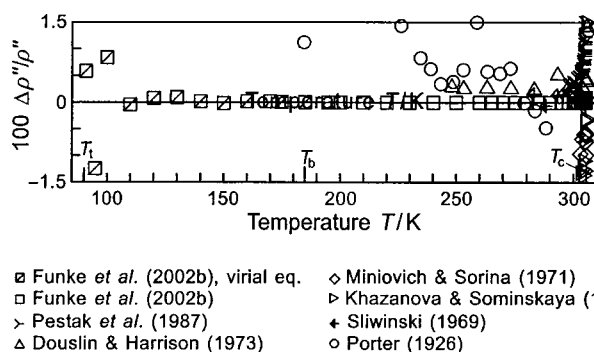


Fig. 4. Percentage deviations $100\Delta\rho''/\rho''=100(\rho''_{exp}-\rho''_{calc})/\rho''_{exp}$ of the selected data for the saturated-vapor density ρ'' from values calculated from the equation for the saturated-vapor density, Eq. (2.6).

tive of the investigation was rather the determination of the critical parameters of ethane than the actual speed of sound data themselves. Accordingly, no estimates are given for the relevant uncertainties. Resonator techniques generally perform best at low densities, while uncertainties of the measured speeds of sound will increase substantially when approaching the critical point, see Trusler (1991). Nonetheless, these data give important information on the speed of sound in the vicinity of the critical point of ethane.

The pulse-echo technique, as applied by Vangeel (1976) and Tsumura and Straty (1977), is considered to be the most appropriate method for the determination of saturated-liquid speeds of sound. Tsumura and Straty (1977) report uncertainties of the measured variables of 0.01% in pressure, 0.05 K in temperature, and 0.06%–0.1% in speed of sound, while the purity of the ethane is reported as 99.98%. Vangeel (1976) gives estimated total uncertainties of 0.2% in speed of sound. The uncertainties of both data sets are expected to be higher at low temperatures near the triple point due to dispersion effects and at high temperatures when approaching the critical temperature. In both regions, greater inconsistencies between the data sets can be observed that exceed the combined claimed uncertainties. The values of the speed of sound published by Poole and Aziz (1972) deviate systematically from the more reliable data by Vangeel (1976) and Tsumura and Straty (1977).

2.7.2. Heat Capacities

While no data are available for the heat capacity of either the saturated liquid or the saturated vapor, four data sets

TABLE 7. Summary of the data sets for the saturated-vapor density of ethane

Authors	Number of data	Temperature range/K	Group
Funke <i>et al.</i> (2002b)	32 ^a	185–305	1
Pestak <i>et al.</i> (1987)	39	299–305	3
Douslin & Harrison (1973)	13	248–305	3
Khazanova & Sominskaya (1971)	13	303–305	3
Miniovich & Sorina (1971)	8	303–305	3
Sliwinski (1969)	11	283–305	3
Porter (1926)	14	185–288	3

^aAdditionally, 12 values were calculated from a virial equation at temperatures from 91 to 170 K.

TABLE 8. Summary of the data sets for the speed of sound on the vapor–liquid phase boundary of ethane

Authors	Number of data		Temperature range/K	Group
	w'	w''		
Colgate <i>et al.</i> (1992)	14	8	304–305	2
Tsumura & Straty (1977)	55	—	90–305	1
Vangeel (1976)	44	—	98–288	1
Poole & Aziz (1972)	25	—	92–199	2

TABLE 9. Summary of the data sets for the heat capacity along the saturated-liquid line of ethane

Authors	Number of data	Temperature range/K	Group
Roder (1976b)	106	93–301	1
Witt & Kemp (1937)	29	92–180	3
Wiebe <i>et al.</i> (1930)	50	97–295	3
Eucken & Hauck (1928)	18	100–270	3

containing experimental values of heat capacities c_σ along the saturated-liquid line have been published. They are summarized in Table 9. Amongst the older data sets, the results of Wiebe *et al.* (1930) and Witt and Kemp (1937) are consistent within 0.7%, while the results of Eucken and Hauck (1928) deviate from these by up to 20%. Only the most recent data set, published by Roder (1976b), was used for the development of the new equation of state. The reported total uncertainties of the heat capacities are less than 0.5% except for the vicinity of the critical temperature where the uncertainties increase to 5%. Roder (1976b) expects potential undetected systematic errors to be less than 2%.

The relation between the dimensionless Helmholtz energy and c_σ contains the first derivative of the vapor pressure (see Table 23). Direct inclusion of this property in the nonlinear fit therefore involves an interlocked relation to the Maxwell criterion as given by Eq. (4.2). To avoid numerical problems, the specific heat capacities along the saturated-liquid line have been transformed into specific isobaric heat capacities at the saturated-liquid line according to

$$c'_p(T) = c_\sigma(T) - \frac{T}{\rho'^2} \frac{\left(\frac{\partial p}{\partial T}\right)_\rho \frac{dp_s}{dT}}{\left(\frac{\partial p}{\partial \rho}\right)_T}. \quad (2.7)$$

The loss of accuracy associated with this transformation is negligible if accurate preliminary equations are used to calculate the fraction in Eq. (2.7) or if temperatures are near the triple point.

2.7.3. Enthalpy of Vaporization

Experimental data on the enthalpy of vaporization of ethane are given in two sources, which are listed in Table 10. The enthalpy of vaporization is linked directly to the vapor pressure and the orthobaric liquid and vapor densities by the equation of Clausius–Clapeyron. Since these properties are

TABLE 10. Summary of the data sets for the enthalpy of vaporization of ethane

Authors	Number of data	Temperature range/K	Group
Miyazaki <i>et al.</i> (1980)	2	289–301	3
Dana <i>et al.</i> (1926)	11	233–272	3

very accurately known, none of the data for the enthalpy of vaporization were taken into account in the development of the new equation of state.

3. Experimental Data for the Single-Phase Region

This section presents experimental data sets for the thermodynamic properties of ethane in the homogeneous fluid region. General information on all available data sets and more detailed information on the data selected for the development of the new equation of state are presented in the following tables. Where appropriate, the data have been classified into three groups as explained in Sec. 2. Since the data situation in the homogeneous region is more involved than on the phase boundaries, some data sets are assigned to more than one group. Typically, these data sets reside in regions with sparse or poor data and are used only for comparisons in regions where more reliable data are available.

The uncertainties given in the tables usually correspond to estimates reported by the authors. In some studies, however, the stated uncertainties appear overly optimistic or no estimates are given at all. In these cases, we had to estimate more realistic values for the uncertainties. In the tables, these values are presented in parentheses.

3.1. Thermal Properties

3.1.1. $p\rho T$ Data

During the last century, the thermal properties of ethane have been investigated by numerous experimental studies. The fluid region is described with very good quality up to temperatures of 625 K and pressures of 70 MPa. Furthermore, high-pressure data are available up to 673 K and 900 MPa. Many of the 37 available data sets, however, do not meet the level of accuracy aspired to here. Table 11 gives details on the data sets that were assigned to group 1. However, not every data point was used to set up the new equation of state. The number of data actually used is specified in the row “selected data.” Table 12 summarizes the data sets that were assigned to groups 2 and 3.

At temperatures up to 340 K and pressures up to 12 MPa, the thermal behavior of ethane is defined very accurately by the data published by Funke *et al.* (2002a). The measurements have been performed on ethane with a reported purity of 99.9984% using a two-sinker densimeter, which is probably the most accurate technique for the measurement of fluid densities available today. In the vicinity of the critical point, this study is supplemented by the work of Funke *et al.* (2002b) who provide another high accuracy data set measured with the two-sinker densimeter. Details on the experimental setup are given by Kleinrahm and Wagner (1986), Händel *et al.* (1992), and Wagner and Kleinrahm (2004).

The region described by highly accurate $p\rho T$ data is extended to temperatures up to 520 K and pressures up to 30 MPa by the work of Claus *et al.* (2003) who used a single-sinker densimeter. The densimeter was developed by Bracht-

TABLE 11. Summary of the $p\rho T$ data sets that were assigned to group 1. Uncertainties are given where the original articles contain such estimates. Uncertainty values in parentheses were estimated by ourselves

Authors	Number of data		Temperature range/K	Pressure range/MPa	Total uncertainty in density
	Total	Selected			
Claus <i>et al.</i> (2003)	168	168	240–520	1–30	0.02%–0.03%
Funke <i>et al.</i> (2002a)	356	356	140–340	0.2–12	0.015%–0.022%
Funke <i>et al.</i> (2002b)	203	203	303–305	4.7–4.9	0.006%–0.016% ^a
Mansoorian <i>et al.</i> (1981)	91	91	323–473	0.04–5.4	0.033% (0.05%–0.2%)
Golovskii <i>et al.</i> (1978)	112	57	92–270	1.2–60	(0.25%)
Straty & Tsumura (1976b)	477	153	92–320	0.4–38	0.1%–0.2% ^b
Pal <i>et al.</i> (1976)	267	58	157–344	0.52–73	0.2% (0.4%)
Douslin & Harrison (1973)	298	58	248–623	1.2–41	0.03%–0.3%
Tsiklis <i>et al.</i> (1972)	75	75	323–673	200–900	(2%)
Beattie <i>et al.</i> (1939b)	82	20	323–548	6.1–36	(0.2%)

^aTotal uncertainty in pressure. These values also apply for the data reported by Funke *et al.* (2002a) in the temperature range from 298 to 318 K at densities between 120 and 280 kg m⁻³.

^bThese values apply for the selected data, not for the entire data set.

häuser *et al.* (1993) to extend the operating range of the buoyancy method by using a simpler setup without a significant loss of accuracy compared to the two-sinker method, see also Wagner *et al.* (1995) and Wagner and Kleinrahm (2004). The ethane used had a reported purity of 99.99%.

Mansoorian *et al.* (1981) performed measurements in the gas region at pressures reaching down to 0.04 MPa and temperatures from 323 to 473 K using the Burnett method. The purity of the sample is reported to be 99.99%. These data

were used to supplement the aforementioned data sets at low pressures. In this particular region, namely at pressures below 0.69 MPa, a shift of the null position of the differential pressure transducers was identified by the authors to be the dominating source of error leading to uncertainties of up to 0.17% in density at the lowest pressures. The data are consistent with the values reported by Funke *et al.* (2002a) to within 0.05%. At pressures below 0.2 MPa, where no other reliable data are available, we estimate the total uncertainty

TABLE 12. Summary of the $p\rho T$ data sets that were assigned to groups 2 and 3

Authors	Number of data	Temperature range/K	Pressure range/MPa	Group
Byun <i>et al.</i> (2000)	36	373–423	15–276	3
Lau <i>et al.</i> (1997)	46	240–350	1.1–34	3
Hou <i>et al.</i> (1996)	44	300–320	0.11–6.6	3
Guo <i>et al.</i> (1992)	18	273–293	1.3–3.7	2
Weber (1992)	11	320	0.34–4.3	2
Jaeschke & Humphreys (1990) ^a	222	260–360	0.10–27	2
Jaeschke & Humphreys (1990) ^b	121	280–348	0.22–26	2
Lau (1986)	56	240–350	1.1–34	3
Parrish (1984)	9	300–322	5.52–9.65	3
Young (1978)	52	250–300	0.49–1.6	2
Besserer & Robinson (1973)	68	311–394	0.69–10	3
Rodosevich & Miller (1973)	4	91–115	0.02	2
Pope (1972)	191	210–306	0.11–4.95	3
Chui & Canfield (1971)	2	116–161	0.0007–0.024	2
Khazanova & Sominskaya (1971)	87	299–318	0.49–7.4	3
Tomlinson (1971)	61	280–325	4.28–13.80	2
Jensen & Kurata (1969)	7	103–163	0.02–0.05	3
Wallace <i>et al.</i> (1964)	20	248–348	0.07–0.2	2
Michels <i>et al.</i> (1954)	101	273–423	1.6–22	2
Lambert <i>et al.</i> (1949)	5	293–353	0.1	3
Reamer <i>et al.</i> (1944)	183	311–511	0.1–69	3
Beattie <i>et al.</i> (1939a)	86	305	4.87–4.89	3
Michels & Nederbragt (1939)	12	273–323	1.0–6.0	3
Sage <i>et al.</i> (1937)	305	294–394	0.1–24	3
Beattie <i>et al.</i> (1935)	97	298–523	1.1–20	3
Burrell & Jones (1921)	87	288	0.1–3.1	3
Quint (1902)	71	286–326	3.2–3.7	3

^aValues obtained by measurement of the refractive index.

^bValues obtained using a Burnett apparatus.

in this region to be less than 0.2% in density.

Extensive measurements at temperatures up to 623 K and pressures up to 41 MPa have been performed by Douslin and Harrison (1973). The pycnometer-based method involves numerous sources of uncertainties and requires a complex assessment of the measured variables. Reported total uncertainties of the measured densities vary from 0.03% at low temperatures and pressures to 0.3% at the highest temperatures and pressures. The isotherms measured by Douslin and Harrison (1973) exhibit a steeper increase in density with pressure than those published by Claus *et al.* (2003). However, this systematic effect remains within the claimed uncertainties. We used the data of Douslin and Harrison (1973) above 520 K for the development of the new equation of state, deliberately accepting deviations from the data that could be traced back to the aforementioned inconsistencies.

The results of two earlier studies, by Beattie *et al.* (1939b) and Michels *et al.* (1954) show better agreement with the data of Claus *et al.* (2003) at high temperatures. Both studies were performed using piezometric setups. Maximum density deviations from the reference data of Claus *et al.* (2003) are 0.1%. Some of the data of Beattie *et al.* (1939b) have been used for the development of the new equation of state at temperatures above 498 K to complement the data of Douslin and Harrison (1973).

The liquid and the supercritical region, particularly at higher pressures, have been the subject of two more piezometric studies in the 1970s. The data measured by Golovskii *et al.* (1978) were published by Sychev *et al.* (1987). The authors used ethane with a reported purity of 99.99% and stated a total uncertainty of the density values of 0.01%. Considering both the measurement technique and the apparent scatter in the data, this estimate appears to be overly optimistic. The second group, Pal *et al.* (1976), estimated the total uncertainties of their $p\rho T$ data to be 0.2% in density, and reported a purity of the specimen of 99.95%. Both data sets generally agree with the high accuracy data sets to within 0.25% in density, with a few of the values reported by Pal *et al.* (1976) showing notably larger deviations. Data from both sets have been selected at pressures above 30 MPa to direct the shape of the $p\rho T$ surface at elevated pressures.

A slightly better consistency with the reference data is seen in the results reported by Straty and Tsumura (1976b), who used a Burnett apparatus to obtain density values. The data generally agree with the values reported by Funke *et al.* (2002a) to within 0.2%, except for the near-critical region. The ethane sample is stated to be 99.98% pure, total uncertainties of the density values are estimated to be 1% in the vicinity of the critical point and 0.1%–0.2% elsewhere. The values were not used in regions where data from the work of Funke *et al.* (2002a) are available, but they could be used at temperatures below 240 K to expand the reliably measured region towards higher and lower pressures.

At very high pressures, up to 900 MPa, and temperatures up to 673 K, Tsiklis *et al.* (1972) obtained density values using a high-pressure piezometer. In view of the extreme experimental conditions, the accuracy of the data may be

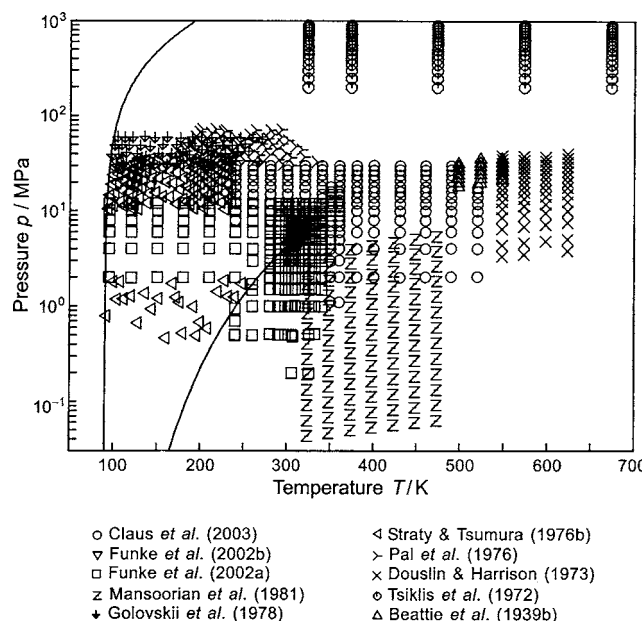


FIG. 5. Distribution of the experimental $p\rho T$ data used to develop the residual part of the equation of state, Eq. (4.1), in a p - T diagram.

considered as uncertain. However, the results provide important information on the thermal behavior of ethane in the high-pressure region.

In a p - T diagram, Fig. 5 shows the $p\rho T$ data that were used to establish the new equation of state. Although a number of additional studies are available, some of which provide very reliable data for the thermal properties, none of them were selected for the development of the new equation of state. In most cases, the range of parameters investigated lies completely within the region covered by high accuracy data.

3.1.2. Virial Coefficients

Table 13 summarizes the available data sets for the second and third virial coefficients of ethane. Except for the values calculated by Klimeck (2000) these virial coefficients only cover temperatures above 190 K. Values of the virial coefficients are usually established by isothermal fits to $p\rho T$ measurements. Consequently, such virial coefficients do not contain much new information which is not given by the genuine $p\rho T$ data. In any case, if one includes virial coefficients in the development of an equation of state, then only those values should be used that were derived from very accurate $p\rho T$ data. Therefore, only the B values of Funke *et al.* (2002a), which are based on the most accurate $p\rho T$ data and are given for temperatures from 240 to 340 K, were used to develop the new equation of state. For low temperatures from 71 to 200 K there are second virial coefficients calculated by Klimeck (2000) from a square-well potential given by Mason and Spurling (1969). These values were used in the development of the new equation of state in order

TABLE 13. Summary of the data sets for the second and third virial coefficients of ethane

Authors	Number of data		Temperature range/K
	B	C	
Funke <i>et al.</i> (2002a)	14 ^a	14	240–340
Klimeck (2000)	44 ^{a,b}	14	71–200
Estrada-Alexanders & Trusler (1997)	20	—	200–600
Hou <i>et al.</i> (1996)	2	2	300–320
Bell <i>et al.</i> (1992)	3	—	290–310
Kerl & Häusler (1984)	5	—	299–365
Holste <i>et al.</i> (1982)	1	1	300
Mansoorian <i>et al.</i> (1981)	7	7	323–473
Rigby <i>et al.</i> (1980)	4	—	273–323
Hahn <i>et al.</i> (1974)	4	—	199–251
Schäfer <i>et al.</i> (1974)	6	—	295–511
Douslin & Harrison (1973)	16	16	273–623
Pope (1972)	5	5	210–306
Stein <i>et al.</i> (1971)	10	—	286–493
Lichtenthaler & Schäfer (1969)	5	—	288–323
Hoover <i>et al.</i> (1968)	3	3	215–273
Huff & Reed (1963)	8	—	273–511
Gunn (1958)	8	—	273–510
Hamann & McManamey (1953)	14	—	303–423
Lambert <i>et al.</i> (1949)	5	—	291–351
Hirschfelder <i>et al.</i> (1942)	10	—	298–523
Eucken & Parts (1933)	15	—	192–273

^aThese values were considered in the development of the new equation of state.

^bSee Table 14.

to ensure reasonable plots of the virial coefficients at low temperatures. Since these data are not readily published, they are given in Table 14.

3.2. Speeds of Sound

Over the course of the last 2 decades, the importance of experimental data for the isentropic speed of sound in the development of equations of state has increased profoundly. The main reason is the development of highly precise measurement techniques, see Trusler (1991). Today, the highest accuracy is attained by spherical resonators. Especially in the low-density region, where fluid modes and resonator modes remain uncoupled, this method yields the same reliability as the most accurate density measurements. At higher densities the coupling between resonator and fluid modes gains impact on the resonance frequencies, leading to a significant loss of accuracy. For this reason, reliable measurements in high-density regions, especially in the liquid phase, are not feasible with this technique.

Estrada-Alexanders and Trusler (1997) established the most comprehensive and most accurate data set available for the speed of sound in gaseous ethane using a spherical resonator. The measurements were conducted on 99.99% pure ethane along isotherms between 220 and 450 K. The highest density on each isotherm corresponds to approximately $0.8\rho_c$ at subcritical temperatures and to $0.5\rho_c$ at supercritical temperatures to ensure that coupling effects between resona-

TABLE 14. Data for the second virial coefficients B calculated by Klimeck (2000) from a square-well potential

T/K	$B/(cm^3 mol^{-1})$	T/K	$B/(cm^3 mol^{-1})$
71	-5956.62	137	-942.48
74	-5160.99	140	-897.02
77	-4517.31	143	-855.02
80	-3989.65	146	-816.14
83	-3551.94	149	-780.05
86	-3184.96	152	-746.48
89	-2874.30	155	-715.20
92	-2608.98	158	-685.99
95	-2380.56	161	-658.66
98	-2182.48	164	-633.04
101	-2009.54	167	-608.99
104	-1857.61	170	-586.38
107	-1723.38	173	-565.09
110	-1604.16	176	-545.01
113	-1497.75	179	-526.04
116	-1402.33	182	-508.10
119	-1316.42	185	-491.12
122	-1238.76	188	-475.02
125	-1168.29	191	-459.73
128	-1104.13	194	-445.21
131	-1045.52	197	-431.39
134	-991.82	200	-418.23

tor and fluid modes remain negligible. All data from this study were considered in the development of the equation of state presented here.

Trusler and Costa Gomes (1996) used a similar setup to conduct measurements for the Groupe Européen de Recherches Gazières. The estimated total uncertainties of the speed of sound values are given as 0.025%. Nevertheless, their results are approximately 0.02% lower than the values reported by Estrada-Alexanders and Trusler (1997). At 300 K, these discrepancies reach up to -0.06%, which is clearly beyond the combined estimated uncertainties. On the 350 K isotherm, values have been measured at pressures to 20 MPa, with the density being more than $1.6\rho_c$. These values are subject to a substantially larger uncertainty. We assume they are accurate to within 0.15% and included them in the development of the new equation of state since they give important information on the crossover from low-density to high-density speeds of sound at supercritical states.

The results of two more measurement runs with spherical resonators are available. The values reported by Boyes (1992) are in excellent agreement with the data reported by Estrada-Alexanders and Trusler (1997). Differences are less than 0.005% except for the 300 K isotherm, where deviations of up to +0.025% can be observed. The data published by Lemming (1989) are generally consistent with the results of the other authors to within 0.02%. At 350 K, however, the speeds of sound reported by Lemming (1989) are about +0.035% higher than the values obtained by Estrada-Alexanders and Trusler (1997).

With the exception of a few values, all available data sets that were obtained with spherical resonators are mutually consistent within 0.05% in speed of sound, which confirms the remarkable quality of the data.

TABLE 15. Summary of the data sets for the speed of sound that were assigned to group 1. Uncertainties are given where the original articles contain such estimates. Uncertainty values in parentheses were estimated by ourselves

Authors	Number of data		Temperature range/K	Pressure range/MPa	Total uncertainty in speed of sound
	Total	Selected			
Estrada-Alexanders & Trusler (1997)	186	186	220–450	0.01–10	0.01% (up to 0.05%)
Trusler & Costa Gomez (1996)	52	7	250–350	0.03–19.60	0.025% (0.15%)
Boyes (1992)	71	51	210–360	0.02–1	(0.02% up to 0.05%)
Lemming (1989)	163	127	223–351	0.02–0.6	0.007 (up to 0.05%)
Tsumura & Straty (1977)	154	154	100–323	3.56–36.83	0.06%–0.1% ^a

^aClose to the critical point the uncertainties are expected to be higher than these estimates.

The most important set of calorific data for ethane at higher densities was published by Tsumura and Straty (1977). The authors obtained values for the speed of sound by the pulse-echo method in large parts of the liquid and supercritical regions. The ethane sample is stated to be 99.98% pure, and the authors report their experimental uncertainties of the different variables to be 0.01% in pressure, 0.05 K in temperature, and 0.06%–0.1% in speed of sound, with the highest uncertainties occurring in the proximity of the critical point. From this, the total uncertainties in the speeds of sound can be estimated to be 0.06%–0.1% except for the near-critical region, where higher uncertainties are expected.

Table 15 gives details on the data sets that were selected for the development of the new equation of state. These data are also shown in a *p*-*T* diagram in Fig. 6. The data sets that were assigned to groups 2 and 3 are compiled in Table 16.

3.3. Isochoric Heat Capacities

Four of the total of five experimental studies that are available for the isochoric heat capacity of ethane investigated the near-critical region or the critical isochore. Berestov *et al.* (1973) investigated the influence of gravity on the isochoric

heat capacity of pure fluids in the vicinity of the critical point. The calorimetric measurements were performed to verify predictions from scaled equations of state. The authors do not give any details on the purity of the ethane sample or on the numerical value of the density investigated. The isochore on which the measurements were conducted is referred to as “critical.” Plotting the absolute values against temperature reveals good consistency to reliable measurements performed by Haase and Tillmann (1994), see Sec. 5.3.2. All of the data reported by Berestov *et al.* (1973) were obtained within $|T - T_c| < 0.15$ K. Due to its functional form (see the statement at the end of Sec. 4.2.1), the new equation of state cannot reproduce the steep increase in isochoric heat capacity that is observed in this immediate vicinity of the critical point. Only the three values at the greatest distance from the critical temperature were included in the development of the new equation of state. Since the authors do not give a density value, we chose the critical density used in this work, $\rho = 206.18 \text{ kg m}^{-3}$. Moreover, we did not use the absolute values of temperature as given by Berestov *et al.* (1973), but rather the distance from the critical temperature, $\Delta T = T_{\text{Berestov}} - T_{\text{c,Berestov}}$, and calculated new values $T = T_{\text{c,work}} + \Delta T$ with $T_{\text{c,work}} = 305.322$ K. In this way, we transformed the data to suit the critical parameters chosen in this work.

Haase and Tillman (1994), Shmakov (1973), and Abdulagatov *et al.* (1996) investigated near-critical isochores taking a more general approach. The estimated uncertainties reported by Abdulagatov *et al.* (1996) appear too optimistic. Their experimental heat capacities are 20%–25% higher than those reported by the other authors. The data measured by Haase and Tillmann (1994) and by Shmakov (1973) are mutually consistent. Unfortunately, the authors do not give estimates of the experimental uncertainties. The data reported by Haase and Tillman (1994) were used to establish the new equation of state.

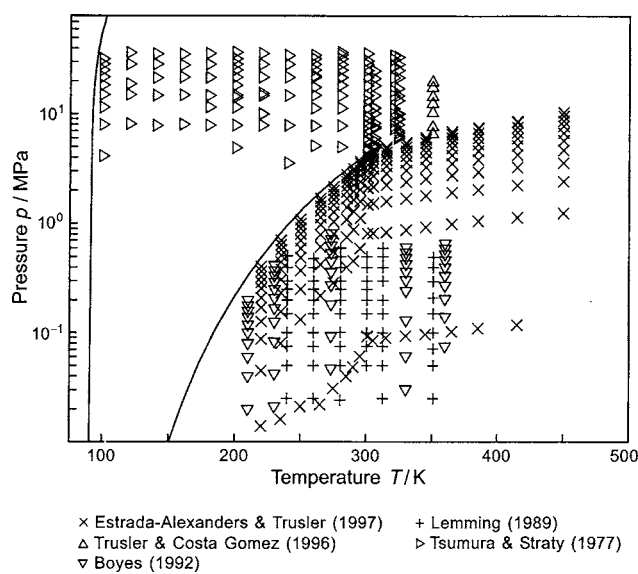


Fig. 6. Distribution of the experimental data for the speed of sound used to develop the residual part of the equation of state, Eq. (4.1), in a *p*-*T* diagram.

TABLE 16. Summary of the data sets for the speed of sound that were assigned to groups 2 and 3

Authors	Number of data	Temperature range/K	Pressure range/MPa	Group
Terres <i>et al.</i> (1957)	99	292–448	0.00–11.77	3
Nouri (1952)	89	304–306	1.18–14.42	2

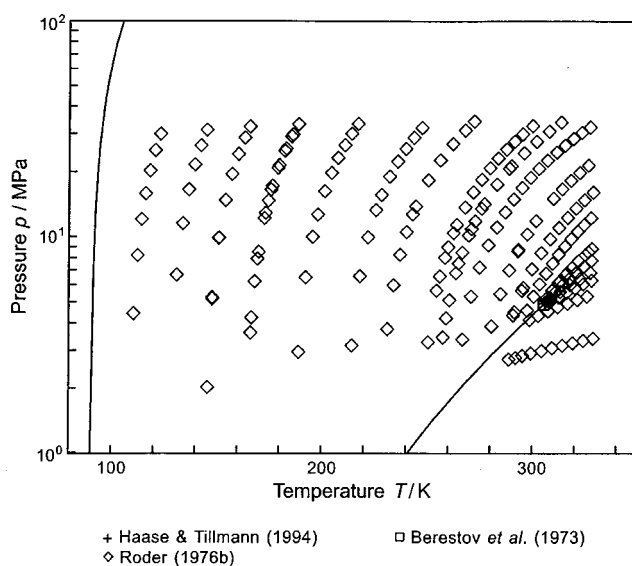


FIG. 7. Distribution of the experimental data for the isochoric heat capacity used to develop the residual part of the equation of state, Eq. (4.1), in a p - T diagram.

Data for the isochoric heat capacity in the remaining fluid regions are of greater importance for the development of a wide-range equation as presented in this work. Such measurements were performed extensively by Roder (1976b). The reported uncertainties in c_v are 0.5%–5% excluding possible systematic errors. The data give important information on the temperature derivative of the Helmholtz energy. The selected data are shown in a p - T diagram in Fig. 7, while details on the available data sets are summarized in Tables 17 and 18.

3.4. Isobaric Heat Capacities

This section is divided into two parts. The first part presents values obtained for the isobaric heat capacity of the real fluid. Just like the other properties discussed in this chapter, these isobaric heat capacities were obtained by measurements. The second section is concerned with the data situation for the isobaric heat capacity of ethane in the ideal-gas state. These data were established either via theoretical approaches or by extrapolating real fluid data to the ideal-gas

TABLE 18. Summary of the data sets for the isochoric heat capacity that were assigned to groups 2 and 3

Authors	Number of data	Temperature range/K	Density range/(kg m ⁻³)	Group
Abdulagatov <i>et al.</i> (1996)	100	305–376	203	2–3

state and were used in this work to set up the equation for the Helmholtz energy of the ideal gas given in Sec. 4.1.

3.4.1. Experimental Results for the Real Fluid

Most of the nine data sets available for the isobaric heat capacity of real fluid ethane are of poor quality. Kistiakowski and Rice (1939) obtained their data by adiabatic expansion of the gas sample, the other data sets were established by flow calorimetry. The data are of little importance for the development of the new equation of state because the thermodynamic behavior of the fluid is essentially defined by the highly accurate $p\rho T$ and speed of sound data.

The mostly supercritical data published by Ernst and Hochberg (1989) and the data obtained in the gas region by Bender (1982) complement each other. The values measured by Bier *et al.* (1976b) are consistent with the data by Bender (1982) but they reveal systematic deviations from the more recent data by Ernst and Hochberg (1989) at higher temperatures and pressures. We assume the newer data to be more reliable and hence used the values reported by Ernst and Hochberg (1989) and by Bender (1982) to establish the new equation of state. A p - T plot of the selected data is shown in Fig. 8, details on the data sets are presented in Table 19. The data sets that were assigned to groups 2 and 3 are summarized in Table 20.

The isobaric heat capacities reported by Lammers *et al.* (1978) and van Kasteren and Zeldenerust (1979) appear to be inconsistent with reliable data of other properties. In the course of the development of the equation of state presented here, preliminary equations were set up to check the consistency of the different data sets. All preliminary equations that could represent the values of the isochoric heat capacity reported by Roder (1976b) and the speed of sound data published by Tsumura and Straty (1977) within their experimental uncertainties predicted lower isobaric heat capacities than

TABLE 17. Summary of the data sets for the isochoric heat capacity that were assigned to group 1. Uncertainties are given where the original articles contain such estimates. Uncertainty values in parentheses were estimated by ourselves

Authors	Number of data		Temperature range/K	Density range/(kg m ⁻³)	Total uncertainty in isochoric heat capacity
	Total	Selected			
Haase & Tillmann (1994)	11	11	305–317	202	(5%)
Roder (1976b)	209	209	110–329	48–610	2%–5%
Berestov <i>et al.</i> (1973)	24	3	305–306	— ^a	1.5% (5%)
Shmakov (1973)	158	— ^b	295–315	205	— ^b

^aThe density is denoted as “critical” in the article. We therefore assigned the critical density used in this work, $\rho = 206.18 \text{ kg m}^{-3}$.

^bThe data were not available when the new equation of state was developed. No estimates for the experimental uncertainties could be drawn from the original article.

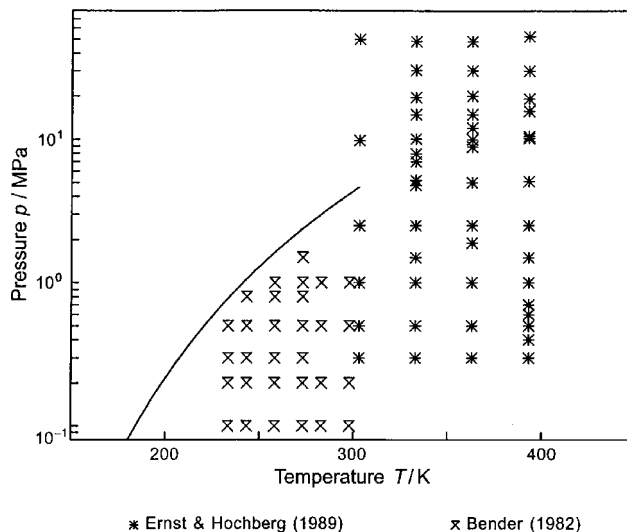


FIG. 8. Distribution of the experimental data for the isobaric heat capacity used to develop the residual part of the equation of state, Eq. (4.1), in a p - T diagram.

the values obtained by Lammers *et al.* (1978) and van Kasteren and Zeldernrust (1979). The data of Furtado (1973) exhibit large scatter and substantial deviations from the more reliable values reported by other authors. Roder (1976b) already noted these inconsistencies that amount up to 10% in c_p in some cases. The values reported by Miyazaki *et al.* (1980) were obtained by interpretation of their enthalpy measurements, see Sec. 3.5. Friend *et al.* (1991) have already discussed the large errors attributed to these data.

3.4.2. Results for the Ideal-Gas State

Two methods are widely used to establish data for the ideal-gas isobaric heat capacity. The first method uses experimental data for caloric properties extrapolated to the limit of zero density. Major sources of uncertainties are the measurements themselves and the extrapolation of real fluid data to zero pressure to get the ideal-gas values. The temperature range where such data are available is restricted to the operating range of the corresponding experimental set-ups. Today, the most reliable of such data are extrapolated from measurements of the speed of sound taken with spherical resonators. Three data sets are available that have been established in this way. Estrada-Alexanders and Trusler (1997) obtained ideal-gas values consistent with their highly accurate data for the speed of sound (see Sec. 3.2), by extrapolating their experimental results. These values were used to establish the equation for the Helmholtz energy of

the ideal gas presented in Sec. 4.1. The reported uncertainties of the c_p data are less than 0.05%. The data also agree well with values reported by Boyes (1992), although the uncertainties in c_p of 0.002%, estimated by Boyes, are certainly too optimistic. The values measured by Esper *et al.* (1995) systematically deviate from the aforementioned data by up to 0.4% and were not selected.

The second method to determine the heat capacity of ideal gases uses theoretical approaches that depend on molecular constants measured by spectroscopy. Such property models usually consider contributions from molecular translation, rotation, and vibration. For more complex polyatomic molecules, such as ethane, internal rotation has to be considered as well. In some cases, excited electronic states may become relevant at very high temperatures. For higher accuracy, especially at elevated temperatures, interactions between different energetic modes will have to be considered. Although the inclusion of such anharmonicity corrections is state-of-the-art for many simple molecules, none of the seven data sets available for ethane accounts for these effects. While the four earlier studies may be considered as obsolete, the more recent works by Gurvich *et al.* (1991), Pamidimukkala *et al.* (1982), and Chao *et al.* (1973) differ mainly with respect to the consideration of internal rotation. We selected the values reported by Gurvich *et al.* (1991) for the development of the equation for the ideal-gas Helmholtz energy. The c_p data are consistent with the results of Estrada-Alexanders and Trusler (1997) within 0.05%. Information on the data sets published for the ideal-gas heat capacity of ethane is reported in Table 21.

3.5. Enthalpy Differences and Throttling Coefficients

Three reports containing experimental values for enthalpy differences of ethane and four studies of the Joule–Thomson coefficient, $\mu = (\partial T / \partial p)_h$, are available. Miyazaki *et al.* (1980) gave additional results for the isothermal throttling coefficient $\delta_T = (\partial h / \partial p)_T$. The data sets are summarized in Table 22. Although none of the data were included in the development of the equation of state presented here, most of them are used for comparisons.

The enthalpy differences measured by Miyazaki *et al.* (1980) show large deviations from the predictions of all reliable equations of state available in the literature. None of the preliminary equations developed in the course of this work was able to give a reasonable representation of the data. Friend *et al.* (1991) encountered similar problems with values for the isobaric heat capacity that Miyazaki *et al.*

TABLE 19. Summary of the data sets for the isobaric heat capacity that were assigned to group 1. Uncertainties are given as estimated by the authors

Authors	Number of data		Temperature range/K	Pressure range/MPa	Total uncertainty in isobaric heat capacity
	Total	Selected			
Ernst & Hochberg (1989)	52	52	303–393	0.3–53	0.2%–1.2%
Bender (1982)	36	36	233–298	0.1–1.5	0.1%–0.15%

TABLE 20. Summary of the data sets for the isobaric heat capacity that were assigned to groups 2 and 3

Authors	Number of data	Temperature range/K	Pressure range/MPa	Group
Miyazaki <i>et al.</i> (1980)	30	298–323	4.47–13.00	3
van Kasteren & Zeldenerst (1979)	30	110–270	3.20–5.07	3
Lammers <i>et al.</i> (1978)	14	120–240	3.20–5.70	3
Bier <i>et al.</i> (1976b)	121	283–473	0.10–10.00	2
Furtado (1973)	299	100–378	1.38–12.07	3
Dailey & Felsing (1943)	7	347–603	0.10	3
Kistiakowski & Rice (1939)	4	272–365	0.10	2

(1980) deduced from their enthalpy measurements. We therefore decided to disregard these values.

The enthalpy differences published by Grini (1994) and Grini *et al.* (1996) are in better agreement with the selected data. Nevertheless, the stated standard deviation of 0.21% is not quite comprehensible, and systematic deviations of 0.5%–1% from enthalpy differences calculated from preliminary equations were evident throughout the development of the new equation of state.

The measurements of the Joule–Thomson coefficient performed by Bender (1982) and Bier *et al.* (1976b) were carried out with the same equipment as the corresponding measurements of the isobaric heat capacities (see Sec. 3.4.1). The earliest experimental values for Joule–Thomson coefficients were reported by Sage *et al.* (1937). They deviate from the results of Bier *et al.* (1976b) by up to 20%. No further consideration was given to these data.

4. The New Equation of State

The equation of state for ethane presented here is a fundamental equation explicit in the Helmholtz energy a as a function

of density ρ and temperature T . This equation is expressed in dimensionless form, $\alpha=a/(RT)$, and is separated into two parts, an ideal-gas part, α^o , and a residual part, α^r , that accounts for intermolecular forces, so that

$$\frac{\alpha(\rho, T)}{RT} = \alpha(\delta, \tau) = \alpha^o(\delta, \tau) + \alpha^r(\delta, \tau), \quad (4.1)$$

where $\delta=\rho/\rho_c$ is the reduced density and $\tau=T_c/T$ is the inverse reduced temperature with the critical density $\rho_c=206.18 \text{ kg m}^{-3}$ and the critical temperature $T_c=305.322 \text{ K}$; $R=0.276\,512\,72 \text{ kJ kg}^{-1} \text{ K}^{-1}$ is the specific gas constant of ethane. The ideal-gas part α^o and the residual part α^r of the dimensionless Helmholtz energy α are given by Eqs. (4.6) and (4.8).

Since Eq. (4.1) is an equation of state in the form of a fundamental equation, all thermodynamic properties can be calculated using combinations of α^o and α^r and their derivatives. These relations are given in Table 23 for the thermodynamic properties considered in this paper. At a given temperature, the vapor pressure and the orthobaric liquid and vapor densities can be obtained by simultaneously solving the phase-equilibrium conditions

TABLE 21. Summary of the data sets for the isobaric heat capacity in the ideal-gas state. Uncertainties are given where the original articles contain such estimates

Authors	Number of data	Temperature range/K	Total uncertainty	Measured property
Data calculated from models based on spectroscopic data				
Gurvich <i>et al.</i> (1991)	61 ^a	100–6000	—	—
Pamidimukkala <i>et al.</i> (1982)	32	0–3000	0.025%–0.3%	—
Chao <i>et al.</i> (1973)	42	0–1500	—	—
Schäfer & Auer (1961)	25	100–1500	—	—
Rossini <i>et al.</i> (1953)	15	100–1500	—	—
Dailey & Felsing (1943)	7	348–603	1%	—
Thompson (1941)	10	291–1000	—	—
Data extrapolated from experimental results				
Estrada-Alexanders & Trusler (1997)	17 ^a	220–450	0.05%	w
Esper <i>et al.</i> (1995)	16	223–351	0.1%–0.2%	w
Boyes (1992)	14	210–360	0.002%	w
Ernst & Hochberg (1989)	4	303–393	0.2%	c_p
Bender (1982)	5	233–283	0.2%	c_p
Bier <i>et al.</i> (1976a)	9	283–473	0.2%	c_p
Kistiakowsky & Rice (1939)	4	272–365	0.3%	c_p
Eucken & Parts (1933)	6	189–292	0.5%–1%	c_p
Heuse (1919)	3	191–288	—	c_p

^aThese data were used to fit the correlation equation for the ideal-gas heat capacity, Eq. (4.5).

TABLE 22. Summary of the data sets for the enthalpy h , the Joule–Thomson coefficient μ , and the isothermal throttling coefficient δ_T

Authors	Number of data			Temperature range/K	Pressure range/MPa	Group
	h	μ	δ_T			
Grini <i>et al.</i> (1996)	60	—	—	154–267	1.16–5.10	2
Grini (1994)	22 ^a	—	—	156–256	0.84–4.07	2
Bender (1982)	—	27	—	233–298	0.30–1.50	2
Miyazaki <i>et al.</i> (1980)	104	6	27	283–326	3.44–6.75	2–3
Bier <i>et al.</i> (1976b)	—	66	—	298–473	0.30–10.0	2
Sage <i>et al.</i> (1937)	—	41	—	294–377	0.10–4.20	3

^aContains also 60 of the values published by Grini *et al.* (1996).

$$\frac{p_s}{RT} = \rho' (1 + \delta' \alpha_{\delta}^r(\delta', \tau)), \quad (4.2a)$$

$$\frac{p_s}{RT} = \rho'' (1 + \delta'' \alpha_{\delta}^r(\delta'', \tau)), \quad (4.2b)$$

$$\frac{p_s}{RT} \left(\frac{1}{\rho''} - \frac{1}{\rho'} \right) - \ln \left(\frac{\rho'}{\rho''} \right) = \alpha^r(\delta', \tau) - \alpha^r(\delta'', \tau). \quad (4.2c)$$

4.1. The Equation for the Helmholtz Energy of the Ideal Gas

The Helmholtz energy of the ideal gas is given by

$$a^\circ(\rho, T) = h^\circ(T) - RT - Ts^\circ(\rho, T). \quad (4.3)$$

The enthalpy $h^\circ(T)$ and the entropy $s^\circ(\rho, T)$ of the ideal gas

TABLE 23. Relations of thermodynamic properties to the ideal-gas part α° , Eq. (4.6), and the residual part α^r , Eq. (4.8), of the dimensionless Helmholtz energy and their derivatives^{a,b}

Property	Relation
Pressure $p = \rho^2 (\partial a / \partial \rho)_T$	$\frac{p(\delta, \tau)}{\rho RT} = 1 + \delta \alpha_{\delta}^r$
Entropy $s = -(\partial a / \partial T)_v$	$\frac{s(\delta, \tau)}{R} = \tau(\alpha_{\tau}^\circ + \alpha_{\tau}^r) - \alpha^\circ - \alpha^r$
Internal energy $u = a + Ts$	$\frac{u(\delta, \tau)}{RT} = \tau(\alpha_{\tau}^\circ + \alpha_{\tau}^r)$
Enthalpy $h = u + pv$	$\frac{h(\delta, \tau)}{RT} = 1 + \tau(\alpha_{\tau}^\circ + \alpha_{\tau}^r) + \delta \alpha_{\delta}^r$
Gibbs free energy $g = h - Ts$	$\frac{g(\delta, \tau)}{RT} = 1 + \alpha^\circ + \alpha^r + \delta \alpha_{\delta}^r$
Isochoric heat capacity $c_v = (\partial u / \partial T)_v$	$\frac{c_v(\delta, \tau)}{R} = -\tau^2(\alpha_{\tau\tau}^\circ + \alpha_{\tau\tau}^r)$
Isobaric heat capacity $c_p = (\partial h / \partial T)_p$	$\frac{c_p(\delta, \tau)}{R} = -\tau^2(\alpha_{\tau\tau}^\circ + \alpha_{\tau\tau}^r) + \frac{(1 + \delta \alpha_{\delta}^r - \delta \tau \alpha_{\delta\tau}^r)^2}{1 + 2 \delta \alpha_{\delta}^r + \delta^2 \alpha_{\delta\delta}^r}$
Saturated-liquid heat capacity $c_\sigma(T) = (\partial h / \partial T)_p + T(\partial p / \partial T)_v \cdot (dp_s / dT) / (-\rho^2(\partial p / \partial \rho)_T _{\rho=\rho_s})$	$\frac{c_\sigma(\tau)}{R} = -\tau^2(\alpha_{\tau\tau}^\circ + \alpha_{\tau\tau}^r) + \frac{1 + \delta' \alpha_{\delta}^r - \delta' \tau \alpha_{\delta\tau}^r}{1 + 2 \delta' \alpha_{\delta}^r + \delta'^2 \alpha_{\delta\delta}^r} \cdot \left[(1 + \delta' \alpha_{\delta}^r - \delta' \tau \alpha_{\delta\tau}^r) - \frac{1}{\rho_c R \delta'} \frac{dp_s}{dT} \right]^c$
Speed of sound $w = (\partial p / \partial \rho)_s^{1/2}$	$\frac{w^2(\delta, \tau)}{RT} = 1 + 2 \delta \alpha_{\delta}^r + \delta^2 \alpha_{\delta\delta}^r - \frac{(1 + \delta \alpha_{\delta}^r - \delta \tau \alpha_{\delta\tau}^r)^2}{\tau^2(\alpha_{\tau\tau}^\circ + \alpha_{\tau\tau}^r)}$
Joule–Thomson coefficient $\mu = (\partial T / \partial p)_h$	$\mu_T(\delta, \tau) R \rho = \frac{-(\delta \alpha_{\delta}^r + \delta^2 \alpha_{\delta\delta}^r + \delta \tau \alpha_{\delta\tau}^r)}{(1 + \delta \alpha_{\delta}^r - \delta \tau \alpha_{\delta\tau}^r)^2 - \tau^2(\alpha_{\tau\tau}^\circ + \alpha_{\tau\tau}^r)(1 + 2 \delta \alpha_{\delta}^r + \delta^2 \alpha_{\delta\delta}^r)}$
Isothermal throttling coefficient $\delta_T = (\partial h / \partial p)_T$	$\delta_T(\delta, \tau) \rho = 1 - \frac{1 + \delta \alpha_{\delta}^r - \delta \tau \alpha_{\delta\tau}^r}{1 + 2 \delta \alpha_{\delta}^r + \delta^2 \alpha_{\delta\delta}^r}$
Second virial coefficient $B(T) = \lim_{\rho \rightarrow 0} (\partial Z / \partial \rho)_T$	$B(\tau) \rho_c = \lim_{\delta \rightarrow 0} \alpha_{\delta}^r(\delta, \tau)$
Third virial coefficient $C(T) = \lim_{\rho \rightarrow 0} \left[\frac{1}{2} (\partial^2 Z / \partial \rho^2)_T \right]$	$C(\tau) \rho_c^2 = \lim_{\delta \rightarrow 0} \alpha_{\delta\delta}^r(\delta, \tau)$

^a $\alpha_{\delta}^r = [\partial \alpha^r / \partial \delta]_\tau, \alpha_{\delta\delta}^r = [\partial^2 \alpha^r / \partial \delta^2]_\tau, \alpha_{\tau}^r = [\partial \alpha^r / \partial \tau]_\delta, \alpha_{\tau\tau}^r = [\partial^2 \alpha^r / \partial \tau^2]_\delta, \alpha_{\delta\tau}^r = [\partial^2 \alpha^r / \partial \delta \partial \tau], \alpha_{\tau\delta}^r = [\partial^2 \alpha^r / \partial \tau \partial \delta], \alpha_{\tau}^\circ = [\partial \alpha^\circ / \partial \tau]_\delta, \alpha_{\tau\tau}^\circ = [\partial^2 \alpha^\circ / \partial \tau^2]_\delta.$

^bFor the specific gas constant R see Eq. (4.1).

^c $dp_s/dT = [\rho'' \cdot \rho' / (\rho'' - \rho')] R [\ln(\rho''/\rho') + \alpha^r(\tau, \delta'') - \alpha^r(\tau, \delta') - \tau(\alpha_{\tau}^r(\tau, \delta'') - \alpha_{\tau}^r(\tau, \delta'))].$

TABLE 24. Coefficients for the correlation equations for the ideal-gas isobaric heat capacity and the ideal-gas part of the Helmholtz energy, Eqs. (4.5) and (4.6)

i	n_i°	θ_i°
1	9.212 802 589	—
2	-4.682 248 550	—
3	3.003 039 265	—
4	1.117 433 359	1.409 105 2332
5	3.467 773 215	4.009 917 0712
6	6.941 944 640	6.596 709 8342
7	5.970 850 948	13.979 810 2659

can be derived from an equation for the ideal-gas isobaric heat capacity $c_p^\circ(T)$. Replacing h° and s° in Eq. (4.3) by the appropriate expressions yields

$$\begin{aligned} a^\circ(\rho, T) = & \int_{T_0}^T c_p^\circ dT + h_0^\circ - RT - T \\ & \times \left[\int_{T_0}^T \frac{c_p^\circ - R}{T} dT - R \ln\left(\frac{\rho}{\rho_0}\right) + s_0^\circ \right], \quad (4.4) \end{aligned}$$

where all variables with the index “0” refer to an arbitrary reference state. Often the enthalpy and the entropy are set to zero at $T_0=298.15$ K and $p_0=0.101\,325$ MPa. The corresponding ideal-gas density is given by $\rho_0=p_0/(RT_0)$.

The data sets published by Estrada-Alexanders and Trusler (1997) and Gurvich *et al.* (1991) were used to fit the following correlation equation for $c_p^\circ(T)$:

$$\frac{c_p^\circ(T)}{R} = 1 + n_3^\circ + \sum_{i=4}^7 n_i^\circ (\theta_i^\circ \tau)^2 \frac{\exp(-\theta_i^\circ \tau)}{[\exp(-\theta_i^\circ \tau) - 1]^2}. \quad (4.5)$$

With the coefficients given in Table 24, Eq. (4.5) reproduces all of the input data within their mutual consistency, which is 0.05%. At temperatures from 700 to 6000 K, the data by Gurvich *et al.* (1991) are represented with deviations of less than 0.01%.

The expression for the Helmholtz energy of the ideal gas can be derived by inserting Eq. (4.5) into Eq. (4.4) and carrying out the integration

$$\begin{aligned} a^\circ = & \ln(\delta) + n_1^\circ + n_2^\circ \tau + n_3^\circ \ln(\tau) \\ & + \sum_{i=4}^7 n_i^\circ \ln[1 - \exp(-\theta_i^\circ \tau)], \quad (4.6) \end{aligned}$$

for the definition of δ and τ see Eq. (4.1). The coefficients n_i° and θ_i° are given in Table 24. The integration constants n_1 and n_2 were chosen to give zero for the ideal-gas enthalpy at $T_0=298.15$ K and the ideal-gas entropy at $T_0=298.15$ K and $p_0=0.101\,325$ MPa. Table 25 compiles the derivatives of the ideal-gas part a° required for the calculation of thermodynamic properties.

TABLE 25. The ideal-gas part a° , Eq. (4.6), of the dimensionless Helmholtz free energy and its derivatives^a

$a^\circ = \ln \delta + n_1^\circ + n_2^\circ \tau + n_3^\circ \ln \tau + \sum_{i=4}^7 n_i^\circ \ln(1 - e^{-\theta_i^\circ \tau})$
$\alpha_\delta^\circ = 1/\delta + 0 + 0 + 0 + 0$
$\alpha_{\delta\delta}^\circ = -1/\delta^2 + 0 + 0 + 0 + 0$
$\alpha_\tau^\circ = 0 + 0 + n_2^\circ + n_3^\circ / \tau + \sum_{i=4}^7 n_i^\circ \theta_i^\circ [(1 - e^{-\theta_i^\circ \tau})^{-1} - 1]$
$\alpha_{\tau\tau}^\circ = 0 + 0 + 0 - n_3^\circ / \tau^2 - \sum_{i=4}^7 n_i^\circ (\theta_i^\circ)^2 e^{-\theta_i^\circ \tau} (1 - e^{-\theta_i^\circ \tau})^{-2}$
$\alpha_{\delta\tau}^\circ = 0 + 0 + 0 + 0 + 0$
$\alpha_\delta^\circ = [\partial a^\circ / \partial \delta]_\tau, \alpha_{\delta\delta}^\circ = [\partial^2 a^\circ / \partial \delta^2]_\tau, \alpha_\tau^\circ = [\partial a^\circ / \partial \tau]_\delta, \alpha_{\tau\tau}^\circ = [\partial^2 a^\circ / \partial \tau^2]_\delta,$
$\alpha_{\delta\tau}^\circ = [\partial^2 a^\circ / \partial \delta \partial \tau]_\delta.$

4.2. The Equation for the Residual Part of the Helmholtz Energy

Unlike the ideal-gas part of the Helmholtz energy, no physically founded models are available that accurately describe the thermodynamic behavior of real fluids over a wide range of parameters. Therefore, an empirical description of the residual Helmholtz energy was developed in this work. State-of-the-art procedures were used to establish the mathematical structure of the correlation equation and to adjust the coefficients. Although certain demands on the functional form as formulated by Span and Wagner (1997) were considered, the terms in the equation are basically empirical.

4.2.1. Fitting Procedures

The coefficients of the equation were determined in a least-squares fit. Therefore, a weighting factor was calculated for each data point using the experimental total uncertainties as stated by the authors. Where only individual uncertainties are given for the different variables, total uncertainties were calculated according to the Gaussian error propagation formula. Where no uncertainties are available or in the case of artificial data points that were used to ensure physically reasonable results, we estimated the uncertainties by thoroughly analyzing the data. The partial derivatives needed for the application of the error propagation formula were calculated from preliminary equations. In some instances, the calculated weights were modified by arbitrary multiplicative factors to increase or reduce the influence of a particular data set on the overall representation of the surface. In this way, the disproportionate influence of single data sets that were assigned overly optimistic uncertainties by the authors could be avoided.

We used a modified adaptation of the well known algorithm by Setzmann and Wagner (1989) to optimize preliminary functional forms for the residual part. Since only linear residua are supported in this algorithm, nonlinear data such as speeds of sound can only be used if they are linearized by appropriate methods, see, e.g., Setzmann and Wagner (1991) and Wagner and Prüß (2002). To improve the representation of the available highly accurate data for the speed of sound,

the final functional form was developed by means of a nonlinear regression analysis developed by Tegeler *et al.* (1997). This algorithm combines linear and nonlinear procedures and enables a direct consideration of both linear and nonlinear data in the development of the functional form. The residuals used in the linear and nonlinear algorithms correspond to common formulations recently explained by Span (2000).

The bank of terms that built the basis for the development of the new equation of state

$$\begin{aligned} \alpha^r = & \sum_{i=1}^4 \sum_{j=0}^{16} n_{ij} \delta^i \tau^{j/4} + \exp(-\delta) \sum_{i=1}^{10} \sum_{j=2}^{20} n_{ij} \delta^i \tau^{j/4} \\ & + \exp(-\delta^2) \sum_{i=2}^{10} \sum_{j=1}^{20} n_{ij} \delta^i \tau^{j/2} \\ & + \exp(-\delta^3) \sum_{i=2}^{14} \sum_{j=5}^{20} n_{ij} \delta^i \tau^j \\ & + \exp(-\delta^4) \sum_{i=2}^{10} \sum_{j=10}^{30} n_{ij} \delta^i \tau^j + \sum_{i=1}^{72} n_i \delta^{d_i} \tau^{t_i} \\ & \times \exp[-\eta_i(\delta - \varepsilon_i)^2 - \beta_i(\tau - \gamma_i)^2], \quad (4.7) \end{aligned}$$

comprises a total of 907 terms, including 68 simple polynomial terms, 767 polynomials combined with exponential functions, and 72 modified Gaussian bell-shaped terms as introduced by Setzmann and Wagner (1991) to improve the representation of data in the critical region. The parameters of these Gaussian terms covered the ranges $1 \leq d_i \leq 3$, $0 \leq t_i \leq 3$, $15 \leq \eta_i \leq 25$, $150 \leq \beta_i \leq 400$, $\varepsilon_i = 1$, and $1.05 \leq \gamma_i \leq 1.25$. The density and temperature exponents of the remaining terms in Eq. (4.7) were chosen according to recommendations given by Span and Wagner (1997) to ensure reliable extrapolation behavior of the equation. Equation (4.7) does not contain nonanalytical terms as applied by Span and Wagner (1996) to CO₂ and by Wagner and Prüß (2002) to H₂O. Due to the absence of really good caloric data in the near critical region, we felt that the additional computations and complexity required by these terms were not justified for the new equation of state for ethane.

4.2.2. Selected Database

The experimental data that were selected to establish the new equation of state have been presented in Secs. 2 and 3. Table 26 gives a brief summary of the data used in the linear optimization procedure and in the nonlinear regression analysis. In addition to the data discussed in the preceding chapters, several data have been generated either for the exclusive use in the linear optimization algorithm or to ensure reasonable behavior of the equation of state in regions where the data available in the literature yield insufficient information. These are:

- (1) Twenty-eight $p\rho T$ data within the high-temperature/high-pressure region calculated from the reference equa-

TABLE 26. Summary of the selected data that were used in the linear and nonlinear optimization algorithms

Property	For details, see	Number of data	
		Linear optimization	Nonlinear regression analysis
$p(\rho, T)$	Table 11	1239	1239
$p(\rho, T)$	Sec. 7.2	28	28
$p_s(T)$		224 ^a	—
$\rho'(T)$		224 ^a	—
$\rho''(T)$		224 ^a	—
$p_s(T)$	Table 5	—	44
$\rho'(T)$	Table 6	—	42
$\rho''(T)$	Table 7	—	44
$B(T)$	Table 13	14	14
$B(T)$	Table 14	44	44
$c_v(\rho, T)$	Table 17	223	223
$c_v(\rho, T)$	Sec. 4.2.2	232	—
$c_p(\rho, T)$	Table 19	88 ^b	88
$c'_p(T)$	Table 9	106 ^b	106
$w(p, T)$	Table 15	525 ^b	525
$w'(T)$	Table 8	99 ^b	99

^aLinearized solution of the Maxwell criterion using data calculated from the ancillary equations, Eqs. (2.4) to (2.6), see Wagner (1972).

^bLinearized data used in the linear optimization procedure, see Setzmann and Wagner (1991) and Wagner and Prüß (2002).

tion of state for nitrogen [Span *et al.* (2000)] and transferred to ethane by a simple corresponding states approach (see Sec. 5.4.1).

- (2) 232 data for the isobaric heat capacity calculated from preliminary equations to ensure a numerically reliable linearization of the experimental speeds of sound published by Estrada-Alexanders and Trusler (1997) and Tsumura and Straty (1977). Details on the linearization procedures are given by Setzmann and Wagner (1991) and Tegeler *et al.* (1997). These data were used only in the linear optimization algorithm.
- (3) 244 data calculated from the ancillary equations, Eqs. (2.4)–(2.6), for a linearized solution of the Maxwell criterion, see Wagner (1972). These data were used only in the linear optimization algorithm.

4.2.3. The Equation for the Residual Part α^r

From the bank of terms as formulated in Eq. (4.7), the optimization algorithms selected the final functional form for the residual part of the dimensionless Helmholtz energy given by

$$\begin{aligned} \alpha^r = & \sum_{i=1}^5 n_i \delta^{d_i} \tau^{t_i} + \sum_{i=6}^{39} n_i \delta^{d_i} \tau^{t_i} \exp(-\delta^{c_i}) \\ & + \sum_{i=40}^{44} n_i \delta^{d_i} \tau^{t_i} \exp[-\eta_i(\delta - \varepsilon_i)^2 - \beta_i(\tau - \gamma_i)^2], \quad (4.8) \end{aligned}$$

for the definition of δ and τ see Eq. (4.1). The final values of the parameters were determined by the nonlinear regression

TABLE 27. Coefficients and exponents of Eq. (4.8)

<i>i</i>	<i>n_i</i>	<i>c_i</i>	<i>d_i</i>	<i>t_i</i>
1	0.834 407 457 352 41	—	1	0.25
2	-0.142 873 606 071 71 × 10 ¹	—	1	1.00
3	0.344 302 422 109 27	—	2	0.25
4	-0.420 966 779 202 65	—	2	0.75
5	0.120 945 008 865 49 × 10 ⁻¹	—	4	0.75
6	-0.579 762 015 973 41	1	1	2.00
7	-0.331 270 378 708 38 × 10 ⁻¹	1	1	4.25
8	-0.117 516 548 941 30	1	2	0.75
9	-0.111 609 578 330 67	1	2	2.25
10	0.621 815 926 544 06 × 10 ⁻¹	1	3	3.00
11	0.984 817 954 344 43 × 10 ⁻¹	1	6	1.00
12	-0.982 685 826 823 58 × 10 ⁻¹	1	6	1.25
13	-0.239 778 310 070 49 × 10 ⁻³	1	7	2.75
14	0.698 856 633 288 21 × 10 ⁻³	1	9	1.00
15	0.196 659 878 033 05 × 10 ⁻⁴	1	10	2.00
16	-0.145 861 522 079 28 × 10 ⁻¹	2	2	2.50
17	0.463 541 005 367 81 × 10 ⁻¹	2	4	5.50
18	0.607 646 221 804 45 × 10 ⁻²	2	4	7.00
19	-0.264 473 301 478 28 × 10 ⁻²	2	5	0.50
20	-0.429 318 726 899 04 × 10 ⁻¹	2	5	5.50
21	0.299 877 865 172 63 × 10 ⁻²	2	6	2.50
22	0.529 193 351 750 10 × 10 ⁻²	2	8	4.00
23	-0.103 838 977 981 98 × 10 ⁻²	2	9	2.00
24	-0.542 603 482 146 94 × 10 ⁻¹	3	2	10.00
25	-0.219 593 629 184 93	3	3	16.00
26	0.353 624 566 503 54	3	3	18.00
27	-0.124 773 901 737 14	3	3	20.00
28	0.184 256 935 915 17	3	4	14.00
29	-0.161 922 564 367 54	3	4	18.00
30	-0.827 708 761 490 64 × 10 ⁻¹	3	5	12.00
31	0.501 607 580 964 37 × 10 ⁻¹	3	5	19.00
32	0.936 143 263 366 55 × 10 ⁻²	3	6	7.00
33	-0.278 391 862 428 64 × 10 ⁻³	3	11	15.00
34	0.235 602 740 714 81 × 10 ⁻⁴	3	14	9.00
35	0.392 383 297 385 27 × 10 ⁻²	4	3	26.00
36	-0.764 883 258 136 18 × 10 ⁻³	4	3	28.00
37	-0.499 443 044 407 30 × 10 ⁻²	4	4	28.00
38	0.185 933 864 071 86 × 10 ⁻²	4	8	22.00
39	-0.614 043 533 311 99 × 10 ⁻³	4	10	13.00
<i>i</i>	<i>n_i</i>	<i>c_i</i>	<i>d_i</i>	<i>t_i</i>
40	-0.233 121 793 679 24 × 10 ⁻²	—	1	0.00
41	0.293 010 479 087 60 × 10 ⁻²	—	1	3.00
42	-0.269 124 728 428 83 × 10 ⁻³	—	3	3.00
43	0.184 138 341 118 14 × 10 ³	—	3	0.00
44	-0.103 971 279 848 54 × 10 ²	—	2	3.00
				η_i β_i γ_i ε_i
				15 150 1.05 1
				15 150 1.05 1
				15 150 1.05 1
				275 1.22 1
				400 1.16 1

analysis and are given in Table 27. The coefficients n_i resulted in a nonlinear fit which is part of the regression analysis.

The new equation of state for ethane, Eq. (4.1), in combination with the formulation for α° , Eq. (4.6), and the formulation for α^r , Eq. (4.8), was constrained to the critical parameters given in Sec. 2.2 by setting the first and second derivatives of pressure with respect to density to zero at the critical point.

The range of validity of the new equation of state for ethane, Eq. (4.1), is based on the region from which reliable experimental data were used to develop the equation. Thus, the range of validity is defined by the following region in temperature and pressure:

$$90.368 \text{ K} \leq T \leq 675 \text{ K}$$

and

$$p \leq 900 \text{ MPa.}$$

The lowest temperature given above corresponds to the triple-point temperature. At pressures above the triple-point pressure the melting line (see Sec. 2.3) forms the range of validity regarding the lowest temperature. In this range of validity of Eq. (4.1), clear statements about the uncertainty of the equation of state can be made. The equation can also be used outside this range of validity, however, with greater uncertainties (see also Sec. 5.4).

The derivatives of the residual part of the equation of state, Eq. (4.1), needed for the property calculations, are presented in Table 28. Estimations for the uncertainties are summarized in Sec. 6.

5. Comparison of the New Equation of State with Experimental Data

This section gives a discussion of the quality of the new equation of state [Eq. (4.1)] based mainly on comparisons with selected experimental data. Most of the figures also show calculations from the equation published by Friend *et al.* (1991), which is commonly accepted as the international standard for the thermodynamic properties of ethane. Since the equation is based on the International Practical Temperature Scale of 1968 (IPTS-68), temperature values were converted to the IPTS-68 scale before values were calculated from this equation.

5.1. The Vapor–Liquid Phase Boundary

5.1.1. Thermal Properties

Since the highly accurate data measured by Funke *et al.* (2002b) cover the entire phase boundary, the comparisons can be restricted to these values. Figure 9 shows comparisons of the thermal saturation properties calculated from Eq. (4.1) to experimental data. Additionally, values calculated from the ancillary equations, Eqs. (2.4)–(2.6), and from the equation of state of Friend *et al.* (1991) are included. Absolute deviations are shown for the vapor pressure and the vapor density at temperatures below 170 K. Due to the small absolute values in this region, absolute deviations are more significant than the divergent relative deviations. Percentage deviations are plotted in the other diagrams.

Equation (4.1) represents the selected data clearly within their experimental uncertainties. Deviations from the vapor-pressure data are within 0.01% above 170 K and within 10 Pa below 170 K. The selected saturated-liquid densities are reproduced within 0.005% up to a temperature of 304.9 K. Approaching the critical temperature, the deviations increase up to 0.12%. The experimental saturated-vapor densities are represented within 0.015% at temperatures up to 305.1 K. Closer to the critical temperature, the deviations reach up to 0.35%. Below 185 K, no experimental saturated-vapor densities are available. Absolute deviations from values calculated from the virial equation of state of Funke *et al.* (2002b) are within 0.0004 kg m⁻³.

TABLE 28. The residual part α^r , Eq. (4.8), of the dimensionless Helmholtz energy and its derivatives^a

$$\begin{aligned} \alpha^r &= \sum_{i=1}^5 n_i \delta^{d_i} \tau^{t_i} + \sum_{i=6}^{39} n_i \delta^{d_i} \tau^{t_i} e^{-\delta^{c_i}} + \sum_{i=40}^{44} n_i \delta^{d_i} \tau^{t_i} e^{-\eta_i(\delta-\varepsilon_i)^2 - \beta_i(\tau-\gamma_i)^2} \\ \alpha_{\delta}^r &= \sum_{i=1}^5 n_i d_i \delta^{d_i-1} \tau^{t_i} + \sum_{i=6}^{39} n_i e^{-\delta^{c_i}} [\delta^{d_i-1} \tau^{t_i} (d_i - c_i \delta^{c_i})] + \sum_{i=40}^{44} n_i \delta^{d_i} \tau^{t_i} e^{-\eta_i(\delta-\varepsilon_i)^2 - \beta_i(\tau-\gamma_i)^2} \left[\frac{d_i}{\delta} - 2\eta_i(\delta-\varepsilon_i) \right] \\ \alpha_{\delta\delta}^r &= \sum_{i=1}^5 n_i d_i (d_i - 1) \delta^{d_i-2} \tau^{t_i} + \sum_{i=6}^{39} n_i e^{-\delta^{c_i}} [\delta^{d_i-2} \tau^{t_i} ((d_i - c_i \delta^{c_i}) (d_i - 1 - c_i \delta^{c_i}) - c_i^2 \delta^{c_i})] + \sum_{i=40}^{44} n_i \tau^{t_i} e^{-\eta_i(\delta-\varepsilon_i)^2 - \beta_i(\tau-\gamma_i)^2} [-2\eta_i \delta^{d_i} + 4\eta_i^2 \delta^{d_i} (\delta-\varepsilon_i)^2 \\ &\quad - 4d_i \eta_i \delta^{d_i-1} (\delta-\varepsilon_i) + d_i (d_i - 1) \delta^{d_i-2}] \\ \alpha_{\tau}^r &= \sum_{i=1}^5 n_i t_i \delta^{d_i} \tau^{t_i-1} + \sum_{i=6}^{39} n_i t_i \delta^{d_i} \tau^{t_i-1} e^{-\delta^{c_i}} + \sum_{i=40}^{44} n_i \delta^{d_i} \tau^{t_i} e^{-\eta_i(\delta-\varepsilon_i)^2 - \beta_i(\tau-\gamma_i)^2} \left[\frac{t_i}{\tau} - 2\beta_i(\tau-\gamma_i) \right] \\ \alpha_{\tau\tau}^r &= \sum_{i=1}^5 n_i t_i (t_i - 1) \delta^{d_i} \tau^{t_i-2} + \sum_{i=6}^{39} n_i t_i (t_i - 1) \delta^{d_i} \tau^{t_i-2} e^{-\delta^{c_i}} + \sum_{i=40}^{44} n_i \delta^{d_i} \tau^{t_i} e^{-\eta_i(\delta-\varepsilon_i)^2 - \beta_i(\tau-\gamma_i)^2} \left[\left(\frac{t_i}{\tau} - 2\beta_i(\tau-\gamma_i) \right)^2 - \frac{t_i}{\tau^2} - 2\beta_i \right] \\ \alpha_{\delta\tau}^r &= \sum_{i=1}^5 n_i d_i t_i \delta^{d_i-1} \tau^{t_i-1} + \sum_{i=6}^{39} n_i t_i \delta^{d_i-1} \tau^{t_i-1} (d_i - c_i \delta^{c_i}) e^{-\delta^{c_i}} + \sum_{i=40}^{44} n_i \delta^{d_i} \tau^{t_i} e^{-\eta_i(\delta-\varepsilon_i)^2 - \beta_i(\tau-\gamma_i)^2} \left[\frac{d_i}{\delta} - 2\eta_i(\delta-\varepsilon_i) \right] \left[\frac{t_i}{\tau} - 2\beta_i(\tau-\gamma_i) \right] \end{aligned}$$

$$^a \alpha_{\delta}^r = [\partial \alpha^r / \partial \delta]_{\tau}, \alpha_{\delta\delta}^r = [\partial^2 \alpha^r / \partial \delta^2]_{\tau}, \alpha_{\tau}^r = [\partial \alpha^r / \partial \tau]_{\delta}, \alpha_{\tau\tau}^r = [\partial^2 \alpha^r / \partial \tau^2]_{\delta}, \alpha_{\delta\tau}^r = [\partial^2 \alpha^r / \partial \delta \partial \tau].$$

The equation of Friend *et al.* (1991) is not able to reproduce the experimental data within their uncertainties. Nonetheless, relative deviations between calculated and measured vapor pressures are within 0.03% for temperatures above 180 K and absolute deviations are within 25 Pa below this point. The maximum deviations from the experimental saturated-liquid densities reach up to 0.12% at temperatures

below 300 K and up to 0.7% above 300 K. The representation of the saturated-vapor densities is particularly poor with deviations from experimental values reaching as much as 0.4% far from the critical temperature and 1.1% above 305 K.

The ancillary equations give a slightly better representation of the experimental data on the phase boundary than the new equation of state. However, if thermodynamically consistent values for all properties on the phase boundary are desired, such values should be calculated from Eq. (4.1).

5.1.2. Caloric Properties

Figure 10 gives comparisons of the caloric properties of saturated-liquid ethane calculated from Eq. (4.1) to selected experimental data. The upper diagram shows speeds of sound measured by Vangeel (1976) and Tsumura and Straty (1977). Both data sets were included in the development of the new equation of state. The two data sets are consistent with each other at temperatures from 120 to 270 K. In this region, both data sets are reproduced by Eq. (4.1) within the reported uncertainties. Above 270 K and below 120 K, however, the discrepancies between the different measurement runs exceed the combined reported uncertainties. Equation (4.1) represents both data sets in these regions within 0.5% which is better than their mutual consistency. The values calculated from the equation of Friend *et al.* (1991) deviate systematically from the measured data. Particularly at temperatures above 220 K, the calculated values are up to 2% higher than the experimental data.

Absolute values of the speed of sound on the phase boundary in the proximity of the critical point are plotted in Fig. 11. Values calculated from Eq. (4.1) and the equation of Friend *et al.* (1991) are plotted as lines. Additionally, measured speeds of sound reported by Colgate *et al.* (1992) for

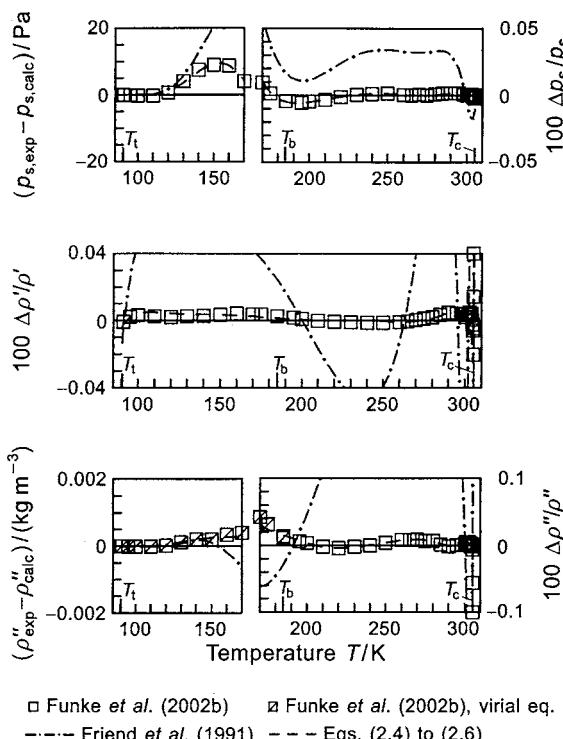


FIG. 9. Absolute and percentage deviations [$100\Delta y_m/y_m = 100(y_{m,\text{exp}} - y_{m,\text{calc}})/y_{m,\text{exp}}$ with $y = p_s, \rho', \rho''$] of the selected thermal data at saturation from values calculated from Eq. (4.1). Values calculated from the ancillary equations, Eqs. (2.4)–(2.6), and from the equation of state of Friend *et al.* (1991) are plotted for comparison.

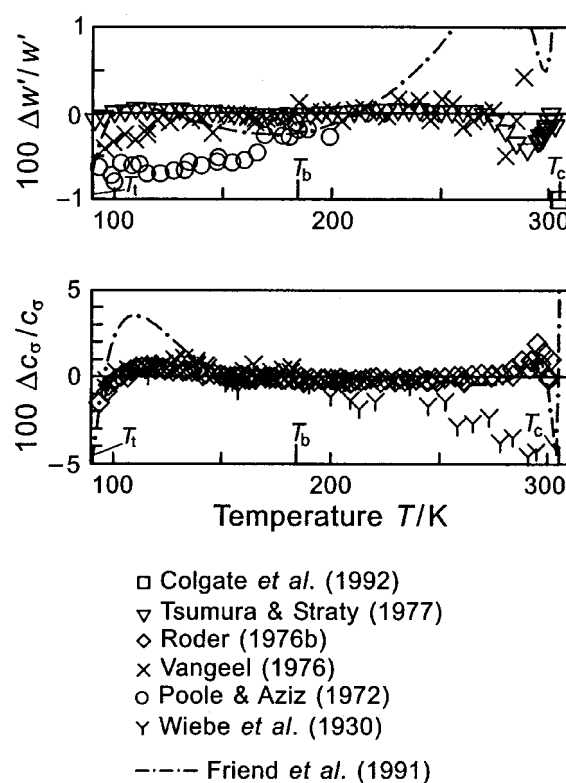


FIG. 10. Percentage deviations deviations $[100\Delta y_m/y_m = 100(y_{m,\exp} - y_{m,\text{calc}})/y_{m,\exp}]$ of experimental data for the speed of sound in the saturated liquid and for the heat capacity along the saturated-liquid line from values calculated from the equation of state, Eq. (4.1). Values calculated from the equation of state of Friend *et al.* (1991) are plotted for comparison.

temperatures $(T_c - T) \leq 0.75$ K and data reported by Tsumura and Straty (1977) are shown. Equation (4.1) provides a better representation of the data than the equation of Friend *et al.* (1991), but without the nonanalytical terms (see

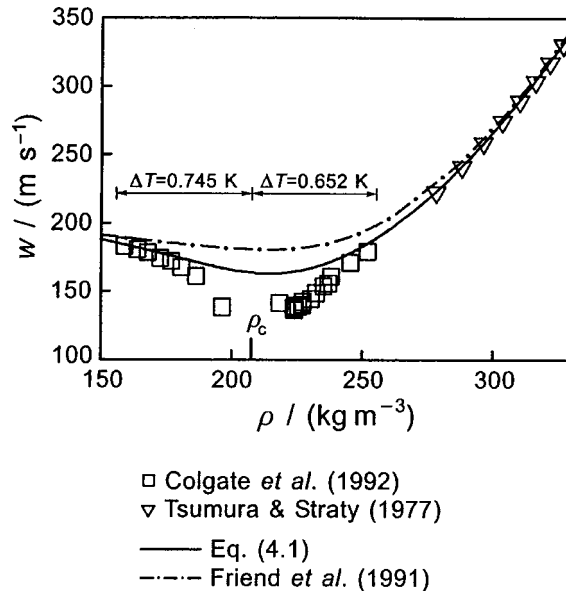


FIG. 11. Representation of the speed of sound on the phase boundary near the critical point. The plotted curves correspond to values calculated from the equation of state, Eq. (4.1), and from the equation of state of Friend *et al.* (1991).

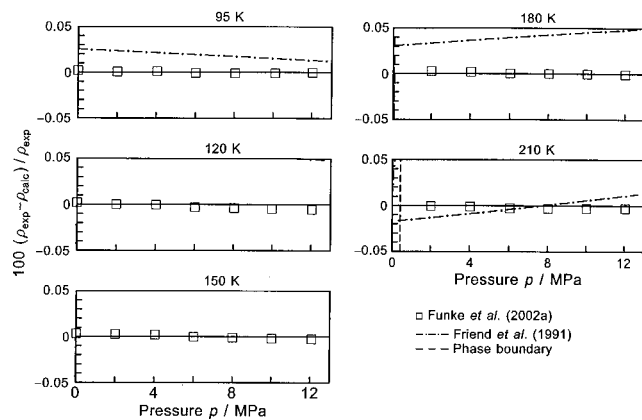


FIG. 12. Percentage density deviations of highly accurate $p\rho T$ data (95–210 K) from values calculated from the equation of state, Eq. (4.1). Values calculated from the equation of state of Friend *et al.* (1991) are plotted for comparison.

the statement at the end of Sec. 4.2.1) it cannot reproduce the sharp decline of the speed of sound towards the critical temperature at the critical density.

The experimental values for the heat capacity along the saturated-liquid line published by Roder (1976b) cover the entire phase boundary. The author reports uncertainties of his measurements to be generally less than 0.5%, increasing to 5% within a few Kelvin of the critical temperature. Additionally, he suggests that undetected systematic errors remain within 2%. The lower diagram in Fig. 10 gives comparisons of these values and of older data measured by Wiebe *et al.* (1930) with values calculated from Eq. (4.1). At temperatures above 100 K, all data are reproduced within the reported uncertainties, even if possible systematic errors are assumed to be zero. Below 100 K, the maximum deviations are less than 1.5%, which is presumably far less than the total uncertainties of the data. The equation of state of Friend *et al.* (1991) also yields a good representation of the data over a large part of the phase boundary. At temperatures from 100 to 150 K, however, the performance of the equation is poor with deviations from the measured values reaching up to +3.5%.

5.2. Single-Phase Region

5.2.1. $p\rho T$ Data

As a result of the measurements performed by Funke *et al.* (2002a, 2002b), the thermal properties of fluid-phase ethane at temperatures from 95 to 340 K and pressures up to 12 MPa are known to the highest degree of accuracy attainable today. These measurements are complemented by the values obtained by Claus *et al.* (2003) at temperatures up to 520 K and pressures up to 30 MPa. These data very precisely define the $p\rho T$ surface in the largest part of the relevant region. No other $p\rho T$ data were included in the development of the new equation of state within the range of parameters covered by these measurements. Comparisons of densities calculated from Eq. (4.1) to the highly accurate $p\rho T$ data are shown in

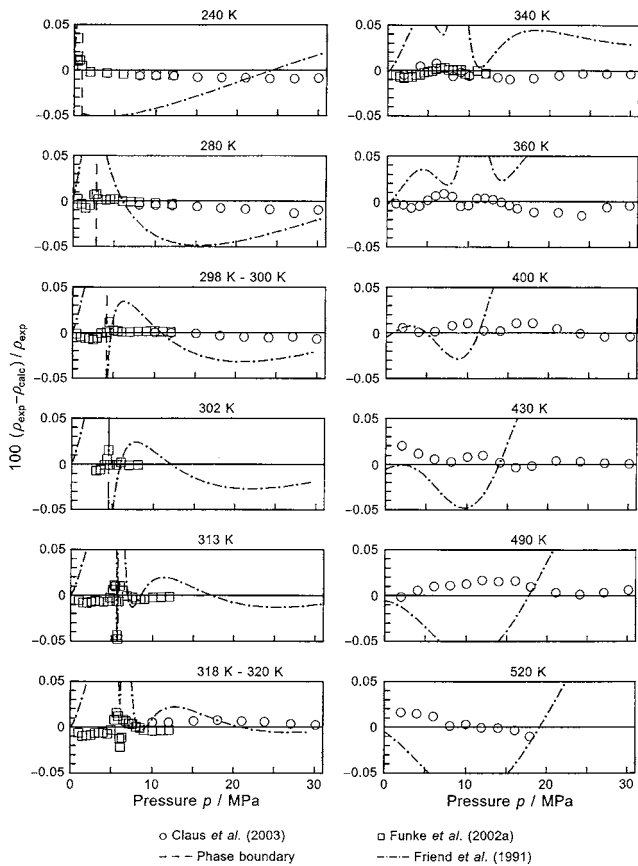


Fig. 13. Percentage density deviations of highly accurate $p\rho T$ data (240–520 K) from values calculated from the equation of state, Eq. (4.1). Values calculated from the equation of state of Friend *et al.* (1991) are plotted for comparison.

Figs. 12 and 13. All data are reproduced clearly within the small experimental uncertainties which are generally 0.02% of the densities measured by Funke *et al.* (2002a) and 0.02%–0.03% of the densities measured by Claus *et al.* (2003). In the extended critical region, total uncertainties are about 0.015% in pressure. This particular region is discussed in more detail in Sec. 5.3. Along the 340 K isotherm, the values published by Claus *et al.* (2003) exhibit slightly oscillating deviations from the values measured by Funke *et al.* (2002a) and from the values calculated from Eq. (4.1). This small but systematic effect can be observed along the higher isotherms as well and may be an indication for experimental errors in the order of 0.01%–0.02% in this region. The authors accounted for these possible errors by estimating the total uncertainties in density to be 0.03% at the higher temperatures.

Over the entire range of parameters shown in Figs. 12 and 13, the deviations between measured densities and values calculated from the equation of state of Friend *et al.* (1991) exceed the experimental uncertainties by far. In the subcritical gaseous region, the calculated densities are systematically higher than the experimental values with maximum deviations of +0.3% close to the phase boundary. Similarly, systematic inconsistencies are observed in the liquid phase with

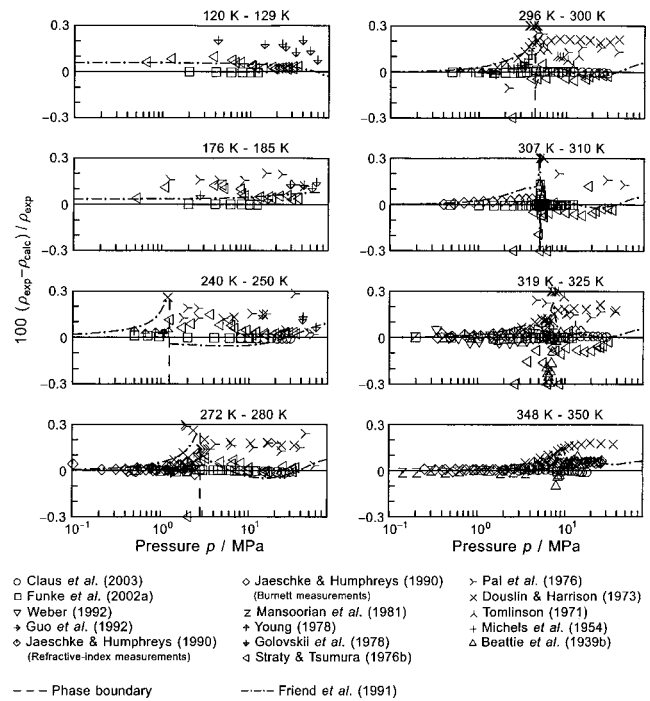


Fig. 14. Percentage density deviations of $p\rho T$ data (120–350 K) assigned to groups 1 and 2 from values calculated from the equation of state, Eq. (4.1). Values calculated from the equation of Friend *et al.* (1991) are plotted for comparison.

maximum deviations reaching 0.1% near the saturated-liquid line. The deviations oscillate along the supercritical isotherms mostly within a margin of 0.05%, but reaching up to 0.3% at higher temperatures and pressures and in the vicinity of the critical isochore.

Figures 14 and 15 show comparisons of densities calculated from Eq. (4.1) to representative sets of group 1 and group 2 $p\rho T$ data for pressures up to 80 MPa. In the liquid

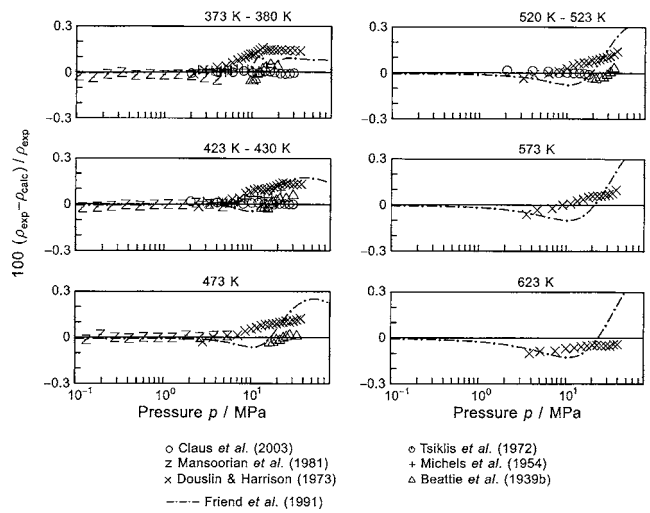


Fig. 15. Percentage density deviations of $p\rho T$ data (373–623 K) assigned to groups 1 and 2 from values calculated from the equation of state, Eq. (4.1). Values calculated from the equation of Friend *et al.* (1991) are plotted for comparison.

region at low temperatures, the densities reported by Straty and Tsumura (1976b) agree best with the measurements of Funke *et al.* (2002a). Inconsistencies remain within 0.05%–0.1% approximately, although the data show a considerable inherent scatter. The data sets of Golovskii *et al.* (1978) and Pal *et al.* (1976) exhibit larger scatter and systematic errors. Some of the densities measured by Pal *et al.* (1976) are more than +0.3% higher than the reference data by Funke *et al.* (2002a). Due to the inherent scatter and the systematic deviations varying with pressure, we could not find a means to methodically adjust these data sets to show better agreement with the reference data. Therefore, these data were used in the development of the new equation of state without any corrections, but only at pressures above 30 MPa and assigning them only moderate weights.

A number of data sets that agree with the group 1 data mostly to within 0.05% exist in the subcritical gaseous region, namely, the values reported by Guo *et al.* (1992), Weber (1992), Jaeschke and Humphreys (1990), Mansoorian *et al.* (1981) and Michels *et al.* (1954). Approaching the saturated-vapor line, however, the density values reported by Jaeschke and Humphreys (1990), and by Michels *et al.* (1954) are higher than the values reported by the other authors by up to +0.15%. None of these data were used to establish the new equation of state.

The densities measured by Douslin and Harrison (1973) are generally higher than the other group 1 data. While these inconsistencies increase with pressure in the low pressure range, the gap remains almost constant at higher pressures. The highest difference is +0.3% in the gas phase and approximately +0.2% at higher densities. Two earlier data sets, published by Michels *et al.* (1954) and Beattie *et al.* (1939b) are in better agreement with the reference data. Equation (4.1) reproduces both data sets with deviations of less than 0.1%, although they were assigned only small weights in the development of the equation. Figure 15 indicates that the gap between the data of Douslin and Harrison (1973) and the other group 1 data decreases with temperature. Friend *et al.* (1991) apparently overfitted the data of Douslin and Harrison (1973) in the gas phase. Their equation reproduces the faulty densities and thus yields values up to

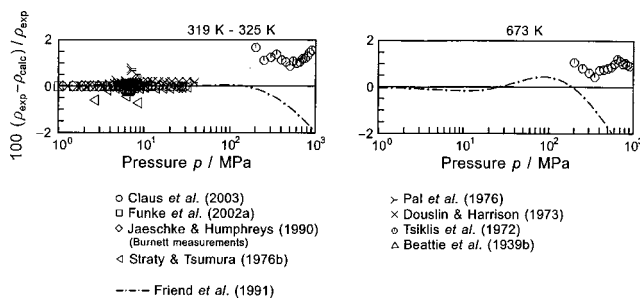


FIG. 16. Percentage density deviations of $p\rho T$ data in the high-pressure region from values calculated from the equation of state, Eq. (4.1). Values calculated from the equation of Friend *et al.* (1991) are plotted for comparison. Note that the range of validity of the equation of Friend *et al.* (1991) is restricted to pressures up to 70 MPa and temperatures up to 625 K.

+0.3% higher than the most accurate data. At higher pressures and temperatures above 370 K, the values oscillate around the reference data and the densities calculated from Eq. (4.1).

The only experimental fluid phase densities above 73 MPa were measured by Tsiklis *et al.* (1972) at temperatures from 323 to 673 K. Comparisons with values calculated from Eq. (4.1) are shown in Fig. 16 for the highest and the lowest isotherm of the investigation. All of the reported densities can be reproduced within 1.6% which is certainly less than the experimental uncertainties. The data are beyond the range of validity of the equation of Friend *et al.* (1991).

5.2.2. Virial Coefficients

Figure 17 shows absolute values of selected data for the second virial coefficient B . Additionally, values calculated from the new equation of state and from the equation of state of Friend *et al.* (1991) are plotted as lines. Equation (4.1) yields a plausible plot of the second virial coefficient over the entire temperature range. The desired sharp decrease towards low temperatures was accomplished by including the data calculated by Klimeck (2000) in the development of the equation. The values reported by Funke *et al.* (2002a) are represented by Eq. (4.1) within 0.6%.

The corresponding diagram for the third virial coefficient C is shown in Fig. 18. Again, the values calculated from Eq. (4.1) show a thermodynamically correct plot, yielding the expected maximum and the succeeding sharp decrease to-

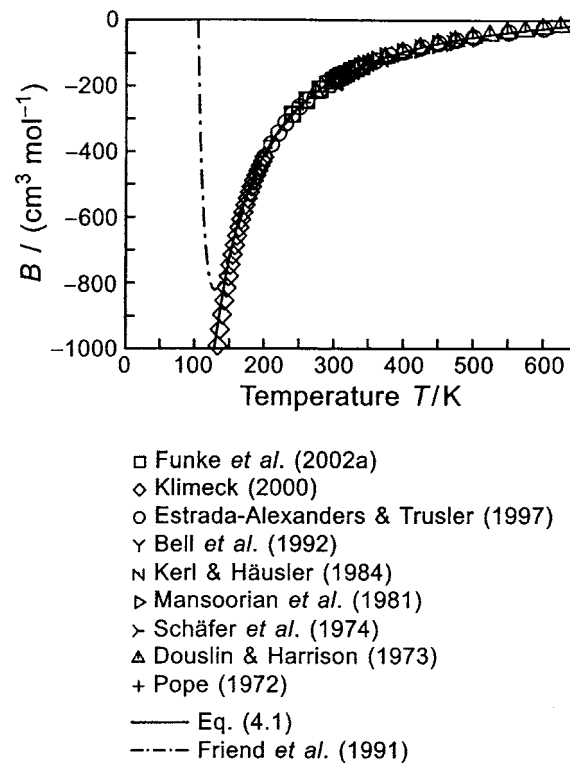


FIG. 17. Representation of data for the second virial coefficient at temperatures up to 650 K. The plotted lines correspond to values calculated from the equation of state, Eq. (4.1), and from the equation of Friend *et al.* (1991).

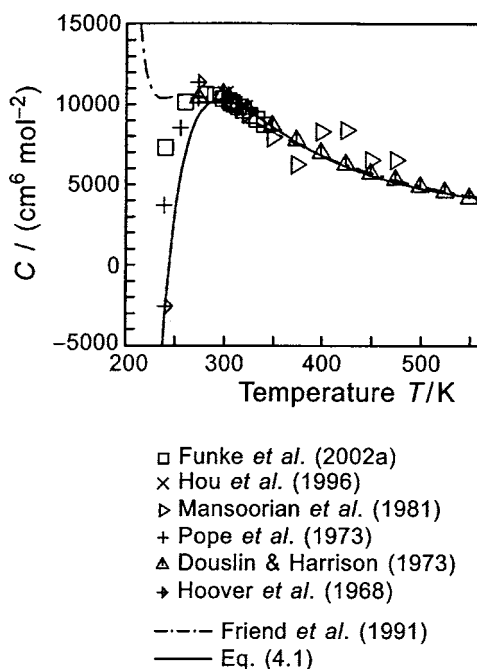


FIG. 18. Representation of data for the third virial coefficient at temperatures up to 650 K. The plotted lines correspond to values calculated from the equation of state, Eq. (4.1), and from the equation of Friend *et al.* (1991).

wards low temperatures. Compared to the data obtained from measurements, the maximum calculated from Eq. (4.1) is located at a slightly higher temperature.

The equation of Friend *et al.* (1991) generates plausible plots of the virial coefficients only in a limited temperature range. Below 130 K, the values of the second virial coefficient abruptly increase towards infinity. Calculated values of the third virial coefficient show a similar sharp increase originating at 230 K, just below the location of the maximum.

5.2.3. Speed of Sound

The values for the speed of sound obtained by Estrada-Alexanders and Trusler (1997) using spherical resonators represent the most accurate description of the caloric properties of ethane now available. The gaseous region from 220 to 450 K is measured with the highest possible accuracy. The data published by Tsumura and Straty (1977) describe the liquid region at temperatures from 100 to 323 K at pressures up to 37 MPa with the highest accuracy available in this particular region today. These two data sets, complemented by the measurements of Trusler and Costa Gomez (1996), make the speed of sound a key property for the description of the thermodynamic behavior of fluid phase ethane.

Figure 19 shows the comparison of speeds of sound calculated from Eq. (4.1) to highly accurate data in the gaseous region on representative isotherms. The vast majority of the data of Estrada-Alexanders and Trusler (1997) are reproduced within 0.01%, which is the uncertainty estimated by the authors, with deviations for only two values at 300 K exceeding 0.015%. The equation of Friend *et al.* (1991) is

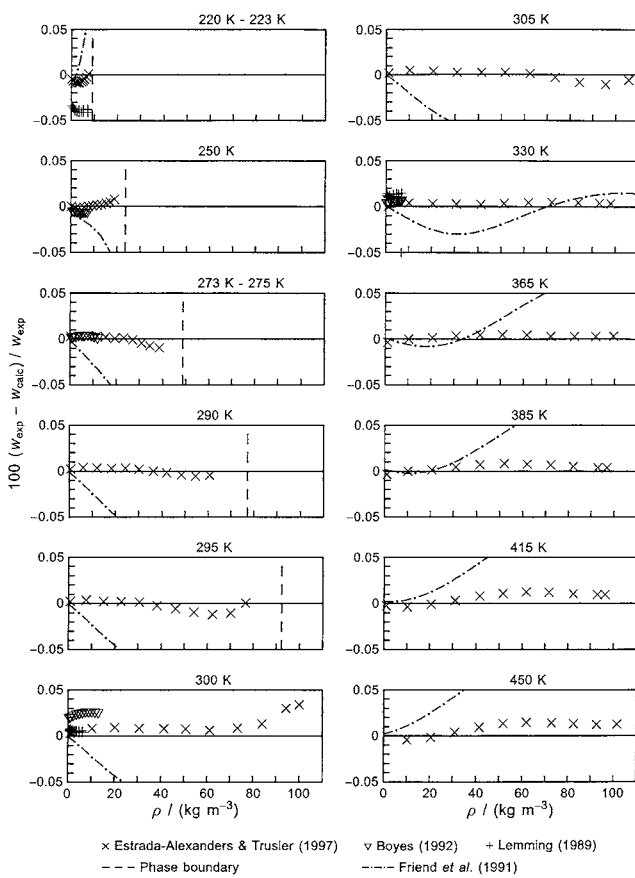


FIG. 19. Percentage deviations of highly accurate speed of sound data for densities up to about half the critical density from values calculated from the equation of state, Eq. (4.1). Values calculated from the equation of Friend *et al.* (1991) are plotted for comparison.

not able to reproduce the data sufficiently. The data were not available when this equation was established and the functional form is not flexible enough to adequately reflect these high precision data. At subcritical temperatures, the equation of Friend *et al.* (1991) systematically predicts lower values with differences reaching up to -0.4% near the phase boundary. These systematic errors decrease towards higher temperatures. At temperatures above 365 K, the speeds of sound calculated from the equation of Friend *et al.* (1991) are too high, with deviations from the experimental data of up to 0.1% .

In Fig. 20, values of the speed of sound from the new equation of state, Eq. (4.1), are compared to the experimental data of Tsumura and Straty (1977) and Trusler and Costa Gomez (1996) in the liquid and supercritical region on characteristic isotherms. The experimental uncertainties of the data shown in the diagrams are $0.06\%-0.15\%$, with the highest uncertainties to be expected near the critical region. The different symbols for the data on the 323 K isotherm denote variations of the measurement technique. Data plotted as triangles or diamonds were measured using the classical pulse-echo technique at frequencies of 10 MHz (triangles) and 1 MHz (diamonds), respectively. Near the critical point, this technique is limited due to the large sound attenuation.

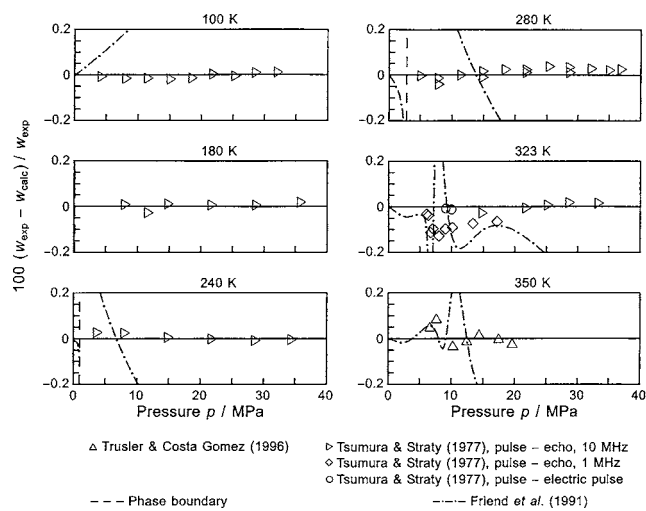


FIG. 20. Percentage deviations of speed of sound data in the liquid and supercritical region from values calculated from the equation of state, Eq. (4.1). Values calculated from the equation of Friend *et al.* (1991) are plotted for comparison.

Therefore, Tsumura and Straty (1977) superimposed the acoustic pulse with the electric signal resulting from the succeeding pulse. The speeds of sound thus measured are considered more reliable at near-critical conditions and are plotted as circles in Fig. 20. The diagrams illustrate the high accuracy of Eq. (4.1) regarding speeds of sound in the liquid and supercritical phase. In the liquid region, all deviations are within 0.06%, and the data at supercritical states are also reproduced clearly within their experimental uncertainties. Speeds of sound obtained on the critical isotherm are attributed with substantially higher uncertainties. These data are discussed separately in Sec. 5.3.2.

An accurate description of the speed of sound in the liquid phase makes high demands on empirical equations of state. Similar to the data in the gaseous phase, the values published by Tsumura and Straty (1977) for the liquid phase could only be represented adequately by equations that were developed using both the linear optimization algorithm and the nonlinear regression analysis (see Sec. 4.2.1). Values calculated from the equation of Friend *et al.* (1991) differ from the experimental data by up to as much as 1%, showing the weakness of this formulation.

5.2.4. Isochoric Heat Capacity

The only reliable data set for the isochoric heat capacity of ethane outside the near-critical region was published by Roder (1976b). Percentage deviations between these data and values calculated from the new equation of state are shown in Fig. 21. The experimental uncertainties estimated by the author correspond to the uncertainties reported for the heat capacities along the saturated-liquid line, i.e., 0.5%–5% plus an additional 2% for possible undetected systematic errors. Equation (4.1) reproduces the data within these uncertainties. The agreement between values calculated from the

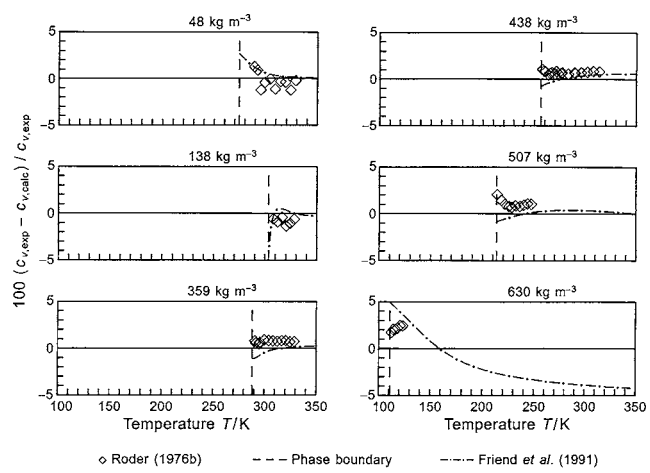


FIG. 21. Percentage deviations of group 1 isochoric heat capacity data from values calculated from the equation of state, Eq. (4.1). Values calculated from the equation of Friend *et al.* (1991) are plotted for comparison.

equation of Friend *et al.* (1991) and the experimental data is generally satisfactory, except for values close to the phase boundary.

5.2.5. Isobaric Heat Capacity

Figure 22 presents comparisons of isobaric heat capacities calculated from Eq. (4.1) to experimental group 1 and 2 c_p data. The data of Bender (1982) are generally reproduced within 0.18%. Ernst and Hochberg (1989) estimate the uncertainties of their results to be 0.2%–1.2%. However, these estimates appear overly optimistic. The agreement with values calculated from the new equation is generally better than 0.5% with a few data points at 333 K deviating by up to 1.5%. We consider these deviations to be clearly within the actual experimental uncertainties. The run of the isobaric heat capacity is basically determined by the highly accurate

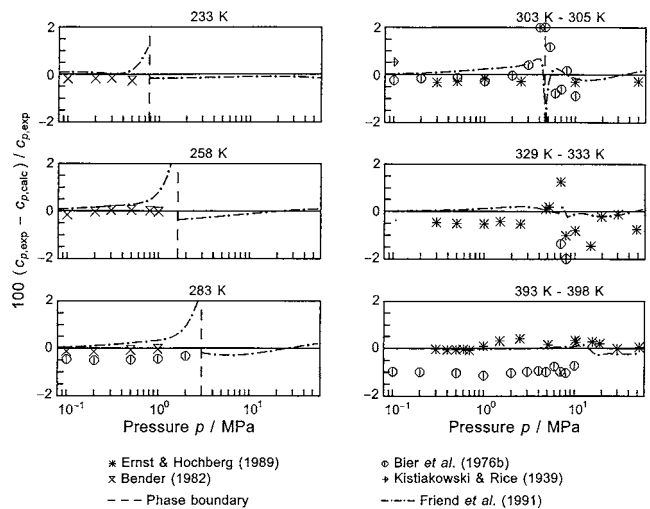


FIG. 22. Percentage deviations of isobaric heat capacity data assigned to groups 1 and 2 from values calculated from the equation of state, Eq. (4.1). Values calculated from the equation of Friend *et al.* (1991) are plotted for comparison.

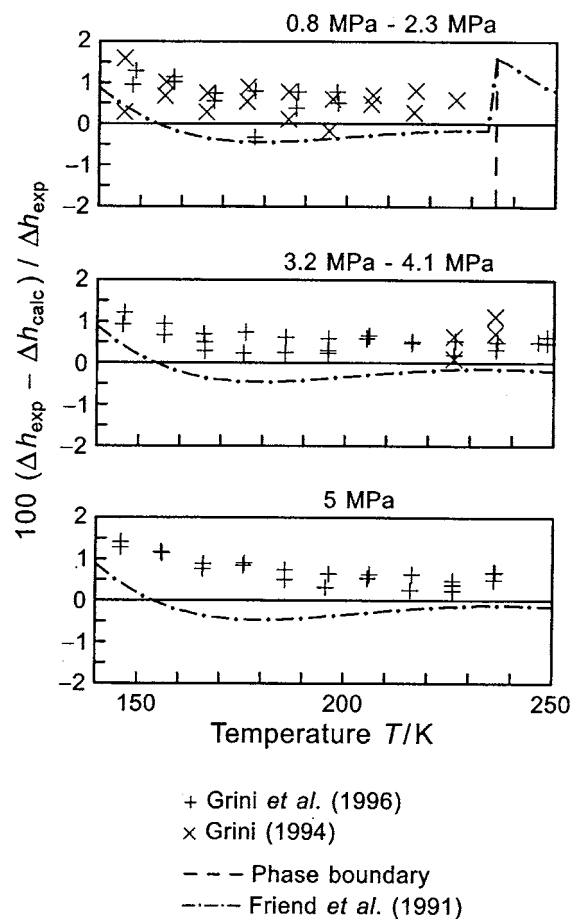


Fig. 23. Percentage deviations of experimental enthalpy differences from values calculated from the equation of state, Eq. (4.1). Deviations between isobaric enthalpy differences for $\Delta T = 1$ K, calculated from the equation of Friend *et al.* (1991) and Eq. (4.1) are plotted for comparison.

data for the thermal properties and the speed of sound. Hence, the measurements of the isobaric heat capacity did not have a wide influence on the development of Eq. (4.1). The data published by Bier *et al.* (1976b) were classified as less reliable than the aforementioned data.

5.2.6. Enthalpy Differences and Throttling Coefficients

Percentage deviations between enthalpy differences, Δh_{exp} , reported by Grini (1994) and Grini *et al.* (1996), and values calculated from Eq. (4.1) are plotted in Fig. 23. All data are reproduced within 1.6%. Additionally, deviations between isobaric enthalpy differences for $\Delta T = 1$ K, calculated from the equation of Friend *et al.* (1991) and the new equation of state, are shown in the diagrams. Both equations yield similar results.

Although the experimental uncertainties of the Joule–Thomson coefficients reported by Bender (1982) are specified to be 0.35%, no preliminary equation could represent the values within this margin. Since the discrepancies between calculated and measured values always decreased with increasing pressure along the isotherms, we suspected systematic errors in the data and performed some plausibility

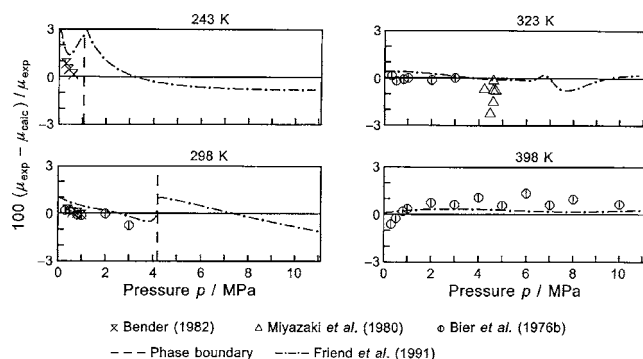


Fig. 24. Percentage deviations of experimental data for the Joule–Thomson coefficient from values calculated from the equation of state, Eq. (4.1). Values calculated from the equation of Friend *et al.* (1991) are plotted for comparison.

checks. We thus could ascertain that a better representation of the measured Joule–Thomson coefficients inevitably led to a significantly worse agreement with the $p\rho T$ measurements of Funke *et al.* (2002a) in the same region. The Joule–Thomson coefficient is defined quite precisely by the highly accurate $p\rho T$ and speed of sound data that are available in the gas region. We hence assume systematic errors in the measurements performed by Bender (1982). Nevertheless, the deviations between these experimental data and values calculated from Eq. (4.1) are less than 0.9%.

Comparisons of μ values calculated from the new equation of state to experimental data are given in Fig. 24. Just like the corresponding c_p data, the measurements of the Joule–Thomson coefficient performed by Bier *et al.* (1976b) and Miyazaki *et al.* (1980) were not considered reliable enough to be included in the development of the new equation. The performance of the equation of Friend *et al.* (1991) and Eq. (4.1) is equivalent in the liquid phase, while Eq. (4.1) is in slightly better agreement with the measurements in the gas phase.

Absolute values of the isothermal throttling coefficient of ethane, calculated from Eq. (4.1) and from the equation of Friend *et al.* (1991) are shown in Fig. 25. Additionally, smoothed values obtained by Miyazaki *et al.* (1980) from their measurements of enthalpy differences are plotted. The run of the throttling coefficient, particularly on the 313.15 K isotherm, is determined mostly by the compressibility and thus by the $p\rho T$ behavior of the fluid. Since both the equations have been fitted to sufficiently precise thermal data, the calculated values can be considered more reliable than the values obtained by measurements in this peculiar region.

5.3. Critical Region

The aim of this work is not to present a universal model for the thermodynamic properties in the critical region, but rather an accurate and comprehensive phenomenological description of the thermodynamic properties of ethane in the entire fluid region. We did not use special nonanalytical terms (see the statement at the end of Sec. 4.2.1), but we chose a purely analytical functional form for the new equa-

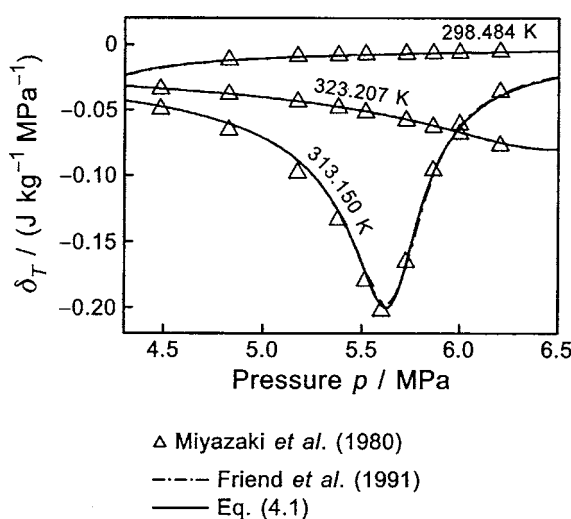


FIG. 25. Representation of experimental data for the isothermal throttling coefficient. The plotted lines correspond to values calculated from the equation of state, Eq. (4.1), and from the equation of Friend *et al.* (1991).

tion of state, i.e., a functional form which can be expanded in a Taylor series about the critical point. Such equations yield finite values for the isochoric heat capacity and the speed of sound at the critical point. Moreover, they result in values for the critical exponents which do not agree with those predicted by renormalization theory. However, it is a common misinterpretation that such equations cannot correctly describe thermodynamic properties in the critical region. In fact, it will be shown in this section that Eq. (4.1) represents highly accurate data for the thermal properties clearly within their experimental uncertainties even in the immediate vicinity of the critical point.

Furthermore, the renormalization theory predicts a weak divergence of the isochoric heat capacity for three-dimensional Ising-like systems without any outer field, e.g., gravity. As a consequence, the speed of sound becomes zero at the critical point. On earth, neither a singularity of the heat capacity nor a value of zero of the speed of sound have been observed in experiments thus far. Unquestionably, however, in the critical region, the isochoric heat capacity increases rapidly towards the critical point, while the speed of sound drops off. Equation (4.1) yields finite values for both heat capacity and speed of sound at the critical point. The range of parameters where Eq. (4.1) cannot reflect the steep increase of the isochoric heat capacity and the sharp decrease of the speed of sound, however, is limited to $|T - T_c| < \approx 0.7 \text{ K}$.

5.3.1. Thermal Properties

The thermal properties of ethane in the critical region have been measured comprehensively by Funke *et al.* (2002a, 2002b). Total experimental uncertainties in pressure are 0.007%–0.016% at $298 \text{ K} \leq T \leq 318 \text{ K}$ and $120 \text{ kg m}^{-3} \leq \rho \leq 280 \text{ kg m}^{-3}$. Comparisons of pressures calculated from

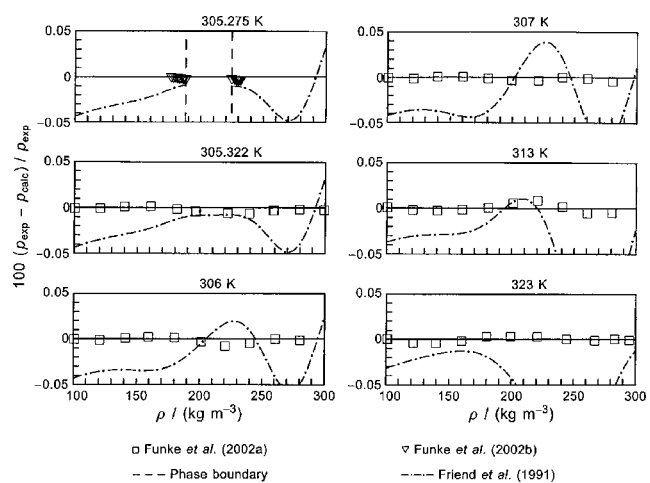


FIG. 26. Percentage pressure deviations of highly accurate $p\rho T$ data in the extended critical region from values calculated from the equation of state, Eq. (4.1). Values calculated from the equation of Friend *et al.* (1991) are plotted for comparison.

Eq. (4.1) to these reference $p\rho T$ data are shown in Fig. 26 for representative isotherms. No other data sets with comparable accuracy are available in this region. All data are represented clearly within their uncertainties. This holds equally for the critical isotherm and slightly sub- and supercritical isotherms as well as for the extended critical region, which is shown in the diagrams for 313 and 323 K in Fig. 26. The equation of Friend *et al.* (1991) represents these data only with appreciable systematic deviations that exceed the uncertainties of the data by far.

5.3.2. Caloric Properties

Figure 27 shows absolute values of the isochoric heat capacity along the critical isochore of ethane, calculated from Eq. (4.1) and from the equation of Friend *et al.* (1991). Additionally, experimental data at densities near the density are included. We can offer no explanation for the striking disagreement between the values measured by Abdulagatov *et al.* (1996) and by the other authors. Considering the data published by Haase and Tillmann (1994), Berestov *et al.* (1973), and Shmakov (1973) to be reliable, it can be seen in Fig. 27 that Eq. (4.1) gives a very good representation of the isochoric heat capacity at $T \geq 306 \text{ K}$. Below the critical temperature, the two-phase isochoric heat capacities are also represented within their experimental uncertainties. Thus, Eq. (4.1) does not reproduce the steep increase of the isochoric heat capacity for $T_c \leq T \leq (T_c + 0.7 \text{ K})$. The equation of Friend *et al.* (1991) yields a decent representation of the experimental data only at $T \geq 309 \text{ K}$.

The representation of speeds of sound on the phase boundary near the critical point was shown in Sec. 5.1.2. In the homogenous critical region, virtually no reliable data for the speed of sound are available. The values measured by Noury (1952), which are the only data in the immediate vicinity of the critical point, exhibit considerable measuring errors. This is noticed in Fig. 28, which shows absolute values of data

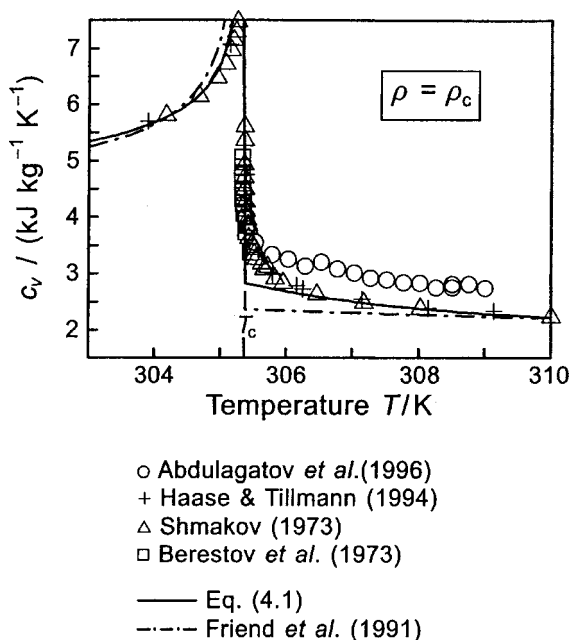


FIG. 27. Representation of the isochoric heat capacity on the critical isochore. The plotted lines correspond to values calculated from the equation of state, Eq. (4.1) and from the equation of Friend *et al.* (1991).

published by Noury (1952) on three isotherms in the critical region. Substantially more accurate values, measured by Tsumura and Straty (1977) at $T=305.3\text{ K}$, are also shown in the diagram. The systematic errors inherent in the data of Noury (1952) are obvious by comparison with the more accurate data. Additionally, values calculated from Eq. (4.1) and the equation of Friend *et al.* (1991) on the corresponding

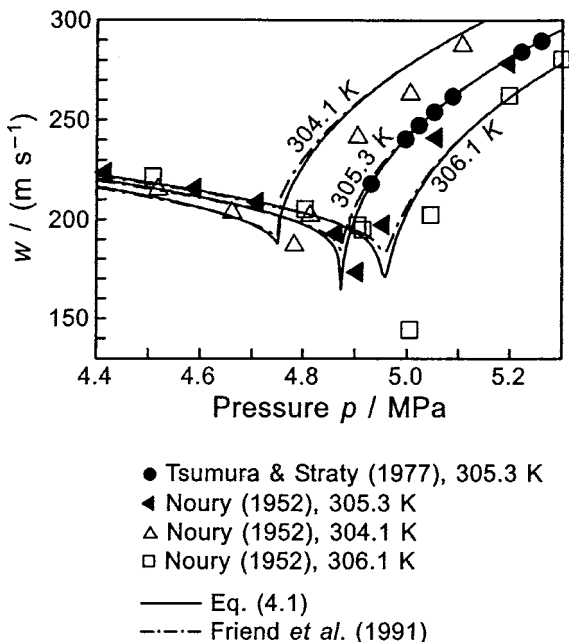


FIG. 28. Representation of the speed of sound on isotherms in the extended critical region. The plotted lines correspond to values calculated from the equation of state, Eq. (4.1) and from the equation of Friend *et al.* (1991).

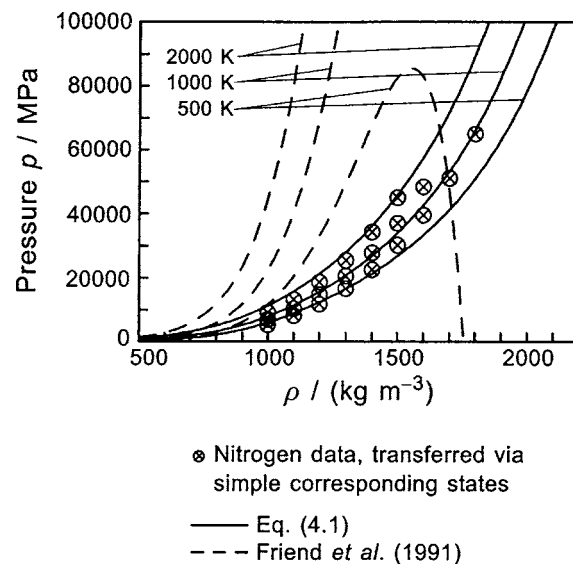


FIG. 29. Representation of data calculated from the reference equation of state for nitrogen [Span *et al.* (2000)] and transferred to ethane by a simple corresponding states approach. The plotted lines correspond to values calculated from the equation of state, Eq. (4.1), and from the equation of Friend *et al.* (1991).

isotherms are plotted as lines. Due to the poor quality of the data, no reliable conclusion can be drawn on the region where the equations yield physically correct values for the speed of sound.

5.4. Extrapolation Behavior

5.4.1. High Pressures and High Temperatures

No experimental data for the thermodynamic properties of ethane are available beyond 900 MPa and 673 K. To ensure reasonable behavior at very high pressures and temperatures, 28 $p\rho T$ data have been calculated from the recent reference equation of state for nitrogen, Span *et al.* (2000), and transferred to ethane by a simple corresponding states approach that goes back to van der Waals (simple substances have the same reduced density δ for the same reduced pressure and temperature, π and τ). These data were used in the development of the new equation of state with low weights. Figure 29 compares these data with values calculated from Eq. (4.1) and from the equation of Friend *et al.* (1991). Equation (4.1) yields reasonable plots of the isotherms in the entire range of parameters. The pressures calculated from the equation of Friend *et al.* (1991) appear to be far too large and, at very high pressures, the isotherms suddenly deviate, as can be seen for the 500 K isotherm, dropping off towards zero and even displaying negative pressures.

5.4.2. Ideal Curves

Ideal curves are frequently used to verify the extrapolation behavior of equations of state. In this work, ideal curves of the compression factor and its first derivatives are considered, namely the classical ideal curve ($Z=1$), the Boyle curve [$(\partial Z/\partial \rho)_T=0$], the Joule–Thomson inversion curve

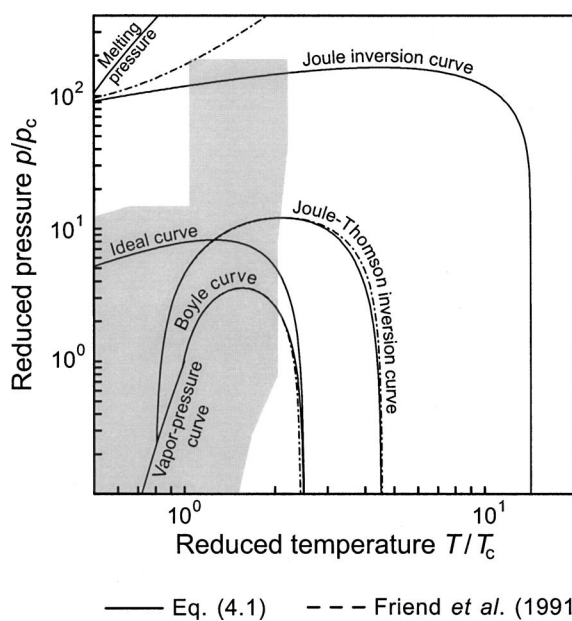


Fig. 30. “Ideal curves” in a double logarithmic p/p_c vs. T/T_c diagram. The curves correspond to values calculated from the equation of state, Eq. (4.1), and from the equation of Friend *et al.* (1991). The area marked in gray corresponds to the region where Eq. (4.1) was fitted to experimental data.

$[(\partial Z/\partial T)_p = 0]$, and the Joule inversion curve $[(\partial Z/\partial T)_p = 0]$. The plots of these characteristic curves, calculated from Eq. (4.1) and from the equation of Friend *et al.* (1991), are shown in Fig. 30. Although no quantitative information should be drawn from the diagram, the plot of the curves calculated from Eq. (4.1) shows reasonable shapes with no sharp inflection points or random oscillations. Each of the curves intersects the abscissa at values of the reduced temperature that compare well to results for other well measured substances, see Span and Wagner (1997). All this indicates qualitatively correct extrapolation behavior of the new equation of state. The equation of Friend *et al.* (1991) yields reasonable plots only for three of the considered ideal curves. The shape of the Joule inversion curve is not plausible and no intersection with the abscissa occurs, indicating that an extrapolation of this equation to high temperatures will give misleading results.

6. Estimated Uncertainty of Calculated Properties

Based on comparisons of calculated properties to available experimental data, estimates for the uncertainty of calculated densities, speeds of sound, isochoric heat capacities, and isobaric heat capacities have been established. These uncertainties are illustrated in tolerance diagrams in Figs. 31–33. All estimates are given as total expanded uncertainties (coverage factor $k=2$ corresponding to a level of confidence of about 95%).

According to the results of the assessment of the extrapolation behavior presented in Sec. 5.4, Eq. (4.1) should yield reasonable results outside of its range of validity at least for

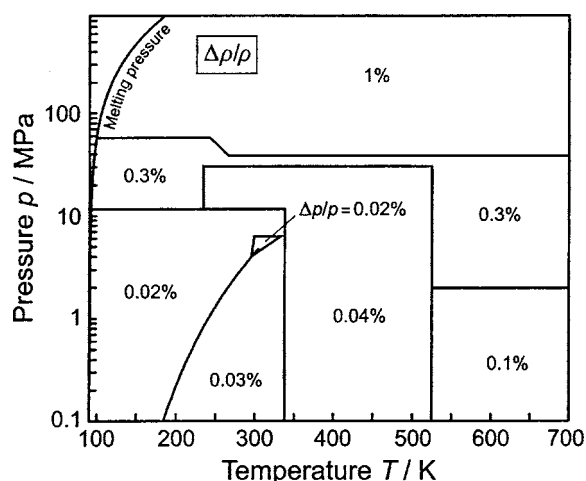


Fig. 31. Tolerance diagram for densities calculated from the equation of state, Eq. (4.1). In the extended critical region the uncertainty in pressure is given.

basic thermodynamic properties like pressure, density, and enthalpy. One should be more careful when extrapolating Eq. (4.1) with regard to caloric properties for which second derivatives of the equation of state are needed, for example, heat capacities and speeds of sound. The uncertainties of these extrapolated properties might be clearly higher than those of the basic properties.

7. Recommendations for Improving the Basis of the Experimental Data

The thermal properties on the vapor–liquid phase boundary are very well measured. There is no need for any improving.

The data situation regarding the $p\rho T$ data in the single-phase region could be clearly improved by having experimental data with uncertainties of less than about 0.05% for the entire temperature range from the melting line to 700 K

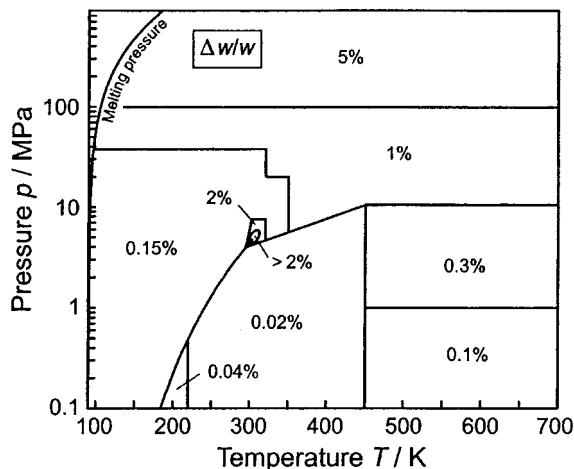


Fig. 32. Tolerance diagram for speeds of sound calculated from the equation of state, Eq. (4.1).

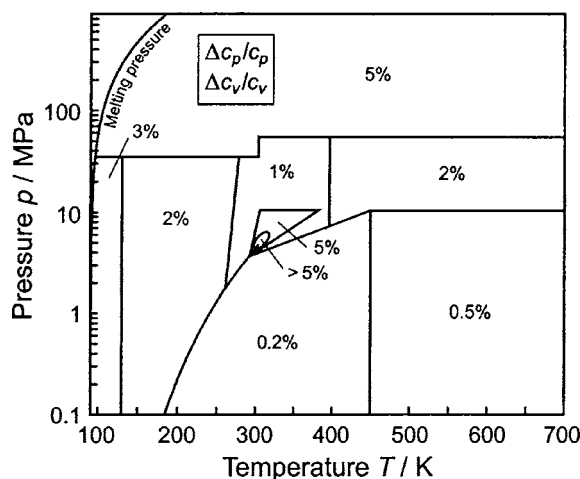


FIG. 33. Tolerance diagram for isobaric and isochoric heat capacities calculated from the equation of state, Eq. (4.1).

and pressures between about 30 and 100 MPa. Moreover, it would be desirable to have $p\rho T$ data with density uncertainties of less than 0.2% for pressures above 100 MPa over the entire temperature range.

As usual, compared with the $p\rho T$ data, the data situation regarding the caloric properties is clearly worse. Concerning the speed of sound, the very good data in the liquid region of Tsumura and Straty (1977) should be supplemented by speed-of-sound measurements below about 5 MPa and above about 40 MPa. Moreover, for pressures above 10 MPa the data should extend to temperatures higher than 350 K, preferably up to about 650 K. The experimental uncertainty of such data should be not higher than 0.05%–0.1% in the speed of sound. It would also be welcomed, when in the gas phase the measurements with the spherical resonator could be extended to higher temperatures.

Experimental data of heat capacities are only really helpful if they are accurate enough. This means that measurements of the isochoric heat capacity should cover the liquid region up to possibly 100 MPa, where the experimental uncertainties should be 0.2%–0.4%. Concerning isobaric heat capacities, it would be desirable to have such data in the gas region and also in the supercritical range up to high pressures and temperatures of up to 500 K or higher. However, these requirements on c_v and c_p measurements might probably be unrealistic. Therefore, it would be all the more important to get $p\rho T$ data and speed of sound data of very good quality that fill the gaps mentioned above.

8. Acknowledgments

We would like to express our gratitude to C. Guder for his many important contributions to this work and to E. W. Lemmon for his very valuable suggestions and advice. We are indebted to the Deutsche Forschungsgemeinschaft (German Research Association) for their financial support of this project.

9. Appendix: Tables of Thermodynamic Properties of Ethane

Table 29 is given here for the saturation properties of ethane as a function of temperature and Table 30 for single-phase state points from 0.1 to 900 MPa from the melting line to 675 K. In order to preserve thermodynamic consistency, all values were calculated from the new equation of state given by Eqs. (4.1), (4.6), and (4.8). The saturation properties were calculated using the phase-equilibrium condition and are also shown in the single-phase table to define the boundary between liquid and vapor state. The melting pressures were calculated from Eq. (2.3).

TABLE 29. Thermodynamic properties of ethane on the vapor–liquid phase boundary as a function of temperature^a

<i>T</i> (K)	<i>p</i> (MPa)	ρ (kg m ⁻³)	<i>h</i> (kJ kg ⁻¹)	<i>s</i> (kJ kg ⁻¹ K ⁻¹)	c_v (kJ kg ⁻¹ K ⁻¹)	c_p (kJ kg ⁻¹ K ⁻¹)	<i>w</i> (m s ⁻¹)
90.368 ^b	0.000 0011	651.529 48 0.000 046	-888.90 -294.12	-5.058 1.524	1.605 0.892	2.326 1.168	2008.69 180.93
92	0.000 0017	649.731 65 0.000 068	-885.11 -292.22	-5.016 1.428	1.591 0.895	2.315 1.171	1996.72 182.48
94	0.000 0029	647.532 28 0.000 11	-880.49 -289.87	-4.966 1.317	1.576 0.899	2.304 1.175	1982.08 184.36
96	0.000 0046	645.335 99 0.000 17	-875.89 -287.52	-4.918 1.211	1.563 0.903	2.295 1.179	1967.48 186.22
98	0.000 0072	643.141 70 0.000 27	-871.31 -285.15	-4.871 1.110	1.551 0.907	2.288 1.183	1952.94 188.05
100	0.000 011	640.948 52 0.000 40	-866.74 -282.78	-4.825 1.015	1.541 0.911	2.283 1.187	1938.44 189.86
102	0.000 017	638.755 69 0.000 59	-862.18 -280.41	-4.779 0.924	1.531 0.915	2.279 1.191	1923.97 191.65
104	0.000 025	636.562 54 0.000 87	-857.62 -278.02	-4.735 0.838	1.523 0.919	2.276 1.195	1909.55 193.42
106	0.000 036	634.368 52 0.001 24	-853.07 -275.63	-4.692 0.756	1.515 0.923	2.274 1.199	1895.14 195.17
108	0.000 052	632.173 12 0.001 75	-848.53 -273.23	-4.649 0.677	1.508 0.927	2.273 1.204	1880.75 196.90
110	0.000 074	629.975 91 0.002 44	-843.98 -270.82	-4.608 0.603	1.502 0.931	2.273 1.208	1866.37 198.61
112	0.000 104	627.776 49 0.003 36	-839.43 -268.41	-4.567 0.532	1.497 0.935	2.274 1.212	1851.99 200.30
114	0.000 144	625.574 51 0.004 56	-834.88 -265.99	-4.526 0.464	1.491 0.940	2.274 1.216	1837.61 201.98
116	0.000 196	623.369 63 0.006 11	-830.33 -263.56	-4.487 0.399	1.487 0.944	2.276 1.221	1823.22 203.63
118	0.000 264	621.161 55 0.008 10	-825.78 -261.13	-4.448 0.337	1.482 0.948	2.278 1.226	1808.81 205.27
120	0.000 352	618.949 97 0.010 62	-821.22 -258.69	-4.410 0.278	1.478 0.953	2.280 1.230	1794.40 206.89
122	0.000 465	616.734 62 0.013 79	-816.66 -256.25	-4.372 0.222	1.475 0.957	2.282 1.235	1779.96 208.49
124	0.000 608	614.515 22 0.017 74	-812.10 -253.80	-4.335 0.168	1.471 0.962	2.284 1.240	1765.51 210.07
126	0.000 787	612.291 49 0.022 60	-807.52 -251.35	-4.298 0.116	1.468 0.967	2.287 1.245	1751.04 211.63
128	0.001 009	610.063 17 0.028 55	-802.95 -248.89	-4.262 0.066	1.465 0.972	2.290 1.251	1736.54 213.17
130	0.001 284	607.829 99 0.035 76	-798.36 -246.43	-4.227 0.019	1.462 0.977	2.293 1.256	1722.03 214.69
132	0.001 620	605.591 68 0.044 45	-793.77 -243.96	-4.192 -0.026	1.459 0.982	2.297 1.262	1707.49 216.19
134	0.002 028	603.347 96 0.054 84	-789.18 -241.50	-4.157 -0.070	1.457 0.987	2.300 1.267	1692.92 217.68
136	0.002 521	601.098 56 0.067 18	-784.57 -239.03	-4.123 -0.112	1.455 0.993	2.304 1.273	1678.34 219.14

TABLE 29. Thermodynamic properties of ethane on the vapor–liquid phase boundary as a function of temperature—Continued

T (K)	p (MPa)	ρ (kg m ⁻³)	h (kJ kg ⁻¹)	s (kJ kg ⁻¹ K ⁻¹)	c_v (kJ kg ⁻¹ K ⁻¹)	c_p (kJ kg ⁻¹ K ⁻¹)	w (m s ⁻¹)
138	0.003 111	598.843 19 0.081 73	−779.96 −236.55	−4.089 −0.152	1.452 0.998	2.307 1.279	1663.73 220.58
140	0.003 814	596.581 56 0.098 80	−775.34 −234.08	−4.056 −0.190	1.450 1.003	2.311 1.284	1649.09 222.01
142	0.004 645	594.313 37 0.118 69	−770.71 −231.61	−4.023 −0.227	1.448 1.008	2.315 1.290	1634.43 223.42
144	0.005 623	592.038 32 0.141 76	−766.08 −229.13	−3.991 −0.262	1.446 1.013	2.319 1.296	1619.75 224.80
146	0.006 766	589.756 10 0.168 36	−761.43 −226.66	−3.959 −0.296	1.445 1.018	2.324 1.301	1605.03 226.17
148	0.008 097	587.466 38 0.198 88	−756.78 −224.18	−3.927 −0.329	1.443 1.022	2.328 1.307	1590.29 227.51
150	0.009 638	585.168 84 0.233 73	−752.12 −221.71	−3.896 −0.360	1.442 1.027	2.333 1.312	1575.53 228.84
152	0.011 413	582.863 12 0.273 35	−747.44 −219.24	−3.865 −0.390	1.440 1.031	2.337 1.317	1560.74 230.14
154	0.013 448	580.548 89 0.318 20	−742.76 −216.77	−3.834 −0.419	1.439 1.036	2.342 1.322	1545.92 231.42
156	0.015 772	578.225 79 0.368 75	−738.07 −214.31	−3.804 −0.447	1.438 1.040	2.347 1.328	1531.07 232.68
158	0.018 414	575.893 43 0.425 52	−733.37 −211.85	−3.774 −0.474	1.437 1.044	2.352 1.333	1516.19 233.91
160	0.021 405	573.551 44 0.489 01	−728.65 −209.40	−3.745 −0.499	1.436 1.048	2.357 1.338	1501.29 235.12
162	0.024 779	571.199 43 0.559 79	−723.93 −206.96	−3.715 −0.524	1.435 1.052	2.363 1.344	1486.35 236.30
164	0.028 570	568.836 98 0.638 42	−719.19 −204.53	−3.686 −0.548	1.435 1.056	2.369 1.349	1471.38 237.45
166	0.032 814	566.463 69 0.725 49	−714.45 −202.10	−3.658 −0.571	1.434 1.061	2.374 1.355	1456.38 238.57
168	0.037 551	564.079 11 0.821 61	−709.69 −199.69	−3.629 −0.594	1.434 1.065	2.381 1.361	1441.35 239.67
170	0.042 819	561.682 81 0.927 42	−704.91 −197.29	−3.601 −0.615	1.433 1.070	2.387 1.368	1426.29 240.73
172	0.048 660	559.274 32 1.043 57	−700.13 −194.91	−3.573 −0.636	1.433 1.075	2.393 1.375	1411.20 241.76
174	0.055 118	556.853 17 1.170 73	−695.33 −192.54	−3.545 −0.656	1.433 1.080	2.400 1.383	1396.07 242.76
176	0.062 235	554.418 86 1.309 60	−690.51 −190.18	−3.518 −0.675	1.433 1.086	2.407 1.391	1380.90 243.72
178	0.070 060	551.970 89 1.460 88	−685.68 −187.85	−3.491 −0.694	1.433 1.092	2.414 1.400	1365.71 244.65
180	0.078 638	549.508 74 1.625 33	−680.84 −185.53	−3.464 −0.712	1.434 1.098	2.421 1.409	1350.47 245.54
182	0.088 019	547.031 86 1.803 68	−675.98 −183.23	−3.437 −0.730	1.434 1.105	2.429 1.419	1335.20 246.39
184	0.098 253	544.539 69 1.996 73	−671.10 −180.95	−3.410 −0.747	1.435 1.112	2.437 1.430	1319.89 247.20

TABLE 29. Thermodynamic properties of ethane on the vapor–liquid phase boundary as a function of temperature—Continued

<i>T</i> (K)	<i>p</i> (MPa)	ρ (kg m ⁻³)	<i>h</i> (kJ kg ⁻¹)	<i>s</i> (kJ kg ⁻¹ K ⁻¹)	c_v (kJ kg ⁻¹ K ⁻¹)	c_p (kJ kg ⁻¹ K ⁻¹)	<i>w</i> (m s ⁻¹)
186	0.109 391	542.031 64 2.205 26	−666.20 −178.69	−3.384 −0.763	1.435 1.119	2.445 1.441	1304.55 247.98
188	0.121 485	539.507 11 2.430 10	−661.29 −176.45	−3.358 −0.779	1.436 1.127	2.454 1.453	1289.17 248.71
190	0.134 591	536.965 48 2.672 08	−656.36 −174.24	−3.332 −0.794	1.437 1.135	2.463 1.466	1273.75 249.41
192	0.148 761	534.406 09 2.932 09	−651.41 −172.04	−3.306 −0.810	1.438 1.143	2.472 1.479	1258.28 250.06
194	0.164 053	531.828 26 3.211 00	−646.44 −169.88	−3.281 −0.824	1.439 1.152	2.482 1.493	1242.78 250.67
196	0.180 524	529.231 30 3.509 73	−641.45 −167.73	−3.255 −0.838	1.441 1.161	2.492 1.507	1227.24 251.24
198	0.198 231	526.614 46 3.829 23	−636.44 −165.61	−3.230 −0.852	1.442 1.170	2.502 1.522	1211.66 251.77
200	0.217 233	523.976 98 4.170 47	−631.41 −163.52	−3.205 −0.865	1.444 1.179	2.512 1.537	1196.04 252.26
202	0.237 590	521.318 06 4.534 44	−626.36 −161.46	−3.180 −0.878	1.445 1.189	2.524 1.553	1180.37 252.70
204	0.259 364	518.636 87 4.922 20	−621.28 −159.42	−3.155 −0.891	1.447 1.198	2.535 1.570	1164.66 253.10
206	0.282 614	515.932 54 5.334 79	−616.18 −157.41	−3.130 −0.903	1.449 1.208	2.547 1.587	1148.91 253.45
208	0.307 404	513.204 15 5.773 35	−611.05 −155.43	−3.106 −0.915	1.452 1.218	2.559 1.604	1133.11 253.76
210	0.333 796	510.450 75 6.239 00	−605.90 −153.48	−3.081 −0.927	1.454 1.228	2.572 1.622	1117.27 254.02
212	0.361 855	507.671 32 6.732 95	−600.71 −151.56	−3.057 −0.939	1.456 1.239	2.586 1.640	1101.38 254.24
214	0.391 644	504.864 82 7.256 44	−595.51 −149.68	−3.033 −0.950	1.459 1.249	2.600 1.659	1085.44 254.41
216	0.423 228	502.030 14 7.810 76	−590.27 −147.83	−3.009 −0.961	1.462 1.259	2.614 1.679	1069.46 254.54
218	0.456 674	499.166 09 8.397 26	−585.00 −146.01	−2.985 −0.971	1.465 1.269	2.629 1.699	1053.42 254.62
220	0.492 046	496.271 45 9.017 35	−579.70 −144.23	−2.961 −0.982	1.468 1.280	2.645 1.720	1037.34 254.65
222	0.529 413	493.344 90 9.672 52	−574.37 −142.49	−2.937 −0.992	1.471 1.290	2.661 1.741	1021.20 254.63
224	0.568 842	490.385 06 10.364 31	−569.01 −140.79	−2.914 −1.002	1.474 1.301	2.678 1.764	1005.01 254.56
226	0.610 401	487.390 45 11.094 37	−563.61 −139.13	−2.890 −1.012	1.478 1.311	2.696 1.786	988.76 254.44
228	0.654 158	484.359 51 11.864 42	−558.17 −137.51	−2.866 −1.021	1.481 1.322	2.715 1.810	972.46 254.27
230	0.700 182	481.290 57 12.676 27	−552.70 −135.94	−2.843 −1.031	1.485 1.333	2.734 1.835	956.09 254.05
232	0.748 545	478.181 85 13.531 88	−547.19 −134.41	−2.820 −1.040	1.489 1.344	2.755 1.861	939.66 253.78

TABLE 29. Thermodynamic properties of ethane on the vapor–liquid phase boundary as a function of temperature—Continued

<i>T</i> (K)	<i>p</i> (MPa)	ρ (kg m ⁻³)	<i>h</i> (kJ kg ⁻¹)	<i>s</i> (kJ kg ⁻¹ K ⁻¹)	c_v (kJ kg ⁻¹ K ⁻¹)	c_p (kJ kg ⁻¹ K ⁻¹)	<i>w</i> (m s ⁻¹)
234	0.799 315	475.031 44 14.433 28	−541.63 −132.93	−2.796 −1.050	1.493 1.355	2.776 1.888	923.17 253.45
236	0.852 564	471.837 30 15.382 66	−536.04 −131.51	−2.773 −1.059	1.498 1.366	2.799 1.916	906.60 253.07
238	0.908 364	468.597 23 16.382 36	−530.40 −130.13	−2.750 −1.068	1.502 1.377	2.822 1.945	889.97 252.64
240	0.966 788	465.308 87 17.434 87	−524.72 −128.82	−2.726 −1.077	1.507 1.388	2.847 1.976	873.25 252.14
242	1.027 908	461.969 65 18.542 86	−518.98 −127.56	−2.703 −1.086	1.512 1.400	2.873 2.009	856.45 251.59
244	1.091 798	458.576 80 19.709 22	−513.20 −126.36	−2.680 −1.094	1.517 1.412	2.901 2.043	839.57 250.98
246	1.158 534	455.127 32 20.937 06	−507.37 −125.23	−2.657 −1.103	1.522 1.423	2.930 2.080	822.59 250.31
248	1.228 191	451.617 92 22.229 75	−501.48 −124.17	−2.633 −1.112	1.528 1.436	2.961 2.119	805.51 249.58
250	1.300 845	448.045 02 23.590 94	−495.53 −123.18	−2.610 −1.121	1.533 1.448	2.994 2.160	788.33 248.79
252	1.376 574	444.404 71 25.024 63	−489.52 −122.27	−2.587 −1.129	1.539 1.461	3.029 2.205	771.03 247.93
254	1.455 457	440.692 67 26.535 17	−483.45 −121.43	−2.564 −1.138	1.546 1.474	3.066 2.252	753.60 247.00
256	1.537 574	436.904 16 28.127 37	−477.32 −120.68	−2.540 −1.147	1.552 1.488	3.106 2.303	736.05 246.01
258	1.623 006	433.033 93 29.806 50	−471.11 −120.03	−2.517 −1.156	1.559 1.502	3.149 2.358	718.36 244.95
260	1.711 835	429.076 17 31.578 45	−464.83 −119.47	−2.493 −1.165	1.566 1.516	3.195 2.418	700.52 243.81
262	1.804 148	425.024 40 33.449 73	−458.47 −119.01	−2.470 −1.174	1.573 1.531	3.244 2.483	682.53 242.61
264	1.900 029	420.871 38 35.427 65	−452.02 −118.66	−2.446 −1.183	1.580 1.546	3.298 2.554	664.38 241.33
266	1.999 567	416.608 96 37.520 45	−445.49 −118.44	−2.422 −1.193	1.588 1.562	3.356 2.632	646.06 239.97
268	2.102 853	412.227 93 39.737 43	−438.86 −118.34	−2.399 −1.203	1.597 1.578	3.420 2.719	627.58 238.54
270	2.209 980	407.717 76 42.089 22	−432.13 −118.38	−2.375 −1.212	1.605 1.595	3.491 2.815	608.92 237.02
272	2.321 044	403.066 36 44.587 99	−425.28 −118.56	−2.350 −1.223	1.614 1.613	3.568 2.922	590.08 235.42
274	2.436 146	398.259 65 47.247 85	−418.32 −118.92	−2.326 −1.233	1.624 1.632	3.655 3.043	571.04 233.73
276	2.555 389	393.281 18 50.085 27	−411.23 −119.45	−2.301 −1.244	1.633 1.652	3.752 3.181	551.77 231.95
278	2.678 881	388.111 45 53.119 68	−403.99 −120.19	−2.276 −1.255	1.644 1.673	3.862 3.339	532.23 230.07
280	2.806 736	382.727 12 56.374 28	−396.59 −121.14	−2.251 −1.267	1.654 1.696	3.987 3.522	512.38 228.10

TABLE 29. Thermodynamic properties of ethane on the vapor–liquid phase boundary as a function of temperature—Continued

<i>T</i> (K)	<i>p</i> (MPa)	<i>ρ</i> (kg m ⁻³)	<i>h</i> (kJ kg ⁻¹)	<i>s</i> (kJ kg ⁻¹ K ⁻¹)	<i>c_v</i> (kJ kg ⁻¹ K ⁻¹)	<i>c_p</i> (kJ kg ⁻¹ K ⁻¹)	<i>w</i> (m s ⁻¹)
282	2.939 073	377.099 93	−389.02	−2.225	1.666	4.132	492.15
		59.877 13	−122.34	−1.279	1.720	3.737	226.01
284	3.076 020	371.195 12	−381.24	−2.199	1.678	4.303	471.46
		63.662 74	−123.83	−1.293	1.745	3.992	223.82
286	3.217 713	364.969 23	−373.24	−2.172	1.692	4.506	450.22
		67.774 29	−125.64	−1.306	1.773	4.300	221.51
288	3.364 299	358.366 67	−364.98	−2.145	1.708	4.753	428.34
		72.267 04	−127.82	−1.321	1.803	4.681	219.07
290	3.515 942	351.314 40	−356.42	−2.117	1.727	5.061	405.70
		77.213 56	−130.45	−1.337	1.835	5.162	216.50
292	3.672 818	343.713 15	−347.48	−2.088	1.749	5.459	382.18
		82.712 39	−133.61	−1.355	1.871	5.791	213.78
294	3.835 131	335.422 19	−338.08	−2.057	1.776	5.995	357.64
		88.903 01	−137.44	−1.375	1.912	6.648	210.88
296	4.003 112	326.230 70	−328.10	−2.025	1.809	6.757	331.84
		95.994 15	−142.14	−1.397	1.959	7.885	207.77
298	4.177 038	315.798 16	−317.30	−1.990	1.852	7.937	304.47
		104.323 07	−148.01	−1.422	2.016	9.826	204.37
300	4.357 255	303.508 79	−305.32	−1.952	1.912	10.022	274.91
		114.500 91	−155.61	−1.453	2.089	13.299	200.51
301	4.449 861	296.305 93	−298.65	−1.931	1.952	11.815	258.98
		120.643 14	−160.39	−1.472	2.136	16.304	198.29
302	4.544 230	288.016 28	−291.29	−1.908	2.005	14.743	241.95
		127.867 74	−166.17	−1.493	2.194	21.215	195.74
303	4.640 463	278.032 97	−282.87	−1.881	2.079	20.373	223.34
		136.781 05	−173.47	−1.520	2.270	30.602	192.59
304	4.738 705	264.891 19	−272.44	−1.848	2.197	35.385	202.16
		148.851 27	−183.59	−1.556	2.386	55.117	188.14
305	4.839 225	241.961 49	−255.73	−1.794	2.470	164.093	175.12
		170.754 82	−202.19	−1.619	2.623	247.460	178.83
305.322 ^c	4.872 200	206.180 00	−230.72	−1.713			

^aFor each temperature, the values on the first line correspond to the saturated-liquid line and the values on the second line correspond to the saturated-vapor line.

^bTriple point.

^cCritical point.

TABLE 30. Thermodynamic properties of ethane in the single-phase region

<i>T</i> (K)	<i>ρ</i> (kg m ⁻³)	<i>u</i> (kJ kg ⁻¹)	<i>h</i> (kJ kg ⁻¹)	<i>s</i> (kJ kg ⁻¹ K ⁻¹)	<i>c_v</i> (kJ kg ⁻¹ K ⁻¹)	<i>c_p</i> (kJ kg ⁻¹ K ⁻¹)	<i>w</i> (m s ⁻¹)
0.1 MPa							
90.384 ^a	651.55	-888.88	-888.73	-5.0574	1.6051	2.3256	2008.97
95	646.47	-878.21	-878.06	-4.9423	1.5694	2.2990	1975.17
100	640.99	-866.77	-866.61	-4.8249	1.5407	2.2826	1938.83
105	635.51	-855.38	-855.22	-4.7137	1.5191	2.2749	1902.75
110	630.02	-844.01	-843.85	-4.6079	1.5024	2.2730	1866.79
115	624.52	-832.64	-832.48	-4.5069	1.4892	2.2749	1830.85
120	619.00	-821.26	-821.10	-4.4100	1.4785	2.2794	1794.85
125	613.45	-809.85	-809.69	-4.3168	1.4696	2.2856	1758.75
130	607.88	-798.40	-798.24	-4.2270	1.4622	2.2932	1722.52
135	602.28	-786.92	-786.75	-4.1403	1.4558	2.3017	1686.14
140	596.64	-775.39	-775.22	-4.0564	1.4503	2.3111	1649.61
145	590.96	-763.81	-763.64	-3.9751	1.4457	2.3213	1612.93
150	585.23	-752.18	-752.01	-3.8963	1.4418	2.3323	1576.07
155	579.45	-740.49	-740.32	-3.8196	1.4387	2.3443	1539.03
160	573.61	-728.74	-728.56	-3.7450	1.4362	2.3572	1501.80
165	567.71	-716.92	-716.74	-3.6722	1.4345	2.3712	1464.37
170	561.73	-705.03	-704.85	-3.6012	1.4335	2.3865	1426.71
175	555.67	-693.05	-692.87	-3.5318	1.4332	2.4032	1388.81
180	549.53	-681.00	-680.81	-3.4638	1.4337	2.4214	1350.64
184.33 ^b	544.13	-670.49	-670.30	-3.4062	1.4347	2.4385	1317.40
184.33 ^c	2.0295	-229.85	-180.58	-0.749 30	1.1128	1.4317	247.33
185	2.0213	-229.09	-179.61	-0.744 07	1.1143	1.4327	247.80
190	1.9626	-223.38	-172.43	-0.705 76	1.1260	1.4405	251.25
195	1.9075	-217.63	-165.21	-0.668 24	1.1376	1.4485	254.61
200	1.8557	-211.83	-157.94	-0.631 46	1.1491	1.4570	257.90
210	1.7608	-200.08	-143.28	-0.559 92	1.1735	1.4762	264.25
220	1.6757	-188.09	-128.41	-0.490 74	1.2002	1.4989	270.34
230	1.5989	-175.84	-113.29	-0.423 55	1.2292	1.5249	276.18
240	1.5291	-163.30	-97.903	-0.358 05	1.2604	1.5535	281.81
250	1.4654	-150.45	-82.215	-0.294 01	1.2933	1.5845	287.25
260	1.4070	-137.28	-66.207	-0.231 23	1.3279	1.6174	292.53
270	1.3532	-123.76	-49.861	-0.169 55	1.3639	1.6521	297.65
280	1.3035	-109.88	-33.161	-0.108 82	1.4012	1.6882	302.63
290	1.2573	-95.626	-16.092	-0.048 93	1.4397	1.7256	307.49
300	1.2144	-80.987	1.3561	0.010 223	1.4791	1.7642	312.23
310	1.1744	-65.954	19.195	0.068 713	1.5194	1.8037	316.88
320	1.1370	-50.518	37.433	0.126 61	1.5604	1.8441	321.43
330	1.1019	-34.673	56.079	0.183 99	1.6020	1.8851	325.89
340	1.0690	-18.411	75.137	0.240 88	1.6440	1.9266	330.28
350	1.0380	-1.7298	94.612	0.297 33	1.6864	1.9686	334.59
360	1.0087	15.375	114.51	0.353 38	1.7291	2.0109	338.84
370	0.981 12	32.906	134.83	0.409 05	1.7720	2.0533	343.02
380	0.954 99	50.864	155.58	0.464 38	1.8149	2.0960	347.15
390	0.930 23	69.250	176.75	0.519 37	1.8579	2.1386	351.22
400	0.906 74	88.063	198.35	0.574 05	1.9007	2.1812	355.24
425	0.852 93	136.96	254.20	0.709 47	2.0072	2.2871	365.07
450	0.805 18	188.50	312.69	0.843 16	2.1122	2.3916	374.65
475	0.762 53	242.62	373.77	0.975 22	2.2150	2.4940	383.97
500	0.724 20	299.29	437.37	1.1057	2.3153	2.5941	393.08
525	0.689 55	358.42	503.45	1.2346	2.4130	2.6915	401.99
550	0.658 07	419.97	571.92	1.3620	2.5079	2.7862	410.71
575	0.629 36	483.84	642.73	1.4879	2.6001	2.8782	419.25
600	0.603 05	549.99	715.81	1.6123	2.6895	2.9674	427.63
625	0.578 86	618.33	791.08	1.7352	2.7762	3.0539	435.85
650	0.556 54	688.80	868.48	1.8566	2.8602	3.1379	443.92
675	0.535 89	761.35	947.95	1.9766	2.9418	3.2193	451.85

TABLE 30. Thermodynamic properties of ethane in the single-phase region—Continued

<i>T</i> (K)	<i>ρ</i> (kg m ⁻³)	<i>u</i> (kJ kg ⁻¹)	<i>h</i> (kJ kg ⁻¹)	<i>s</i> (kJ kg ⁻¹ K ⁻¹)	<i>c_v</i> (kJ kg ⁻¹ K ⁻¹)	<i>c_p</i> (kJ kg ⁻¹ K ⁻¹)	<i>w</i> (m s ⁻¹)
0.5 MPa							
90.449 ^a	651.62	-888.83	-888.06	-5.0568	1.6050	2.3250	2010.12
95	646.62	-878.31	-877.54	-4.9434	1.5699	2.2987	1976.74
100	641.15	-866.87	-866.09	-4.8259	1.5412	2.2823	1940.41
105	635.67	-855.49	-854.70	-4.7148	1.5196	2.2745	1904.36
110	630.19	-844.13	-843.34	-4.6090	1.5029	2.2725	1868.46
115	624.70	-832.77	-831.97	-4.5080	1.4897	2.2744	1832.59
120	619.19	-821.40	-820.59	-4.4111	1.4790	2.2788	1796.66
125	613.65	-810.00	-809.18	-4.3180	1.4701	2.2850	1760.64
130	608.09	-798.56	-797.74	-4.2282	1.4627	2.2924	1724.50
135	602.50	-787.09	-786.26	-4.1415	1.4563	2.3009	1688.21
140	596.87	-775.57	-774.73	-4.0577	1.4509	2.3102	1651.78
145	591.20	-764.00	-763.15	-3.9765	1.4463	2.3203	1615.20
150	585.49	-752.38	-751.52	-3.8976	1.4424	2.3312	1578.45
155	579.72	-740.70	-739.84	-3.8210	1.4392	2.3430	1541.53
160	573.90	-728.96	-728.09	-3.7464	1.4368	2.3558	1504.43
165	568.01	-717.16	-716.28	-3.6737	1.4350	2.3696	1467.13
170	562.06	-705.28	-704.39	-3.6027	1.4340	2.3847	1429.61
175	556.02	-693.33	-692.43	-3.5334	1.4337	2.4012	1391.87
180	549.90	-681.29	-680.38	-3.4655	1.4342	2.4191	1353.88
185	543.68	-669.16	-668.24	-3.3989	1.4355	2.4387	1315.61
190	537.35	-656.92	-655.99	-3.3336	1.4375	2.4602	1277.05
195	530.90	-644.57	-643.63	-3.2694	1.4404	2.4839	1238.16
200	524.32	-632.10	-631.15	-3.2062	1.4441	2.5098	1198.92
210	510.69	-606.74	-605.76	-3.0823	1.4541	2.5702	1119.19
220	496.28	-580.70	-579.70	-2.9611	1.4677	2.6448	1037.44
220.43 ^b	495.64	-579.55	-578.55	-2.9559	1.4683	2.6484	1033.83
220.43 ^c	9.1568	-198.45	-143.85	-0.983 90	1.2822	1.7246	254.65
230	8.6361	-185.44	-127.54	-0.911 47	1.2847	1.6923	262.24
240	8.1679	-171.88	-110.66	-0.839 62	1.3026	1.6869	269.53
250	7.7584	-158.21	-93.762	-0.770 65	1.3267	1.6941	276.34
260	7.3953	-144.36	-76.750	-0.703 93	1.3549	1.7094	282.75
270	7.0698	-130.28	-59.555	-0.639 03	1.3861	1.7304	288.84
280	6.7757	-115.92	-42.127	-0.575 65	1.4198	1.7559	294.66
290	6.5080	-101.25	-24.425	-0.513 54	1.4554	1.7849	300.25
300	6.2629	-86.256	-6.4202	-0.452 50	1.4926	1.8166	305.63
310	6.0373	-70.905	11.913	-0.392 39	1.5312	1.8504	310.84
320	5.8288	-55.187	30.594	-0.333 09	1.5707	1.8860	315.90
330	5.6353	-39.089	49.637	-0.274 49	1.6111	1.9230	320.81
340	5.4552	-22.599	69.057	-0.216 52	1.6522	1.9611	325.61
350	5.2870	-5.7105	88.862	-0.159 11	1.6938	2.0001	330.29
360	5.1294	11.583	109.06	-0.102 21	1.7358	2.0397	334.87
370	4.9815	29.287	129.66	-0.045 78	1.7781	2.0799	339.36
380	4.8423	47.405	150.66	0.010 229	1.8205	2.1205	343.77
390	4.7111	65.938	172.07	0.065 838	1.8630	2.1614	348.10
400	4.5871	84.888	193.89	0.121 08	1.9055	2.2024	352.35
425	4.3050	134.09	250.23	0.257 67	2.0111	2.3050	362.71
450	4.0566	185.87	309.13	0.392 31	2.1155	2.4068	372.70
475	3.8362	240.22	370.56	0.525 13	2.2178	2.5071	382.39
500	3.6390	297.07	434.47	0.656 24	2.3177	2.6055	391.80
525	3.4616	356.37	500.81	0.785 70	2.4151	2.7015	400.96
550	3.3010	418.05	569.53	0.913 54	2.5098	2.7951	409.90
575	3.1549	482.06	640.54	1.0398	2.6017	2.8861	418.63
600	3.0213	548.32	713.81	1.1645	2.6910	2.9745	427.17
625	2.8988	616.76	789.25	1.2877	2.7775	3.0603	435.53
650	2.7859	687.33	866.80	1.4093	2.8614	3.1437	443.73
675	2.6816	759.96	946.41	1.5295	2.9428	3.2245	451.77

TABLE 30. Thermodynamic properties of ethane in the single-phase region—Continued

<i>T</i> (K)	<i>ρ</i> (kg m ⁻³)	<i>u</i> (kJ kg ⁻¹)	<i>h</i> (kJ kg ⁻¹)	<i>s</i> (kJ kg ⁻¹ K ⁻¹)	<i>c_v</i> (kJ kg ⁻¹ K ⁻¹)	<i>c_p</i> (kJ kg ⁻¹ K ⁻¹)	<i>w</i> (m s ⁻¹)
1 MPa							
90.529 ^a	651.71	−888.76	−887.22	−5.0561	1.6049	2.3241	2011.53
95	646.81	−878.44	−876.89	−4.9447	1.5706	2.2984	1978.69
100	641.34	−867.01	−865.45	−4.8273	1.5419	2.2818	1942.37
105	635.88	−855.63	−854.06	−4.7161	1.5202	2.2740	1906.37
110	630.41	−844.28	−842.70	−4.6104	1.5035	2.2719	1870.55
115	624.93	−832.93	−831.33	−4.5094	1.4903	2.2737	1834.76
120	619.43	−821.57	−819.96	−4.4125	1.4796	2.2780	1798.93
125	613.90	−810.18	−808.55	−4.3194	1.4708	2.2841	1763.00
130	608.36	−798.76	−797.11	−4.2297	1.4633	2.2915	1726.96
135	602.78	−787.29	−785.63	−4.1431	1.4569	2.2998	1690.79
140	597.16	−775.79	−774.11	−4.0593	1.4515	2.3090	1654.48
145	591.51	−764.23	−762.54	−3.9781	1.4469	2.3190	1618.03
150	585.81	−752.63	−750.92	−3.8993	1.4430	2.3298	1581.41
155	580.06	−740.97	−739.24	−3.8227	1.4399	2.3414	1544.64
160	574.26	−729.25	−727.51	−3.7482	1.4375	2.3540	1507.69
165	568.40	−717.46	−715.70	−3.6755	1.4357	2.3677	1470.56
170	562.46	−705.60	−703.83	−3.6046	1.4347	2.3825	1433.23
175	556.45	−693.67	−691.87	−3.5353	1.4344	2.3987	1395.68
180	550.36	−681.65	−679.84	−3.4675	1.4349	2.4163	1357.89
185	544.17	−669.55	−667.71	−3.4011	1.4361	2.4356	1319.85
190	537.87	−657.34	−655.48	−3.3358	1.4382	2.4567	1281.54
195	531.46	−645.02	−643.14	−3.2717	1.4410	2.4798	1242.92
200	524.92	−632.58	−630.68	−3.2086	1.4447	2.5053	1203.96
210	511.39	−607.29	−605.34	−3.0850	1.4546	2.5641	1124.92
220	497.12	−581.36	−579.35	−2.9641	1.4681	2.6365	1044.02
230	481.89	−554.62	−552.55	−2.8450	1.4854	2.7275	960.67
240	465.39	−526.86	−524.71	−2.7265	1.5070	2.8460	873.85
241.10 ^b	463.48	−523.73	−521.57	−2.7135	1.5097	2.8614	864.04
241.10 ^c	18.036	−183.56	−128.12	−1.0816	1.3945	1.9938	251.85
250	16.948	−169.78	−110.77	−1.0109	1.3866	1.9154	260.39
260	15.930	−154.60	−91.822	−0.93658	1.4001	1.8798	268.91
270	15.066	−139.47	−73.099	−0.865 91	1.4220	1.8676	276.67
280	14.317	−124.27	−54.425	−0.798 00	1.4489	1.8691	283.85
290	13.656	−108.91	−35.686	−0.732 24	1.4793	1.8799	290.57
300	13.067	−93.335	−16.803	−0.668 23	1.5126	1.8977	296.92
310	12.535	−77.489	2.2842	−0.605 64	1.5480	1.9206	302.96
320	12.053	−61.343	21.622	−0.544 25	1.5852	1.9475	308.73
330	11.612	−44.870	41.244	−0.483 87	1.6237	1.9774	314.29
340	11.207	−28.050	61.179	−0.424 37	1.6633	2.0097	319.64
350	10.833	−10.866	81.445	−0.365 62	1.7036	2.0439	324.83
360	10.486	6.6930	102.06	−0.307 55	1.7446	2.0794	329.86
370	10.163	24.637	123.04	−0.250 07	1.7860	2.1161	334.76
380	9.8607	42.973	144.39	−0.193 15	1.8277	2.1536	339.54
390	9.5779	61.705	166.11	−0.136 71	1.8695	2.1918	344.20
400	9.3123	80.839	188.22	−0.080 73	1.9115	2.2305	348.76
425	8.7131	130.44	245.21	0.057 420	2.0161	2.3283	359.78
450	8.1912	182.56	304.64	0.193 28	2.1196	2.4265	370.32
475	7.7316	237.19	366.53	0.327 10	2.2213	2.5240	380.45
500	7.3232	294.28	430.83	0.459 01	2.3208	2.6201	390.24
525	6.9577	353.79	497.52	0.589 13	2.4177	2.7143	399.72
550	6.6282	415.66	566.53	0.717 54	2.5121	2.8063	408.93
575	6.3296	479.82	637.81	0.844 27	2.6038	2.8960	417.89
600	6.0575	546.23	711.31	0.969 38	2.6928	2.9834	426.64
625	5.8085	614.80	786.96	1.0929	2.7791	3.0683	435.17
650	5.5796	685.48	864.71	1.2149	2.8629	3.1509	443.52
675	5.3685	758.22	944.49	1.3353	2.9442	3.2311	451.70

TABLE 30. Thermodynamic properties of ethane in the single-phase region—Continued

<i>T</i> (K)	<i>ρ</i> (kg m ⁻³)	<i>u</i> (kJ kg ⁻¹)	<i>h</i> (kJ kg ⁻¹)	<i>s</i> (kJ kg ⁻¹ K ⁻¹)	<i>c_v</i> (kJ kg ⁻¹ K ⁻¹)	<i>c_p</i> (kJ kg ⁻¹ K ⁻¹)	<i>w</i> (m s ⁻¹)
1.5 MPa							
90.609 ^a	651.80	-888.69	-886.38	-5.0553	1.6048	2.3233	2012.92
95	647.00	-878.56	-876.24	-4.9460	1.5712	2.2980	1980.63
100	641.54	-867.14	-864.80	-4.8286	1.5425	2.2814	1944.32
105	636.08	-855.77	-853.41	-4.7175	1.5209	2.2735	1908.38
110	630.62	-844.43	-842.05	-4.6118	1.5041	2.2713	1872.62
115	625.15	-833.09	-830.70	-4.5108	1.4909	2.2730	1836.92
120	619.66	-821.74	-819.32	-4.4140	1.4802	2.2773	1801.18
125	614.15	-810.36	-807.92	-4.3209	1.4714	2.2833	1765.36
130	608.62	-798.95	-796.49	-4.2312	1.4639	2.2906	1729.43
135	603.05	-787.50	-785.01	-4.1446	1.4576	2.2988	1693.37
140	597.45	-776.01	-773.50	-4.0609	1.4522	2.3079	1657.17
145	591.81	-764.47	-761.93	-3.9797	1.4476	2.3177	1620.84
150	586.13	-752.88	-750.32	-3.9009	1.4437	2.3284	1584.37
155	580.40	-741.23	-738.65	-3.8244	1.4406	2.3399	1547.74
160	574.62	-729.53	-726.92	-3.7499	1.4381	2.3523	1510.94
165	568.78	-717.76	-715.12	-3.6773	1.4364	2.3657	1473.97
170	562.86	-705.92	-703.26	-3.6065	1.4354	2.3804	1436.81
175	556.88	-694.01	-691.32	-3.5373	1.4351	2.3963	1399.45
180	550.81	-682.02	-679.29	-3.4695	1.4356	2.4136	1361.87
185	544.65	-669.93	-667.18	-3.4032	1.4368	2.4325	1324.06
190	538.39	-657.75	-654.96	-3.3380	1.4389	2.4532	1285.98
195	532.02	-645.46	-642.64	-3.2740	1.4417	2.4759	1247.62
200	525.52	-633.06	-630.20	-3.2110	1.4454	2.5008	1208.96
210	512.08	-607.85	-604.92	-3.0876	1.4552	2.5583	1130.57
220	497.93	-582.01	-578.99	-2.9671	1.4686	2.6286	1050.48
230	482.88	-555.39	-552.29	-2.8484	1.4857	2.7164	968.17
240	466.61	-527.80	-524.58	-2.7305	1.5069	2.8296	882.75
250	448.67	-498.90	-495.56	-2.6120	1.5331	2.9837	792.63
255.09 ^b	438.63	-483.52	-480.10	-2.5508	1.5490	3.0876	744.01
255.09 ^c	27.396	-175.76	-121.01	-1.1431	1.4816	2.2796	246.47
260	26.286	-167.15	-110.09	-1.1007	1.4678	2.1833	252.28
270	24.418	-150.27	-88.837	-1.0205	1.4691	2.0801	262.68
280	22.907	-133.79	-68.310	-0.945 85	1.4853	2.0310	271.80
290	21.639	-117.45	-48.130	-0.875 03	1.5085	2.0085	280.02
300	20.548	-101.08	-28.085	-0.807 07	1.5362	2.0027	287.59
310	19.593	-84.595	-8.0381	-0.741 34	1.5675	2.0082	294.64
320	18.745	-67.913	12.107	-0.677 38	1.6015	2.0220	301.26
330	17.985	-50.983	32.421	-0.614 88	1.6376	2.0417	307.54
340	17.296	-33.770	52.956	-0.553 57	1.6752	2.0659	313.53
350	16.668	-16.243	73.751	-0.493 30	1.7141	2.0935	319.27
360	16.092	1.6197	94.835	-0.433 90	1.7538	2.1237	324.80
370	15.561	19.834	116.23	-0.375 28	1.7942	2.1560	330.13
380	15.068	38.412	137.96	-0.317 34	1.8351	2.1897	335.30
390	14.611	57.365	160.03	-0.260 01	1.8762	2.2247	340.31
400	14.183	76.698	182.46	-0.203 24	1.9175	2.2606	345.20
425	13.228	126.73	240.12	-0.063 43	2.0210	2.3529	356.90
450	12.405	179.20	300.12	0.073 715	2.1237	2.4470	367.99
475	11.687	234.12	362.47	0.208 55	2.2247	2.5414	378.57
500	11.053	291.47	427.18	0.341 29	2.3237	2.6351	388.74
525	10.488	351.19	494.21	0.472 10	2.4203	2.7273	398.54
550	9.9812	413.25	563.53	0.601 07	2.5144	2.8177	408.02
575	9.5236	477.58	635.08	0.728 28	2.6058	2.9061	417.21
600	9.1080	544.13	708.82	0.853 79	2.6946	2.9924	426.15
625	8.7286	612.84	784.68	0.977 66	2.7808	3.0764	434.87
650	8.3806	683.64	862.62	1.0999	2.8644	3.1581	443.37
675	8.0602	756.47	942.57	1.2206	2.9455	3.2377	451.67

TABLE 30. Thermodynamic properties of ethane in the single-phase region—Continued

<i>T</i> (K)	<i>ρ</i> (kg m ⁻³)	<i>u</i> (kJ kg ⁻¹)	<i>h</i> (kJ kg ⁻¹)	<i>s</i> (kJ kg ⁻¹ K ⁻¹)	<i>c_v</i> (kJ kg ⁻¹ K ⁻¹)	<i>c_p</i> (kJ kg ⁻¹ K ⁻¹)	<i>w</i> (m s ⁻¹)
2 MPa							
90.690 ^a	651.89	-888.62	-885.55	-5.0545	1.6048	2.3225	2014.28
95	647.18	-878.68	-875.59	-4.9473	1.5719	2.2977	1982.55
100	641.73	-867.27	-864.15	-4.8299	1.5431	2.2810	1946.26
105	636.29	-855.91	-852.77	-4.7188	1.5215	2.2730	1910.38
110	630.84	-844.58	-841.41	-4.6132	1.5048	2.2707	1874.70
115	625.38	-833.25	-830.06	-4.5122	1.4915	2.2724	1839.08
120	619.90	-821.91	-818.69	-4.4154	1.4808	2.2765	1803.43
125	614.40	-810.54	-807.29	-4.3224	1.4720	2.2825	1767.71
130	608.88	-799.14	-795.86	-4.2327	1.4646	2.2896	1731.88
135	603.33	-787.71	-784.39	-4.1461	1.4582	2.2978	1695.93
140	597.74	-776.23	-772.88	-4.0624	1.4528	2.3067	1659.86
145	592.12	-764.70	-761.32	-3.9813	1.4482	2.3165	1623.65
150	586.45	-753.12	-749.71	-3.9026	1.4444	2.3270	1587.30
155	580.74	-741.49	-738.05	-3.8261	1.4412	2.3383	1550.81
160	574.98	-729.81	-726.33	-3.7517	1.4388	2.3506	1514.17
165	569.15	-718.06	-714.54	-3.6792	1.4371	2.3638	1477.36
170	563.26	-706.24	-702.69	-3.6084	1.4361	2.3782	1440.38
175	557.30	-694.35	-690.76	-3.5392	1.4358	2.3939	1403.21
180	551.26	-682.38	-678.75	-3.4715	1.4363	2.4109	1365.83
185	545.13	-670.32	-666.65	-3.4052	1.4375	2.4295	1328.23
190	538.90	-658.16	-654.45	-3.3402	1.4395	2.4499	1290.39
195	532.57	-645.90	-642.14	-3.2763	1.4424	2.4721	1252.28
200	526.11	-633.53	-629.72	-3.2134	1.4460	2.4964	1213.90
210	512.76	-608.39	-604.49	-3.0903	1.4558	2.5526	1136.15
220	498.74	-582.64	-578.63	-2.9700	1.4691	2.6210	1056.85
230	483.84	-556.15	-552.01	-2.8517	1.4860	2.7058	975.52
240	467.80	-528.71	-524.44	-2.7343	1.5069	2.8141	891.42
250	450.19	-500.05	-495.61	-2.6167	1.5326	2.9593	803.18
260	430.26	-469.69	-465.04	-2.4968	1.5645	3.1702	708.23
266.01 ^b	416.59	-450.26	-445.46	-2.4224	1.5884	3.3567	645.98
266.01 ^c	37.530	-171.73	-118.44	-1.1930	1.5619	2.6328	239.97
270	36.030	-163.75	-108.24	-1.1549	1.5427	2.4845	245.72
280	33.056	-145.02	-84.520	-1.0686	1.5330	2.2873	257.97
290	30.770	-127.17	-62.171	-0.990 21	1.5442	2.1928	268.34
300	28.911	-109.69	-40.516	-0.916 79	1.5643	2.1437	277.51
310	27.348	-92.345	-19.212	-0.846 94	1.5901	2.1204	285.81
320	26.000	-74.975	1.9469	-0.779 76	1.6199	2.1137	293.45
330	24.819	-57.482	23.100	-0.714 67	1.6529	2.1185	300.57
340	23.770	-39.796	44.344	-0.651 25	1.6882	2.1314	307.28
350	22.828	-21.866	65.747	-0.589 21	1.7252	2.1502	313.63
360	21.974	-3.6543	87.363	-0.528 32	1.7635	2.1735	319.68
370	21.195	14.866	109.23	-0.468 41	1.8027	2.2000	325.49
380	20.480	33.715	131.37	-0.409 36	1.8427	2.2292	331.07
390	19.820	52.909	153.82	-0.351 06	1.8830	2.2602	336.46
400	19.208	72.460	176.58	-0.293 42	1.9237	2.2928	341.67
425	17.854	122.95	234.97	-0.151 87	2.0260	2.3788	354.07
450	16.701	175.80	295.55	-0.013 37	2.1278	2.4684	365.72
475	15.702	231.03	358.40	0.122 52	2.2282	2.5594	376.77
500	14.827	288.63	423.52	0.256 12	2.3267	2.6504	387.31
525	14.052	348.58	490.91	0.387 62	2.4229	2.7406	397.42
550	13.360	410.83	560.54	0.517 16	2.5166	2.8293	407.17
575	12.736	475.33	632.36	0.644 86	2.6078	2.9163	416.59
600	12.172	542.03	706.34	0.770 78	2.6964	3.0014	425.73
625	11.658	610.87	782.42	0.895 00	2.7824	3.0845	434.61
650	11.188	681.79	860.55	1.0176	2.8658	3.1654	443.25
675	10.756	754.73	940.67	1.1385	2.9468	3.2442	451.69

TABLE 30. Thermodynamic properties of ethane in the single-phase region—Continued

<i>T</i> (K)	<i>ρ</i> (kg m ⁻³)	<i>u</i> (kJ kg ⁻¹)	<i>h</i> (kJ kg ⁻¹)	<i>s</i> (kJ kg ⁻¹ K ⁻¹)	<i>c_v</i> (kJ kg ⁻¹ K ⁻¹)	<i>c_p</i> (kJ kg ⁻¹ K ⁻¹)	<i>w</i> (m s ⁻¹)
3 MPa							
90.850 ^a	652.07	-888.48	-883.87	-5.0530	1.6047	2.3209	2016.96
95	647.55	-878.93	-874.30	-4.9499	1.5732	2.2970	1986.36
100	642.12	-867.53	-862.86	-4.8325	1.5444	2.2801	1950.12
105	636.70	-856.19	-851.48	-4.7215	1.5227	2.2720	1914.35
110	631.27	-844.88	-840.13	-4.6159	1.5060	2.2696	1878.82
115	625.83	-833.57	-828.78	-4.5150	1.4928	2.2711	1843.37
120	620.37	-822.25	-817.41	-4.4183	1.4821	2.2751	1807.91
125	614.90	-810.90	-806.03	-4.3253	1.4732	2.2808	1772.38
130	609.40	-799.53	-794.60	-4.2357	1.4658	2.2878	1736.76
135	603.87	-788.11	-783.15	-4.1492	1.4595	2.2958	1701.03
140	598.32	-776.66	-771.64	-4.0655	1.4541	2.3045	1665.19
145	592.72	-765.16	-760.10	-3.9845	1.4495	2.3140	1629.23
150	587.09	-753.61	-748.50	-3.9059	1.4457	2.3243	1593.14
155	581.41	-742.01	-736.85	-3.8295	1.4426	2.3353	1556.93
160	575.69	-730.36	-725.15	-3.7552	1.4402	2.3472	1520.58
165	569.90	-718.64	-713.38	-3.6828	1.4384	2.3601	1484.09
170	564.06	-706.86	-701.55	-3.6121	1.4374	2.3741	1447.45
175	558.14	-695.01	-689.64	-3.5431	1.4372	2.3893	1410.64
180	552.16	-683.08	-677.65	-3.4755	1.4376	2.4058	1373.65
185	546.08	-671.07	-665.58	-3.4094	1.4389	2.4237	1336.47
190	539.92	-658.97	-653.41	-3.3445	1.4409	2.4433	1299.08
195	533.65	-646.76	-641.14	-3.2807	1.4437	2.4647	1261.48
200	527.26	-634.45	-628.76	-3.2180	1.4473	2.4881	1223.62
210	514.10	-609.46	-603.62	-3.0954	1.4570	2.5417	1147.10
220	500.31	-583.89	-577.89	-2.9757	1.4700	2.6064	1069.28
230	485.72	-557.62	-551.44	-2.8582	1.4867	2.6859	989.81
240	470.10	-530.49	-524.11	-2.7418	1.5071	2.7856	908.11
250	453.09	-502.25	-495.63	-2.6256	1.5317	2.9157	823.20
260	434.11	-472.54	-465.63	-2.5080	1.5617	3.0963	733.32
270	412.09	-440.67	-433.39	-2.3863	1.5996	3.3757	635.17
280	384.46	-405.10	-397.29	-2.2551	1.6515	3.9166	521.43
282.90 ^b	374.48	-393.56	-385.55	-2.2134	1.6713	4.2054	482.92
282.90 ^c	61.540	-171.72	-122.97	-1.2852	1.7308	3.8457	225.04
290	55.401	-153.13	-98.979	-1.2014	1.6618	3.0580	239.18
300	49.821	-130.92	-70.707	-1.1055	1.6417	2.6575	254.11
310	45.853	-110.57	-45.140	-1.0217	1.6476	2.4762	266.21
320	42.770	-91.050	-20.908	-0.944 73	1.6648	2.3798	276.63
330	40.253	-71.929	2.5998	-0.872 39	1.6888	2.3272	285.91
340	38.130	-52.955	25.722	-0.803 36	1.7176	2.3007	294.34
350	36.299	-33.976	48.671	-0.736 84	1.7498	2.2913	302.12
360	34.692	-14.889	71.586	-0.672 29	1.7845	2.2933	309.38
370	33.264	4.3758	94.565	-0.609 33	1.8209	2.3036	316.22
380	31.980	23.869	117.68	-0.547 69	1.8586	2.3199	322.70
390	30.817	43.627	140.98	-0.487 17	1.8972	2.3406	328.88
400	29.755	63.677	164.50	-0.427 61	1.9364	2.3647	334.79
425	27.455	115.20	224.47	-0.282 21	2.0359	2.4349	348.64
450	25.542	168.86	286.32	-0.140 83	2.1359	2.5137	361.42
475	23.916	224.75	350.19	-0.002 70	2.2350	2.5970	373.38
500	22.510	282.91	416.18	0.132 66	2.3325	2.6821	384.66
525	21.279	343.32	484.30	0.265 60	2.4280	2.7678	395.39
550	20.189	405.97	554.56	0.396 32	2.5211	2.8529	405.65
575	19.216	470.82	626.94	0.525 00	2.6117	2.9371	415.52
600	18.339	537.82	701.40	0.651 75	2.6999	3.0198	425.03
625	17.545	606.93	777.92	0.776 67	2.7855	3.1008	434.24
650	16.822	678.09	856.43	0.899 84	2.8687	3.1801	443.17
675	16.159	751.25	936.90	1.0213	2.9494	3.2574	451.85

TABLE 30. Thermodynamic properties of ethane in the single-phase region—Continued

<i>T</i> (K)	<i>ρ</i> (kg m ⁻³)	<i>u</i> (kJ kg ⁻¹)	<i>h</i> (kJ kg ⁻¹)	<i>s</i> (kJ kg ⁻¹ K ⁻¹)	<i>c_v</i> (kJ kg ⁻¹ K ⁻¹)	<i>c_p</i> (kJ kg ⁻¹ K ⁻¹)	<i>w</i> (m s ⁻¹)
4 MPa							
91.010 ^a	652.25	-888.33	-882.20	-5.0515	1.6047	2.3192	2019.56
95	647.92	-879.17	-873.00	-4.9525	1.5745	2.2964	1990.12
100	642.51	-867.79	-861.56	-4.8352	1.5457	2.2793	1953.94
105	637.10	-856.47	-850.19	-4.7242	1.5240	2.2710	1918.29
110	631.69	-845.18	-838.84	-4.6186	1.5072	2.2684	1882.91
115	626.27	-833.89	-827.50	-4.5178	1.4940	2.2698	1847.64
120	620.84	-822.59	-816.14	-4.4211	1.4833	2.2736	1812.36
125	615.39	-811.26	-804.76	-4.3282	1.4745	2.2792	1777.03
130	609.91	-799.91	-793.35	-4.2386	1.4670	2.2861	1741.61
135	604.41	-788.52	-781.90	-4.1522	1.4607	2.2938	1706.09
140	598.88	-777.09	-770.41	-4.0687	1.4554	2.3024	1670.48
145	593.32	-765.62	-758.87	-3.9877	1.4508	2.3116	1634.76
150	587.72	-754.10	-747.29	-3.9092	1.4470	2.3216	1598.93
155	582.08	-742.53	-735.66	-3.8329	1.4439	2.3324	1562.99
160	576.39	-730.91	-723.97	-3.7586	1.4415	2.3440	1526.93
165	570.64	-719.22	-712.21	-3.6863	1.4398	2.3565	1490.74
170	564.84	-707.48	-700.40	-3.6158	1.4388	2.3701	1454.43
175	558.97	-695.67	-688.51	-3.5469	1.4385	2.3848	1417.97
180	553.04	-683.78	-676.55	-3.4795	1.4390	2.4008	1381.36
185	547.02	-671.81	-664.50	-3.4134	1.4402	2.4181	1344.58
190	540.91	-659.76	-652.37	-3.3487	1.4422	2.4370	1307.63
195	534.71	-647.61	-640.13	-3.2851	1.4450	2.4576	1270.50
200	528.40	-635.36	-627.79	-3.2226	1.4485	2.4801	1233.15
210	515.41	-610.50	-602.74	-3.1004	1.4581	2.5314	1157.78
220	501.84	-585.10	-577.12	-2.9813	1.4711	2.5929	1081.35
230	487.53	-559.04	-550.83	-2.8645	1.4874	2.6676	1003.58
240	472.29	-532.18	-523.71	-2.7490	1.5074	2.7599	924.04
250	455.82	-504.33	-495.55	-2.6341	1.5313	2.8776	842.02
260	437.65	-475.17	-466.03	-2.5183	1.5598	3.0352	756.29
270	417.01	-444.21	-434.62	-2.3998	1.5946	3.2636	664.70
280	392.25	-410.46	-400.27	-2.2749	1.6394	3.6463	563.04
290	358.86	-371.27	-360.13	-2.1341	1.7096	4.5495	439.39
295.96 ^b	326.41	-340.54	-328.28	-2.0255	1.8084	6.7404	332.33
295.96 ^c	95.855	-183.77	-142.04	-1.3963	1.9584	7.8578	207.83
300	84.773	-165.36	-118.18	-1.3161	1.8159	4.8051	221.78
310	71.710	-135.28	-79.497	-1.1892	1.7365	3.3168	242.82
320	64.272	-111.10	-48.862	-1.0919	1.7251	2.8734	257.91
330	59.027	-89.054	-21.288	-1.0070	1.7338	2.6638	270.27
340	54.982	-68.027	4.7242	-0.929 34	1.7527	2.5496	280.96
350	51.699	-47.505	29.866	-0.856 46	1.7781	2.4849	290.48
360	48.944	-27.206	54.520	-0.787 00	1.8078	2.4497	299.14
370	46.576	-6.9584	78.923	-0.720 14	1.8405	2.4334	307.14
380	44.505	13.353	103.23	-0.655 32	1.8755	2.4299	314.60
390	42.669	33.805	127.55	-0.592 14	1.9119	2.4355	321.62
400	41.022	54.455	151.96	-0.530 34	1.9494	2.4477	328.27
425	37.541	107.18	213.73	-0.380 58	2.0459	2.4971	343.59
450	34.722	161.75	276.95	-0.236 05	2.1440	2.5626	357.50
475	32.371	218.36	341.93	-0.095 54	2.2417	2.6367	370.34
500	30.368	277.10	408.82	0.041 692	2.3382	2.7152	382.34
525	28.633	338.01	477.71	0.176 11	2.4329	2.7958	393.66
550	27.111	401.08	548.62	0.308 05	2.5254	2.8771	404.42
575	25.761	466.28	621.56	0.437 73	2.6155	2.9581	414.71
600	24.553	533.60	696.51	0.565 32	2.7033	3.0383	424.58
625	23.464	602.98	773.46	0.690 96	2.7886	3.1172	434.09
650	22.475	674.39	852.36	0.814 73	2.8714	3.1947	443.28
675	21.574	747.77	933.18	0.936 73	2.9519	3.2706	452.20

TABLE 30. Thermodynamic properties of ethane in the single-phase region—Continued

<i>T</i> (K)	<i>ρ</i> (kg m ⁻³)	<i>u</i> (kJ kg ⁻¹)	<i>h</i> (kJ kg ⁻¹)	<i>s</i> (kJ kg ⁻¹ K ⁻¹)	<i>c_v</i> (kJ kg ⁻¹ K ⁻¹)	<i>c_p</i> (kJ kg ⁻¹ K ⁻¹)	<i>w</i> (m s ⁻¹)
5 MPa							
91.170 ^a	652.43	-888.19	-880.53	-5.0499	1.6047	2.3176	2022.10
95	648.29	-879.41	-871.70	-4.9551	1.5759	2.2957	1993.84
100	642.89	-868.05	-860.27	-4.8378	1.5470	2.2784	1957.73
105	637.51	-856.74	-848.90	-4.7268	1.5252	2.2700	1922.21
110	632.12	-845.47	-837.56	-4.6213	1.5084	2.2673	1886.99
115	626.72	-834.20	-826.22	-4.5205	1.4952	2.2685	1851.88
120	621.31	-822.92	-814.87	-4.4239	1.4845	2.2722	1816.79
125	615.88	-811.61	-803.50	-4.3310	1.4757	2.2777	1781.64
130	610.43	-800.28	-792.09	-4.2416	1.4683	2.2844	1746.43
135	604.95	-788.92	-780.65	-4.1552	1.4620	2.2919	1711.12
140	599.45	-777.51	-769.17	-4.0717	1.4566	2.3003	1675.73
145	593.92	-766.07	-757.65	-3.9909	1.4521	2.3093	1640.25
150	588.35	-754.58	-746.08	-3.9124	1.4483	2.3191	1604.67
155	582.74	-743.04	-734.46	-3.8362	1.4452	2.3295	1568.99
160	577.08	-731.44	-722.78	-3.7621	1.4428	2.3408	1533.21
165	571.38	-719.80	-711.05	-3.6898	1.4411	2.3530	1497.32
170	565.62	-708.09	-699.25	-3.6194	1.4401	2.3662	1461.33
175	559.79	-696.31	-687.38	-3.5506	1.4399	2.3805	1425.21
180	553.90	-684.47	-675.44	-3.4833	1.4403	2.3959	1388.96
185	547.94	-672.55	-663.42	-3.4175	1.4415	2.4127	1352.58
190	541.89	-660.54	-651.31	-3.3529	1.4435	2.4310	1316.04
195	535.76	-648.44	-639.11	-3.2895	1.4463	2.4509	1279.35
200	529.52	-636.24	-626.80	-3.2272	1.4498	2.4725	1242.50
210	516.69	-611.51	-601.84	-3.1054	1.4593	2.5216	1168.22
220	503.33	-586.27	-576.34	-2.9868	1.4721	2.5802	1093.08
230	489.28	-560.41	-550.19	-2.8706	1.4883	2.6506	1016.88
240	474.39	-533.81	-523.27	-2.7560	1.5079	2.7365	939.29
250	458.40	-506.30	-495.39	-2.6422	1.5311	2.8440	859.81
260	440.93	-477.63	-466.29	-2.5281	1.5586	2.9836	777.57
270	421.40	-447.41	-435.55	-2.4121	1.5911	3.1760	691.15
280	398.70	-414.98	-402.44	-2.2917	1.6312	3.4689	598.06
290	370.37	-378.88	-365.38	-2.1617	1.6858	4.0096	492.98
300	327.98	-334.24	-318.99	-2.0046	1.7873	5.7005	359.63
310	123.88	-181.86	-141.49	-1.4246	1.9621	8.6868	211.10
320	95.552	-138.95	-86.625	-1.2501	1.8157	4.0927	237.07
330	83.351	-110.44	-50.451	-1.1387	1.7915	3.2810	254.00
340	75.479	-85.789	-19.545	-1.0464	1.7946	2.9401	267.54
350	69.690	-62.874	8.8728	-0.964 06	1.8103	2.7607	279.10
360	65.131	-40.848	35.920	-0.887 86	1.8335	2.6579	289.32
370	61.387	-19.280	62.171	-0.815 93	1.8617	2.5978	298.55
380	58.219	2.0809	87.963	-0.747 14	1.8932	2.5641	307.02
390	55.484	23.393	113.51	-0.680 78	1.9272	2.5478	314.89
400	53.082	44.764	138.96	-0.616 35	1.9627	2.5435	322.27
425	48.137	98.878	202.75	-0.461 67	2.0559	2.5658	339.05
450	44.246	154.47	267.47	-0.313 71	2.1519	2.6151	354.04
475	41.065	211.86	333.62	-0.170 66	2.2483	2.6785	367.72
500	38.394	271.23	401.46	-0.031 49	2.3438	2.7495	380.40
525	36.107	332.65	471.13	0.104 46	2.4377	2.8246	392.28
550	34.118	396.15	542.71	0.237 64	2.5296	2.9017	403.50
575	32.365	461.73	616.22	0.368 34	2.6192	2.9794	414.16
600	30.807	529.37	691.67	0.496 78	2.7066	3.0569	424.37
625	29.408	599.04	769.06	0.623 13	2.7915	3.1337	434.16
650	28.144	670.69	848.35	0.747 52	2.8741	3.2094	443.60
675	26.995	744.30	929.52	0.870 04	2.9544	3.2838	452.73

TABLE 30. Thermodynamic properties of ethane in the single-phase region—Continued

<i>T</i> (K)	<i>ρ</i> (kg m ⁻³)	<i>u</i> (kJ kg ⁻¹)	<i>h</i> (kJ kg ⁻¹)	<i>s</i> (kJ kg ⁻¹ K ⁻¹)	<i>c_v</i> (kJ kg ⁻¹ K ⁻¹)	<i>c_p</i> (kJ kg ⁻¹ K ⁻¹)	<i>w</i> (m s ⁻¹)
6 MPa							
91.330 ^a	652.61	-888.05	-878.86	-5.0484	1.6048	2.3160	2024.58
95	648.65	-879.65	-870.40	-4.9576	1.5772	2.2951	1997.51
100	643.28	-868.30	-858.97	-4.8404	1.5483	2.2776	1961.49
105	637.91	-857.02	-847.61	-4.7295	1.5265	2.2690	1926.10
110	632.54	-845.76	-836.27	-4.6240	1.5097	2.2662	1891.03
115	627.16	-834.51	-824.94	-4.5233	1.4964	2.2673	1856.10
120	621.77	-823.25	-813.60	-4.4267	1.4857	2.2709	1821.19
125	616.36	-811.97	-802.23	-4.3339	1.4769	2.2762	1786.23
130	610.93	-800.66	-790.83	-4.2445	1.4695	2.2827	1751.21
135	605.49	-789.31	-779.40	-4.1582	1.4632	2.2901	1716.12
140	600.01	-777.93	-767.93	-4.0748	1.4579	2.2982	1680.94
145	594.50	-766.51	-756.42	-3.9940	1.4534	2.3071	1645.69
150	588.96	-755.05	-744.86	-3.9156	1.4496	2.3166	1610.35
155	583.39	-743.54	-733.25	-3.8395	1.4465	2.3268	1574.93
160	577.77	-731.98	-721.59	-3.7655	1.4441	2.3378	1539.43
165	572.10	-720.36	-709.87	-3.6933	1.4424	2.3496	1503.83
170	566.38	-708.69	-698.09	-3.6230	1.4415	2.3624	1468.14
175	560.60	-696.95	-686.25	-3.5543	1.4412	2.3763	1432.35
180	554.76	-685.14	-674.33	-3.4872	1.4417	2.3913	1396.46
185	548.85	-673.26	-662.33	-3.4214	1.4429	2.4076	1360.45
190	542.86	-661.30	-650.25	-3.3570	1.4448	2.4252	1324.32
195	536.78	-649.26	-638.08	-3.2938	1.4476	2.4444	1288.06
200	530.61	-637.11	-625.80	-3.2316	1.4511	2.4652	1251.66
210	517.95	-612.51	-600.92	-3.1102	1.4605	2.5124	1178.42
220	504.77	-587.41	-575.53	-2.9921	1.4732	2.5683	1104.50
230	490.98	-561.74	-549.52	-2.8765	1.4891	2.6349	1029.75
240	476.40	-535.38	-522.78	-2.7627	1.5084	2.7153	953.95
250	460.85	-508.18	-495.16	-2.6500	1.5312	2.8141	876.72
260	444.00	-479.93	-466.42	-2.5373	1.5578	2.9392	797.46
270	425.39	-450.34	-436.24	-2.4234	1.5888	3.1050	715.23
280	404.25	-418.93	-404.09	-2.3065	1.6256	3.3408	628.54
290	379.06	-384.79	-368.96	-2.1833	1.6719	3.7188	534.75
300	346.19	-345.80	-328.47	-2.0461	1.7376	4.4938	428.64
310	290.95	-293.44	-272.82	-1.8638	1.8677	7.5519	296.37
320	158.25	-189.14	-151.23	-1.4781	1.9726	9.4521	218.30
330	118.29	-139.36	-88.642	-1.2852	1.8664	4.6261	239.00
340	101.61	-107.46	-48.414	-1.1650	1.8434	3.5955	255.32
350	91.230	-80.636	-14.868	-1.0678	1.8461	3.1645	268.84
360	83.769	-56.090	15.535	-0.982 10	1.8613	2.9378	280.52
370	77.989	-32.734	44.200	-0.903 56	1.8840	2.8063	290.91
380	73.298	-10.024	71.834	-0.829 86	1.9117	2.7272	300.33
390	69.366	12.351	98.849	-0.759 68	1.9428	2.6799	309.00
400	65.995	34.586	125.50	-0.692 20	1.9762	2.6534	317.05
425	59.256	90.306	191.56	-0.532 01	2.0658	2.6412	335.16
450	54.110	147.02	257.90	-0.380 33	2.1597	2.6711	351.13
475	49.988	205.26	325.29	-0.234 61	2.2547	2.7223	365.58
500	46.578	265.30	394.11	-0.093 42	2.3492	2.7850	378.88
525	43.690	327.26	464.59	0.044 115	2.4423	2.8541	391.26
550	41.199	391.21	536.85	0.178 55	2.5336	2.9267	402.89
575	39.021	457.17	610.94	0.310 28	2.6228	3.0009	413.92
600	37.094	525.14	686.89	0.439 58	2.7098	3.0757	424.42
625	35.372	595.10	764.72	0.566 65	2.7944	3.1502	434.47
650	33.823	667.00	844.40	0.691 64	2.8768	3.2241	444.13
675	32.418	740.83	925.92	0.814 69	2.9568	3.2970	453.45

TABLE 30. Thermodynamic properties of ethane in the single-phase region—Continued

<i>T</i> (K)	<i>ρ</i> (kg m ⁻³)	<i>u</i> (kJ kg ⁻¹)	<i>h</i> (kJ kg ⁻¹)	<i>s</i> (kJ kg ⁻¹ K ⁻¹)	<i>c_v</i> (kJ kg ⁻¹ K ⁻¹)	<i>c_p</i> (kJ kg ⁻¹ K ⁻¹)	<i>w</i> (m s ⁻¹)
7 MPa							
91.490 ^a	652.79	-887.91	-877.19	-5.0469	1.6049	2.3145	2027.01
95	649.02	-879.89	-869.10	-4.9602	1.5786	2.2944	2001.14
100	643.66	-868.55	-857.68	-4.8430	1.5496	2.2768	1965.22
105	638.31	-857.29	-846.32	-4.7321	1.5277	2.2681	1929.96
110	632.96	-846.05	-834.99	-4.6267	1.5109	2.2651	1895.06
115	627.60	-834.82	-823.66	-4.5260	1.4976	2.2661	1860.29
120	622.23	-823.57	-812.32	-4.4295	1.4869	2.2695	1825.56
125	616.84	-812.31	-800.96	-4.3367	1.4781	2.2747	1790.79
130	611.44	-801.02	-789.58	-4.2474	1.4707	2.2810	1755.97
135	606.01	-789.70	-778.15	-4.1612	1.4644	2.2883	1721.08
140	600.57	-778.35	-766.69	-4.0778	1.4591	2.2962	1686.12
145	595.09	-766.95	-755.19	-3.9971	1.4546	2.3048	1651.09
150	589.58	-755.52	-743.64	-3.9188	1.4508	2.3141	1615.99
155	584.03	-744.03	-732.05	-3.8428	1.4478	2.3241	1580.82
160	578.45	-732.50	-720.40	-3.7688	1.4454	2.3348	1545.58
165	572.82	-720.92	-708.70	-3.6968	1.4437	2.3463	1510.27
170	567.14	-709.28	-696.94	-3.6266	1.4428	2.3588	1474.88
175	561.40	-697.58	-685.11	-3.5580	1.4425	2.3722	1439.41
180	555.61	-685.81	-673.21	-3.4910	1.4430	2.3868	1403.85
185	549.74	-673.97	-661.24	-3.4254	1.4442	2.4026	1368.20
190	543.81	-662.06	-649.18	-3.3611	1.4461	2.4197	1332.46
195	537.79	-650.06	-637.04	-3.2980	1.4489	2.4382	1296.61
200	531.69	-637.96	-624.80	-3.2360	1.4524	2.4583	1260.66
210	519.17	-613.48	-600.00	-3.1150	1.4617	2.5036	1188.41
220	506.19	-588.53	-574.70	-2.9973	1.4743	2.5571	1115.63
230	492.62	-563.03	-548.82	-2.8823	1.4900	2.6203	1042.24
240	478.35	-536.89	-522.25	-2.7693	1.5091	2.6957	968.06
250	463.18	-509.97	-494.85	-2.6574	1.5314	2.7872	892.85
260	446.88	-482.10	-466.44	-2.5460	1.5573	2.9005	816.19
270	429.06	-453.05	-436.74	-2.4339	1.5871	3.0460	737.45
280	409.16	-422.46	-405.35	-2.3198	1.6218	3.2424	655.74
290	386.18	-389.72	-371.59	-2.2013	1.6632	3.5296	569.69
300	358.13	-353.67	-334.13	-2.0744	1.7155	4.0122	477.31
310	320.13	-311.45	-289.58	-1.9284	1.7890	5.0560	375.61
320	256.48	-253.66	-226.36	-1.7280	1.9081	8.1224	270.19
330	174.00	-180.88	-140.65	-1.4641	1.9369	7.2387	236.17
340	136.48	-134.59	-83.303	-1.2927	1.8939	4.6820	247.87
350	117.56	-101.37	-41.822	-1.1724	1.8828	3.7469	261.48
360	105.43	-73.176	-6.7841	-1.0737	1.8896	3.3080	273.85
370	96.677	-47.427	24.980	-0.986 64	1.9066	3.0665	284.96
380	89.894	-23.005	54.865	-0.906 93	1.9303	2.9223	295.05
390	84.399	0.66618	83.606	-0.832 27	1.9583	2.8330	304.31
400	79.805	23.923	111.64	-0.761 30	1.9895	2.7778	312.89
425	70.897	81.476	180.21	-0.594 99	2.0755	2.7229	332.08
450	64.302	139.43	248.29	-0.439 34	2.1673	2.7302	348.88
475	59.127	198.58	316.97	-0.290 82	2.2609	2.7676	363.99
500	54.906	259.31	386.80	-0.147 55	2.3544	2.8213	377.81
525	51.370	321.84	458.11	-0.008 41	2.4468	2.8840	390.63
550	48.346	386.26	531.05	0.127 31	2.5376	2.9519	402.64
575	45.719	452.61	605.72	0.260 08	2.6263	3.0225	413.97
600	43.406	520.91	682.18	0.390 23	2.7129	3.0944	424.74
625	41.350	591.16	760.45	0.518 01	2.7972	3.1667	435.02
650	39.506	663.32	840.51	0.643 62	2.8793	3.2387	444.88
675	37.839	737.38	922.37	0.767 19	2.9591	3.3100	454.38

TABLE 30. Thermodynamic properties of ethane in the single-phase region—Continued

<i>T</i> (K)	<i>ρ</i> (kg m ⁻³)	<i>u</i> (kJ kg ⁻¹)	<i>h</i> (kJ kg ⁻¹)	<i>s</i> (kJ kg ⁻¹ K ⁻¹)	<i>c_v</i> (kJ kg ⁻¹ K ⁻¹)	<i>c_p</i> (kJ kg ⁻¹ K ⁻¹)	<i>w</i> (m s ⁻¹)
8 MPa							
91.649 ^a	652.97	-887.77	-875.52	-5.0454	1.6050	2.3129	2029.39
95	649.38	-880.12	-867.80	-4.9627	1.5800	2.2938	2004.74
100	644.04	-868.81	-856.38	-4.8456	1.5509	2.2761	1968.92
105	638.71	-857.55	-845.03	-4.7347	1.5290	2.2671	1933.80
110	633.37	-846.33	-833.70	-4.6294	1.5121	2.2641	1899.06
115	628.03	-835.12	-822.38	-4.5287	1.4988	2.2649	1864.47
120	622.68	-823.90	-811.05	-4.4323	1.4881	2.2682	1829.91
125	617.32	-812.66	-799.70	-4.3396	1.4793	2.2732	1795.33
130	611.94	-801.39	-788.32	-4.2503	1.4719	2.2794	1760.70
135	606.54	-790.09	-776.90	-4.1641	1.4657	2.2865	1726.01
140	601.12	-778.76	-765.45	-4.0809	1.4603	2.2943	1691.26
145	595.67	-767.39	-753.96	-4.0002	1.4559	2.3027	1656.45
150	590.19	-755.98	-742.42	-3.9220	1.4521	2.3117	1621.58
155	584.67	-744.52	-730.84	-3.8460	1.4491	2.3215	1586.66
160	579.12	-733.02	-719.21	-3.7722	1.4467	2.3319	1551.68
165	573.52	-721.47	-707.52	-3.7002	1.4450	2.3431	1516.64
170	567.88	-709.86	-695.77	-3.6301	1.4441	2.3552	1481.54
175	562.19	-698.20	-683.97	-3.5616	1.4438	2.3683	1446.38
180	556.44	-686.47	-672.09	-3.4947	1.4443	2.3825	1411.15
185	550.63	-674.67	-660.14	-3.4293	1.4455	2.3978	1375.85
190	544.74	-662.79	-648.11	-3.3651	1.4474	2.4143	1340.48
195	538.78	-650.84	-635.99	-3.3021	1.4502	2.4322	1305.03
200	532.74	-638.80	-623.78	-3.2403	1.4536	2.4516	1269.50
210	520.37	-614.43	-599.06	-3.1197	1.4629	2.4953	1198.18
220	507.56	-589.62	-573.85	-3.0025	1.4754	2.5465	1126.49
230	494.22	-564.28	-548.10	-2.8880	1.4910	2.6066	1054.36
240	480.22	-538.34	-521.68	-2.7756	1.5098	2.6777	981.69
250	465.42	-511.68	-494.50	-2.6646	1.5318	2.7628	908.30
260	449.60	-484.16	-466.37	-2.5543	1.5571	2.8664	833.92
270	432.47	-455.58	-437.08	-2.4438	1.5861	2.9959	758.16
280	413.59	-425.67	-406.32	-2.3319	1.6191	3.1638	680.45
290	392.26	-394.00	-373.60	-2.2171	1.6573	3.3936	600.14
300	367.29	-359.86	-338.08	-2.0967	1.7029	3.7365	516.47
310	336.32	-321.88	-298.09	-1.9657	1.7594	4.3197	428.84
320	294.34	-277.08	-249.90	-1.8128	1.8327	5.4434	340.14
330	235.51	-221.48	-187.51	-1.6209	1.9113	6.8792	271.63
340	181.00	-166.43	-122.23	-1.4259	1.9239	5.8070	254.26
350	149.44	-125.06	-71.530	-1.2789	1.9133	4.4632	260.63
360	130.49	-92.107	-30.801	-1.1641	1.9152	3.7583	271.10
370	117.62	-63.337	4.6813	-1.0668	1.9279	3.3738	281.76
380	108.08	-36.830	37.190	-0.980 14	1.9480	3.1465	291.86
390	100.60	-11.626	67.894	-0.900 37	1.9733	3.0051	301.30
400	94.508	12.812	97.460	-0.825 51	2.0024	2.9148	310.13
425	83.039	72.416	168.76	-0.652 59	2.0848	2.8100	329.98
450	74.799	131.71	238.66	-0.492 76	2.1745	2.7918	347.39
475	68.460	191.82	308.68	-0.341 34	2.2668	2.8143	363.00
500	63.362	253.29	379.55	-0.195 93	2.3594	2.8582	377.25
525	59.133	316.40	451.69	-0.055 16	2.4511	2.9142	390.43
550	55.546	381.30	525.32	0.081 840	2.5414	2.9772	402.75
575	52.449	448.05	600.58	0.215 64	2.6297	3.0441	414.35
600	49.736	516.69	677.54	0.346 65	2.7159	3.1131	425.34
625	47.334	587.23	756.24	0.475 15	2.8000	3.1831	435.82
650	45.187	659.65	836.70	0.601 36	2.8818	3.2532	445.85
675	43.252	733.94	918.90	0.725 44	2.9614	3.3229	455.50

TABLE 30. Thermodynamic properties of ethane in the single-phase region—Continued

<i>T</i> (K)	<i>ρ</i> (kg m ⁻³)	<i>u</i> (kJ kg ⁻¹)	<i>h</i> (kJ kg ⁻¹)	<i>s</i> (kJ kg ⁻¹ K ⁻¹)	<i>c_v</i> (kJ kg ⁻¹ K ⁻¹)	<i>c_p</i> (kJ kg ⁻¹ K ⁻¹)	<i>w</i> (m s ⁻¹)
10 MPa							
91.967 ^a	653.33	-887.49	-872.18	-5.0424	1.6053	2.3099	2034.04
95	650.10	-880.59	-865.21	-4.9678	1.5828	2.2926	2011.83
100	644.79	-869.30	-853.79	-4.8507	1.5535	2.2745	1976.23
105	639.49	-858.08	-842.45	-4.7400	1.5314	2.2653	1941.41
110	634.20	-846.90	-831.13	-4.6347	1.5145	2.2620	1906.99
115	628.90	-835.72	-819.82	-4.5341	1.5011	2.2625	1872.74
120	623.59	-824.54	-808.50	-4.4378	1.4904	2.2656	1838.53
125	618.27	-813.33	-797.16	-4.3452	1.4816	2.2704	1804.32
130	612.93	-802.11	-785.79	-4.2560	1.4743	2.2763	1770.06
135	607.58	-790.86	-774.40	-4.1700	1.4681	2.2830	1735.76
140	602.21	-779.57	-762.96	-4.0868	1.4628	2.2905	1701.42
145	596.81	-768.25	-751.49	-4.0063	1.4583	2.2985	1667.04
150	591.39	-756.89	-739.98	-3.9282	1.4546	2.3072	1632.62
155	585.93	-745.48	-728.42	-3.8524	1.4516	2.3164	1598.17
160	580.45	-734.04	-716.81	-3.7788	1.4493	2.3263	1563.69
165	574.92	-722.55	-705.15	-3.7070	1.4476	2.3370	1529.18
170	569.35	-711.00	-693.44	-3.6371	1.4467	2.3485	1494.63
175	563.74	-699.41	-681.67	-3.5688	1.4464	2.3609	1460.06
180	558.08	-687.75	-669.83	-3.5021	1.4469	2.3742	1425.46
185	552.35	-676.03	-657.92	-3.4369	1.4481	2.3886	1390.82
190	546.57	-664.24	-645.94	-3.3730	1.4500	2.4042	1356.15
195	540.72	-652.37	-633.88	-3.3103	1.4527	2.4210	1321.45
200	534.80	-640.43	-621.73	-3.2488	1.4562	2.4391	1286.72
210	522.70	-616.27	-597.14	-3.1288	1.4654	2.4798	1217.15
220	510.22	-591.71	-572.11	-3.0124	1.4777	2.5270	1147.46
230	497.28	-566.68	-546.57	-2.8989	1.4930	2.5818	1077.63
240	483.78	-541.12	-520.45	-2.7877	1.5114	2.6456	1007.64
250	469.62	-514.92	-493.63	-2.6782	1.5329	2.7204	937.43
260	454.63	-487.99	-465.99	-2.5699	1.5574	2.8088	866.92
270	438.64	-460.19	-437.39	-2.4619	1.5850	2.9148	795.96
280	421.36	-431.35	-407.62	-2.3537	1.6159	3.0445	724.40
290	402.42	-401.24	-376.39	-2.2441	1.6505	3.2073	652.16
300	381.28	-369.54	-343.31	-2.1320	1.6894	3.4187	579.32
310	357.14	-335.77	-307.77	-2.0154	1.7333	3.7061	506.34
320	328.78	-299.22	-268.80	-1.8918	1.7828	4.1091	434.79
330	294.87	-259.08	-225.16	-1.7575	1.8369	4.6315	369.55
340	255.88	-215.48	-176.40	-1.6120	1.8884	5.0696	319.90
350	217.58	-171.62	-125.66	-1.4649	1.9224	4.9685	293.79
360	186.98	-131.93	-78.445	-1.3319	1.9407	4.4525	286.76
370	164.73	-97.190	-36.483	-1.2169	1.9566	3.9614	289.09
380	148.42	-66.125	1.2515	-1.1162	1.9755	3.6077	295.16
390	136.02	-37.471	36.048	-1.0258	1.9983	3.3674	302.58
400	126.22	-10.368	68.857	-0.94273	2.0247	3.2049	310.38
425	108.60	53.811	145.89	-0.75585	2.1017	2.9923	329.47
450	96.552	116.03	219.60	-0.58733	2.1879	2.9187	347.04
475	87.595	178.19	292.35	-0.42997	2.2778	2.9091	363.06
500	80.566	241.20	365.32	-0.28026	2.3687	2.9326	377.77
525	74.841	305.52	439.14	-0.13622	2.4592	2.9746	391.40
550	70.052	371.39	514.14	0.0033445	2.5485	3.0274	404.12
575	65.963	438.96	590.56	0.13921	2.6360	3.0868	416.08
600	62.414	508.29	668.51	0.27191	2.7216	3.1500	427.41
625	59.294	579.43	748.08	0.40181	2.8051	3.2153	438.18
650	56.523	652.37	829.29	0.52921	2.8865	3.2816	448.47
675	54.038	727.10	912.16	0.65431	2.9657	3.3482	458.34

TABLE 30. Thermodynamic properties of ethane in the single-phase region—Continued

T (K)	ρ (kg m ⁻³)	u (kJ kg ⁻¹)	h (kJ kg ⁻¹)	s (kJ kg ⁻¹ K ⁻¹)	c_v (kJ kg ⁻¹ K ⁻¹)	c_p (kJ kg ⁻¹ K ⁻¹)	w (m s ⁻¹)
15 MPa							
92.758 ^a	654.22	-886.78	-863.86	-5.0350	1.6063	2.3024	2045.13
95	651.87	-881.72	-858.71	-4.9802	1.5898	2.2898	2029.01
100	646.64	-870.51	-847.31	-4.8633	1.5599	2.2709	1994.10
105	641.43	-859.37	-835.98	-4.7528	1.5375	2.2611	1960.06
110	636.23	-848.27	-824.69	-4.6477	1.5204	2.2571	1926.45
115	631.02	-837.18	-813.41	-4.5474	1.5069	2.2571	1893.04
120	625.80	-826.08	-802.12	-4.4513	1.4962	2.2596	1859.68
125	620.59	-814.98	-790.81	-4.3589	1.4874	2.2637	1826.33
130	615.36	-803.85	-779.48	-4.2700	1.4801	2.2690	1792.96
135	610.12	-792.70	-768.12	-4.1843	1.4739	2.2751	1759.58
140	604.86	-781.52	-756.72	-4.1014	1.4687	2.2817	1726.19
145	599.59	-770.31	-745.30	-4.0213	1.4643	2.2889	1692.81
150	594.30	-759.07	-733.83	-3.9435	1.4607	2.2967	1659.43
155	588.99	-747.80	-722.33	-3.8681	1.4578	2.3049	1626.07
160	583.65	-736.48	-710.78	-3.7948	1.4555	2.3137	1592.73
165	578.29	-725.13	-699.19	-3.7234	1.4539	2.3232	1559.42
170	572.89	-713.73	-687.55	-3.6539	1.4530	2.3333	1526.15
175	567.46	-702.29	-675.86	-3.5861	1.4528	2.3442	1492.91
180	561.99	-690.80	-664.11	-3.5199	1.4533	2.3558	1459.71
185	556.48	-679.25	-652.30	-3.4552	1.4545	2.3684	1426.55
190	550.93	-667.65	-640.42	-3.3919	1.4564	2.3819	1393.44
195	545.32	-655.98	-628.48	-3.3298	1.4591	2.3965	1360.38
200	539.66	-644.25	-616.46	-3.2690	1.4625	2.4121	1327.38
210	528.16	-620.57	-592.17	-3.1505	1.4715	2.4467	1261.58
220	516.38	-596.55	-567.51	-3.0357	1.4835	2.4862	1196.09
230	504.28	-572.17	-542.42	-2.9243	1.4984	2.5312	1130.99
240	491.80	-547.36	-516.86	-2.8155	1.5162	2.5822	1066.33
250	478.89	-522.08	-490.76	-2.7089	1.5368	2.6398	1002.21
260	465.47	-496.27	-464.04	-2.6041	1.5600	2.7049	938.70
270	451.46	-469.86	-436.63	-2.5007	1.5859	2.7783	875.89
280	436.76	-442.79	-408.44	-2.3982	1.6144	2.8613	813.93
290	421.27	-414.98	-379.37	-2.2962	1.6453	2.9549	753.01
300	404.85	-386.36	-349.30	-2.1943	1.6786	3.0606	693.47
310	387.38	-356.84	-318.12	-2.0920	1.7142	3.1793	635.77
320	368.73	-326.35	-285.67	-1.9890	1.7520	3.3115	580.60
330	348.81	-294.85	-251.85	-1.8849	1.7915	3.4551	528.86
340	327.64	-262.34	-216.56	-1.7796	1.8322	3.6013	481.90
350	305.46	-228.98	-179.88	-1.6733	1.8729	3.7306	441.39
360	282.89	-195.12	-142.09	-1.5669	1.9122	3.8164	408.76
370	260.82	-161.28	-103.77	-1.4619	1.9491	3.8361	384.58
380	240.21	-128.05	-65.603	-1.3601	1.9834	3.7878	368.37
390	221.70	-95.829	-28.169	-1.2628	2.0160	3.6939	358.78
400	205.51	-64.769	8.2189	-1.1707	2.0477	3.5828	354.12
425	174.15	8.4169	94.549	-0.961 27	2.1278	3.3381	355.22
450	152.25	77.442	175.96	-0.775 08	2.2118	3.1909	364.67
475	136.24	144.65	254.75	-0.604 69	2.2989	3.1220	376.82
500	123.99	211.50	332.48	-0.445 20	2.3875	3.1028	389.62
525	114.23	278.83	410.14	-0.293 64	2.4759	3.1140	402.30
550	106.24	347.14	488.34	-0.148 14	2.5635	3.1441	414.57
575	99.529	416.73	567.44	-0.007 48	2.6496	3.1861	426.37
600	93.791	487.78	647.71	0.129 15	2.7340	3.2358	437.68
625	88.809	560.37	729.27	0.262 33	2.8164	3.2904	448.52
650	84.430	634.59	812.25	0.392 50	2.8969	3.3480	458.93
675	80.539	710.44	896.69	0.519 96	2.9753	3.4074	468.94

TABLE 30. Thermodynamic properties of ethane in the single-phase region—Continued

<i>T</i> (K)	<i>ρ</i> (kg m ⁻³)	<i>u</i> (kJ kg ⁻¹)	<i>h</i> (kJ kg ⁻¹)	<i>s</i> (kJ kg ⁻¹ K ⁻¹)	<i>c_v</i> (kJ kg ⁻¹ K ⁻¹)	<i>c_p</i> (kJ kg ⁻¹ K ⁻¹)	<i>w</i> (m s ⁻¹)
20 MPa							
93.543 ^a	655.10	-886.07	-855.55	-5.0278	1.6075	2.2953	2055.78
95	653.60	-882.81	-852.21	-4.9924	1.5967	2.2872	2045.56
100	648.45	-871.67	-840.82	-4.8756	1.5663	2.2676	2011.43
105	643.32	-860.60	-829.52	-4.7653	1.5435	2.2571	1978.21
110	638.20	-849.58	-818.24	-4.6604	1.5261	2.2527	1945.41
115	633.08	-838.57	-806.98	-4.5603	1.5125	2.2521	1912.80
120	627.96	-827.57	-795.72	-4.4644	1.5017	2.2541	1880.25
125	622.83	-816.55	-784.44	-4.3723	1.4930	2.2577	1847.70
130	617.70	-805.52	-773.14	-4.2837	1.4857	2.2624	1815.16
135	612.57	-794.46	-761.81	-4.1982	1.4796	2.2679	1782.62
140	607.42	-783.38	-750.46	-4.1156	1.4745	2.2739	1750.10
145	602.27	-772.28	-739.07	-4.0357	1.4702	2.2804	1717.61
150	597.10	-761.15	-727.65	-3.9583	1.4666	2.2873	1685.17
155	591.92	-749.99	-716.20	-3.8832	1.4638	2.2947	1652.79
160	586.72	-738.79	-704.71	-3.8102	1.4616	2.3026	1620.47
165	581.50	-727.57	-693.17	-3.7392	1.4601	2.3110	1588.23
170	576.26	-716.30	-681.59	-3.6701	1.4592	2.3201	1556.07
175	570.99	-705.00	-669.97	-3.6027	1.4590	2.3297	1523.99
180	565.69	-693.65	-658.30	-3.5369	1.4595	2.3401	1492.01
185	560.37	-682.26	-646.57	-3.4726	1.4607	2.3512	1460.12
190	555.01	-670.82	-634.78	-3.4098	1.4627	2.3631	1428.34
195	549.62	-659.33	-622.94	-3.3482	1.4653	2.3759	1396.68
200	544.18	-647.78	-611.02	-3.2879	1.4687	2.3896	1365.13
210	533.18	-624.49	-586.98	-3.1706	1.4776	2.4197	1302.43
220	521.98	-600.93	-562.62	-3.0573	1.4894	2.4539	1240.33
230	510.55	-577.06	-537.89	-2.9474	1.5040	2.4922	1178.91
240	498.86	-552.85	-512.76	-2.8404	1.5215	2.5350	1118.29
250	486.87	-528.25	-487.17	-2.7360	1.5416	2.5823	1058.58
260	474.55	-503.24	-461.09	-2.6337	1.5642	2.6345	999.89
270	461.87	-477.77	-434.47	-2.5332	1.5893	2.6915	942.38
280	448.77	-451.81	-407.25	-2.4342	1.6166	2.7536	886.21
290	435.22	-425.33	-379.38	-2.3365	1.6461	2.8207	831.57
300	421.18	-398.30	-350.82	-2.2396	1.6776	2.8926	778.73
310	406.62	-370.70	-321.51	-2.1436	1.7109	2.9687	728.00
320	391.54	-342.51	-291.43	-2.0481	1.7458	3.0482	679.76
330	375.92	-313.75	-260.54	-1.9530	1.7821	3.1297	634.43
340	359.82	-284.42	-228.84	-1.8584	1.8195	3.2108	592.46
350	343.32	-254.59	-196.34	-1.7642	1.8576	3.2880	554.34
360	326.57	-224.35	-163.11	-1.6706	1.8960	3.3561	520.55
370	309.79	-193.83	-129.27	-1.5778	1.9343	3.4095	491.53
380	293.25	-163.18	-94.983	-1.4864	1.9720	3.4437	467.46
390	277.25	-132.60	-60.464	-1.3967	2.0090	3.4567	448.25
400	262.07	-102.23	-25.915	-1.3093	2.0454	3.4502	433.55
425	228.69	-27.876	59.581	-1.1019	2.1344	3.3815	412.70
450	202.15	44.132	143.07	-0.911 03	2.2226	3.2999	407.05
475	181.38	114.53	224.79	-0.734 27	2.3111	3.2432	409.60
500	164.96	184.25	305.49	-0.568 70	2.3996	3.2172	416.34
525	151.72	254.04	385.86	-0.411 84	2.4877	3.2166	425.10
550	140.82	324.45	466.47	-0.261 84	2.5746	3.2348	434.79
575	131.67	395.82	547.71	-0.117 39	2.6600	3.2662	444.83
600	123.87	468.40	629.86	0.022 444	2.7438	3.3067	454.90
625	117.11	542.33	713.10	0.158 36	2.8256	3.3535	464.86
650	111.19	617.70	797.57	0.290 87	2.9055	3.4045	474.62
675	105.96	694.59	883.35	0.420 36	2.9833	3.4583	484.15

TABLE 30. Thermodynamic properties of ethane in the single-phase region—Continued

<i>T</i> (K)	<i>ρ</i> (kg m ⁻³)	<i>u</i> (kJ kg ⁻¹)	<i>h</i> (kJ kg ⁻¹)	<i>s</i> (kJ kg ⁻¹ K ⁻¹)	<i>c_v</i> (kJ kg ⁻¹ K ⁻¹)	<i>c_p</i> (kJ kg ⁻¹ K ⁻¹)	<i>w</i> (m s ⁻¹)
25 MPa							
94.322 ^a	655.98	-885.36	-847.25	-5.0207	1.6086	2.2885	2066.22
95	655.29	-883.85	-845.70	-5.0043	1.6036	2.2848	2061.59
100	650.22	-872.78	-834.33	-4.8877	1.5725	2.2645	2028.31
105	645.17	-861.79	-823.04	-4.7775	1.5493	2.2534	1995.91
110	640.13	-850.84	-811.79	-4.6728	1.5316	2.2485	1963.91
115	635.09	-839.91	-800.55	-4.5729	1.5180	2.2475	1932.06
120	630.05	-828.99	-789.31	-4.4772	1.5072	2.2490	1900.26
125	625.02	-818.06	-778.06	-4.3854	1.4984	2.2522	1868.47
130	619.98	-807.11	-766.78	-4.2970	1.4912	2.2564	1836.69
135	614.94	-796.14	-755.49	-4.2117	1.4852	2.2614	1804.92
140	609.90	-785.16	-744.17	-4.1294	1.4801	2.2668	1773.19
145	604.85	-774.15	-732.82	-4.0497	1.4759	2.2727	1741.53
150	599.80	-763.12	-721.44	-3.9726	1.4724	2.2790	1709.94
155	594.73	-752.07	-710.03	-3.8977	1.4696	2.2857	1678.43
160	589.66	-740.98	-698.58	-3.8251	1.4675	2.2928	1647.03
165	584.57	-729.87	-687.10	-3.7544	1.4660	2.3004	1615.74
170	579.46	-718.72	-675.58	-3.6856	1.4652	2.3085	1584.56
175	574.34	-707.54	-664.02	-3.6186	1.4651	2.3171	1553.51
180	569.20	-696.33	-652.41	-3.5531	1.4656	2.3264	1522.60
185	564.04	-685.07	-640.75	-3.4893	1.4669	2.3364	1491.82
190	558.86	-673.78	-629.04	-3.4268	1.4688	2.3470	1461.20
195	553.65	-662.43	-617.28	-3.3657	1.4715	2.3584	1430.72
200	548.41	-651.04	-605.46	-3.3059	1.4748	2.3706	1400.42
210	537.84	-628.10	-581.62	-3.1896	1.4837	2.3974	1340.33
220	527.12	-604.93	-557.50	-3.0773	1.4953	2.4275	1281.03
230	516.25	-581.48	-533.06	-2.9687	1.5098	2.4611	1222.62
240	505.19	-557.75	-508.26	-2.8632	1.5270	2.4982	1165.19
250	493.93	-533.70	-483.08	-2.7604	1.5468	2.5389	1108.88
260	482.45	-509.29	-457.48	-2.6600	1.5691	2.5830	1053.80
270	470.72	-484.52	-431.41	-2.5616	1.5937	2.6305	1000.11
280	458.74	-459.35	-404.85	-2.4650	1.6204	2.6813	947.94
290	446.48	-433.77	-377.78	-2.3700	1.6492	2.7349	897.46
300	433.95	-407.76	-350.15	-2.2764	1.6798	2.7911	848.87
310	421.12	-381.31	-321.95	-2.1839	1.7120	2.8494	802.39
320	408.01	-354.43	-293.16	-2.0925	1.7458	2.9088	758.23
330	394.64	-327.12	-263.77	-2.0021	1.7808	2.9687	716.65
340	381.05	-299.39	-233.78	-1.9126	1.8169	3.0278	677.88
350	367.28	-271.29	-203.22	-1.8240	1.8538	3.0848	642.13
360	353.40	-242.84	-172.10	-1.7363	1.8912	3.1381	609.57
370	339.51	-214.11	-140.48	-1.6497	1.9290	3.1859	580.37
380	325.73	-185.16	-108.41	-1.5641	1.9669	3.2263	554.64
390	312.17	-156.06	-75.978	-1.4799	2.0047	3.2581	532.41
400	298.97	-126.90	-43.277	-1.3971	2.0423	3.2806	513.59
425	268.26	-54.108	39.084	-1.1974	2.1353	3.3006	480.16
450	241.67	18.049	121.49	-1.0090	2.2268	3.2897	462.28
475	219.34	89.555	203.53	-0.83155	2.3174	3.2740	454.91
500	200.79	160.77	285.27	-0.66384	2.4071	3.2674	454.16
525	185.34	232.12	367.01	-0.50432	2.4956	3.2739	457.44
550	172.35	304.01	449.07	-0.35163	2.5826	3.2927	463.12
575	161.31	376.75	531.73	-0.20465	2.6679	3.3219	470.19
600	151.82	450.56	615.23	-0.06252	2.7514	3.3590	478.06
625	143.56	525.59	699.73	0.075461	2.8329	3.4020	486.34
650	136.32	601.97	785.37	0.20980	2.9125	3.4493	494.81
675	129.89	679.75	872.22	0.34092	2.9900	3.4996	503.33

TABLE 30. Thermodynamic properties of ethane in the single-phase region—Continued

<i>T</i> (K)	<i>ρ</i> (kg m ⁻³)	<i>u</i> (kJ kg ⁻¹)	<i>h</i> (kJ kg ⁻¹)	<i>s</i> (kJ kg ⁻¹ K ⁻¹)	<i>c_v</i> (kJ kg ⁻¹ K ⁻¹)	<i>c_p</i> (kJ kg ⁻¹ K ⁻¹)	<i>w</i> (m s ⁻¹)
50 MPa							
98.136 ^a	660.30	-881.76	-806.04	-4.9872	1.6126	2.2588	2118.07
100	658.54	-877.76	-801.84	-4.9448	1.6011	2.2516	2107.34
105	653.82	-867.09	-790.62	-4.8353	1.5760	2.2385	2078.73
110	649.12	-856.47	-779.44	-4.7313	1.5574	2.2319	2050.19
115	644.44	-845.88	-768.29	-4.6322	1.5434	2.2293	2021.58
120	639.77	-835.30	-757.14	-4.5373	1.5325	2.2293	1992.88
125	635.11	-824.72	-745.99	-4.4463	1.5240	2.2309	1964.13
130	630.46	-814.14	-734.83	-4.3587	1.5171	2.2335	1935.39
135	625.83	-803.55	-723.66	-4.2744	1.5114	2.2367	1906.69
140	621.21	-792.95	-712.47	-4.1930	1.5068	2.2403	1878.09
145	616.60	-782.35	-701.26	-4.1143	1.5030	2.2442	1849.62
150	612.00	-771.72	-690.02	-4.0381	1.4999	2.2483	1821.31
155	607.41	-761.09	-678.77	-3.9643	1.4975	2.2527	1793.18
160	602.83	-750.44	-667.50	-3.8927	1.4957	2.2573	1765.26
165	598.25	-739.78	-656.20	-3.8232	1.4945	2.2622	1737.54
170	593.69	-729.09	-644.87	-3.7556	1.4939	2.2675	1710.05
175	589.13	-718.39	-633.52	-3.6898	1.4940	2.2731	1682.79
180	584.58	-707.67	-622.14	-3.6257	1.4947	2.2792	1655.77
185	580.03	-696.93	-610.73	-3.5631	1.4961	2.2857	1628.99
190	575.48	-686.17	-599.28	-3.5021	1.4982	2.2927	1602.46
195	570.94	-675.38	-587.80	-3.4424	1.5009	2.3002	1576.19
200	566.40	-664.56	-576.28	-3.3841	1.5042	2.3082	1550.18
210	557.33	-642.83	-553.11	-3.2711	1.5130	2.3260	1498.97
220	548.26	-620.95	-529.76	-3.1624	1.5245	2.3460	1448.90
230	539.19	-598.92	-506.19	-3.0576	1.5387	2.3682	1400.03
240	530.11	-576.70	-482.38	-2.9563	1.5554	2.3927	1352.42
250	521.03	-554.29	-458.33	-2.8581	1.5745	2.4192	1306.16
260	511.94	-531.66	-433.99	-2.7627	1.5960	2.4477	1261.30
270	502.83	-508.80	-409.37	-2.6698	1.6197	2.4779	1217.93
280	493.73	-485.70	-384.43	-2.5791	1.6453	2.5098	1176.10
290	484.62	-462.34	-359.17	-2.4904	1.6729	2.5429	1135.88
300	475.51	-438.72	-333.57	-2.4036	1.7021	2.5772	1097.31
310	466.40	-414.82	-307.62	-2.3186	1.7328	2.6123	1060.45
320	457.32	-390.65	-281.32	-2.2351	1.7649	2.6481	1025.32
330	448.26	-366.20	-254.66	-2.1530	1.7982	2.6842	991.96
340	439.23	-341.47	-227.63	-2.0724	1.8325	2.7205	960.39
350	430.25	-316.46	-200.25	-1.9930	1.8676	2.7568	930.62
360	421.33	-291.17	-172.50	-1.9148	1.9035	2.7928	902.63
370	412.48	-265.61	-144.39	-1.8378	1.9400	2.8284	876.43
380	403.72	-239.78	-115.93	-1.7619	1.9770	2.8633	851.97
390	395.07	-213.69	-87.128	-1.6871	2.0143	2.8975	829.24
400	386.53	-187.34	-57.986	-1.6133	2.0518	2.9308	808.17
425	365.80	-120.40	16.285	-1.4332	2.1462	3.0098	762.47
450	346.10	-52.020	92.448	-1.2591	2.2404	3.0822	725.90
475	327.60	17.714	170.34	-1.0907	2.3336	3.1483	697.36
500	310.39	88.732	249.82	-0.92761	2.4254	3.2093	675.68
525	294.52	161.01	330.78	-0.76963	2.5154	3.2667	659.70
550	279.95	234.53	413.13	-0.61639	2.6035	3.3218	648.32
575	266.62	309.32	496.86	-0.46753	2.6894	3.3757	640.60
600	254.44	385.41	581.92	-0.32273	2.7731	3.4291	635.78
625	243.32	462.82	668.31	-0.18167	2.8547	3.4824	633.23
650	233.14	541.57	756.04	-0.04405	2.9341	3.5355	632.46
675	223.82	621.70	845.09	0.090375	3.0113	3.5887	633.08

TABLE 30. Thermodynamic properties of ethane in the single-phase region—Continued

<i>T</i> (K)	<i>ρ</i> (kg m ⁻³)	<i>u</i> (kJ kg ⁻¹)	<i>h</i> (kJ kg ⁻¹)	<i>s</i> (kJ kg ⁻¹ K ⁻¹)	<i>c_v</i> (kJ kg ⁻¹ K ⁻¹)	<i>c_p</i> (kJ kg ⁻¹ K ⁻¹)	<i>w</i> (m s ⁻¹)
75 MPa							
101.82 ^a	664.49	-878.11	-765.24	-4.9566	1.6152	2.2356	2169.89
105	661.67	-871.50	-758.15	-4.8880	1.5996	2.2276	2153.58
110	657.25	-861.15	-747.03	-4.7846	1.5805	2.2200	2127.64
115	652.84	-850.83	-735.94	-4.6860	1.5664	2.2167	2101.41
120	648.46	-840.52	-724.86	-4.5917	1.5558	2.2159	2074.97
125	644.10	-830.22	-713.78	-4.5012	1.5476	2.2167	2048.41
130	639.75	-819.93	-702.69	-4.4142	1.5411	2.2185	2021.84
135	635.43	-809.63	-691.60	-4.3305	1.5359	2.2208	1995.32
140	631.13	-799.32	-680.49	-4.2497	1.5316	2.2235	1968.93
145	626.84	-789.01	-669.36	-4.1716	1.5282	2.2263	1942.70
150	622.58	-778.69	-658.22	-4.0961	1.5255	2.2294	1916.68
155	618.34	-768.36	-647.07	-4.0229	1.5234	2.2325	1890.88
160	614.11	-758.02	-635.90	-3.9520	1.5218	2.2359	1865.33
165	609.91	-747.68	-624.71	-3.8831	1.5209	2.2395	1840.04
170	605.72	-737.32	-613.50	-3.8162	1.5206	2.2434	1815.01
175	601.55	-726.95	-602.27	-3.7511	1.5208	2.2476	1790.26
180	597.40	-716.57	-591.02	-3.6877	1.5217	2.2521	1765.78
185	593.26	-706.17	-579.75	-3.6260	1.5232	2.2571	1741.58
190	589.14	-695.76	-568.45	-3.5657	1.5253	2.2624	1717.66
195	585.03	-685.33	-557.13	-3.5069	1.5281	2.2682	1694.02
200	580.94	-674.87	-545.77	-3.4494	1.5315	2.2745	1670.67
210	572.80	-653.89	-522.96	-3.3381	1.5403	2.2886	1624.84
220	564.71	-632.80	-499.99	-3.2312	1.5517	2.3047	1580.19
230	556.68	-611.58	-476.86	-3.1284	1.5656	2.3228	1536.74
240	548.70	-590.21	-453.53	-3.0291	1.5821	2.3430	1494.54
250	540.77	-568.68	-429.99	-2.9330	1.6010	2.3651	1453.62
260	532.89	-546.96	-406.22	-2.8398	1.6221	2.3890	1414.01
270	525.06	-525.04	-382.20	-2.7492	1.6453	2.4147	1375.75
280	517.28	-502.91	-357.92	-2.6609	1.6706	2.4419	1338.87
290	509.56	-480.55	-333.36	-2.5747	1.6976	2.4704	1303.38
300	501.89	-457.95	-308.51	-2.4904	1.7263	2.5001	1269.31
310	494.27	-435.09	-283.36	-2.4080	1.7565	2.5309	1236.67
320	486.72	-411.98	-257.89	-2.3271	1.7880	2.5625	1205.46
330	479.23	-388.60	-232.10	-2.2478	1.8206	2.5948	1175.68
340	471.82	-364.95	-205.99	-2.1698	1.8543	2.6277	1147.32
350	464.47	-341.02	-179.55	-2.0932	1.8888	2.6609	1120.37
360	457.20	-316.81	-152.77	-2.0177	1.9241	2.6944	1094.80
370	450.01	-292.32	-125.66	-1.9434	1.9600	2.7280	1070.59
380	442.91	-267.55	-98.213	-1.8703	1.9963	2.7616	1047.70
390	435.90	-242.49	-70.430	-1.7981	2.0331	2.7951	1026.11
400	428.99	-217.14	-42.312	-1.7269	2.0701	2.8285	1005.78
425	412.15	-152.54	29.432	-1.5529	2.1634	2.9107	960.17
450	396.00	-86.192	103.20	-1.3843	2.2567	2.9906	921.45
475	380.58	-18.132	178.94	-1.2205	2.3494	3.0677	888.91
500	365.92	51.602	256.56	-1.0613	2.4407	3.1419	861.82
525	352.06	122.97	336.01	-0.906 25	2.5303	3.2132	839.48
550	338.97	195.95	417.20	-0.755 18	2.6181	3.2820	821.26
575	326.66	270.49	500.09	-0.607 81	2.7037	3.3485	806.56
600	315.10	346.59	584.61	-0.463 93	2.7872	3.4129	794.86
625	304.25	424.21	670.72	-0.323 33	2.8686	3.4757	785.69
650	294.08	503.35	758.38	-0.185 82	2.9478	3.5369	778.64
675	284.54	583.97	847.55	-0.051 21	3.0248	3.5968	773.38

TABLE 30. Thermodynamic properties of ethane in the single-phase region—Continued

<i>T</i> (K)	<i>ρ</i> (kg m ⁻³)	<i>u</i> (kJ kg ⁻¹)	<i>h</i> (kJ kg ⁻¹)	<i>s</i> (kJ kg ⁻¹ K ⁻¹)	<i>c_v</i> (kJ kg ⁻¹ K ⁻¹)	<i>c_p</i> (kJ kg ⁻¹ K ⁻¹)	<i>w</i> (m s ⁻¹)
100 MPa							
105.39 ^a	668.55	-874.40	-724.83	-4.9286	1.6191	2.2184	2220.05
110	664.69	-865.07	-714.62	-4.8338	1.6017	2.2113	2197.93
115	660.52	-854.97	-703.57	-4.7356	1.5878	2.2076	2173.49
120	656.37	-844.89	-692.54	-4.6416	1.5775	2.2066	2148.75
125	652.25	-834.82	-681.51	-4.5515	1.5697	2.2071	2123.85
130	648.15	-824.75	-670.47	-4.4650	1.5637	2.2084	2098.93
135	644.07	-814.68	-659.42	-4.3816	1.5589	2.2103	2074.07
140	640.02	-804.61	-648.36	-4.3012	1.5550	2.2125	2049.36
145	636.00	-794.53	-637.30	-4.2235	1.5519	2.2148	2024.83
150	632.00	-784.44	-626.22	-4.1484	1.5495	2.2172	2000.54
155	628.03	-774.35	-615.12	-4.0756	1.5477	2.2198	1976.50
160	624.08	-764.25	-604.02	-4.0051	1.5464	2.2225	1952.73
165	620.15	-754.15	-592.90	-3.9367	1.5456	2.2254	1929.24
170	616.25	-744.04	-581.76	-3.8702	1.5454	2.2285	1906.04
175	612.37	-733.91	-570.61	-3.8055	1.5458	2.2319	1883.13
180	608.51	-723.78	-559.44	-3.7426	1.5467	2.2356	1860.50
185	604.67	-713.63	-548.26	-3.6813	1.5483	2.2397	1838.17
190	600.86	-703.47	-537.05	-3.6215	1.5505	2.2442	1816.13
195	597.07	-693.30	-525.81	-3.5631	1.5532	2.2491	1794.38
200	593.30	-683.10	-514.55	-3.5061	1.5566	2.2545	1772.91
210	585.81	-662.65	-491.95	-3.3959	1.5654	2.2667	1730.85
220	578.41	-642.10	-469.21	-3.2901	1.5766	2.2809	1689.94
230	571.08	-621.43	-446.33	-3.1883	1.5904	2.2971	1650.19
240	563.83	-600.62	-423.27	-3.0902	1.6066	2.3153	1611.61
250	556.65	-579.66	-400.01	-2.9953	1.6252	2.3354	1574.23
260	549.54	-558.52	-376.55	-2.9033	1.6461	2.3574	1538.04
270	542.50	-537.19	-352.86	-2.8139	1.6690	2.3811	1503.07
280	535.54	-515.65	-328.92	-2.7268	1.6938	2.4064	1469.33
290	528.64	-493.89	-304.73	-2.6419	1.7205	2.4332	1436.84
300	521.82	-471.89	-280.25	-2.5590	1.7488	2.4613	1405.58
310	515.07	-449.65	-255.50	-2.4778	1.7785	2.4904	1375.57
320	508.39	-427.14	-230.44	-2.3982	1.8096	2.5206	1346.80
330	501.79	-404.37	-205.08	-2.3202	1.8418	2.5516	1319.26
340	495.26	-381.32	-179.41	-2.2436	1.8750	2.5833	1292.93
350	488.81	-357.99	-153.41	-2.1682	1.9091	2.6156	1267.80
360	482.44	-334.38	-127.09	-2.0941	1.9439	2.6483	1243.84
370	476.14	-310.47	-100.45	-2.0211	1.9794	2.6813	1221.02
380	469.93	-286.26	-73.468	-1.9491	2.0153	2.7145	1199.32
390	463.81	-261.76	-46.156	-1.8782	2.0516	2.7479	1178.71
400	457.76	-236.96	-18.510	-1.8082	2.0882	2.7813	1159.14
425	443.04	-173.65	52.063	-1.6371	2.1804	2.8645	1114.60
450	428.87	-108.47	124.70	-1.4710	2.2729	2.9465	1075.84
475	415.28	-41.429	199.37	-1.3095	2.3647	3.0269	1042.28
500	402.26	27.435	276.03	-1.1523	2.4553	3.1051	1013.38
525	389.83	98.091	354.61	-0.998 93	2.5443	3.1811	988.61
550	377.98	170.50	435.07	-0.849 23	2.6315	3.2549	967.47
575	366.70	244.63	517.34	-0.702 96	2.7167	3.3263	949.52
600	355.97	320.45	601.37	-0.559 92	2.7997	3.3957	934.37
625	345.78	397.91	687.10	-0.419 93	2.8807	3.4631	921.64
650	336.11	476.98	774.50	-0.282 82	2.9596	3.5285	911.04
675	326.93	557.64	863.52	-0.148 45	3.0363	3.5923	902.26
200 MPa							
118.64 ^a	683.67	-859.03	-566.49	-4.8351	1.6550	2.1898	2394.54
120	682.73	-856.46	-563.52	-4.8101	1.6530	2.1899	2388.92
125	679.26	-847.00	-552.56	-4.7207	1.6470	2.1908	2368.17
130	675.83	-837.54	-541.61	-4.6348	1.6425	2.1923	2347.41

TABLE 30. Thermodynamic properties of ethane in the single-phase region—Continued

T (K)	ρ (kg m ⁻³)	u (kJ kg ⁻¹)	h (kJ kg ⁻¹)	s (kJ kg ⁻¹ K ⁻¹)	c_v (kJ kg ⁻¹ K ⁻¹)	c_p (kJ kg ⁻¹ K ⁻¹)	w (m s ⁻¹)
200 MPa							
135	672.42	-828.07	-530.64	-4.5520	1.6391	2.1942	2326.78
140	669.05	-818.60	-519.66	-4.4722	1.6363	2.1961	2306.34
145	665.70	-809.11	-508.68	-4.3951	1.6342	2.1981	2286.15
150	662.39	-799.62	-497.68	-4.3205	1.6325	2.2000	2266.24
155	659.10	-790.12	-486.68	-4.2483	1.6312	2.2019	2246.63
160	655.85	-780.61	-475.67	-4.1784	1.6303	2.2038	2227.33
165	652.62	-771.10	-464.64	-4.1106	1.6299	2.2058	2208.33
170	649.42	-761.57	-453.61	-4.0447	1.6298	2.2080	2189.63
175	646.25	-752.04	-442.56	-3.9806	1.6303	2.2104	2171.23
180	643.11	-742.49	-431.50	-3.9183	1.6312	2.2131	2153.12
185	640.00	-732.93	-420.43	-3.8577	1.6327	2.2160	2135.29
190	636.91	-723.36	-409.34	-3.7985	1.6347	2.2194	2117.73
195	633.85	-713.77	-398.24	-3.7408	1.6373	2.2231	2100.44
200	630.82	-704.16	-387.11	-3.6845	1.6404	2.2273	2083.40
210	624.82	-684.88	-364.79	-3.5756	1.6484	2.2370	2050.07
220	618.93	-665.50	-342.36	-3.4713	1.6589	2.2486	2017.70
230	613.13	-646.01	-319.81	-3.3710	1.6717	2.2623	1986.26
240	607.42	-626.37	-297.11	-3.2744	1.6869	2.2781	1955.72
250	601.80	-606.58	-274.24	-3.1811	1.7044	2.2958	1926.06
260	596.26	-586.61	-251.19	-3.0906	1.7241	2.3155	1897.28
270	590.81	-566.44	-227.93	-3.0028	1.7459	2.3370	1869.37
280	585.44	-546.06	-204.44	-2.9174	1.7695	2.3602	1842.33
290	580.15	-525.45	-180.72	-2.8342	1.7950	2.3850	1816.16
300	574.94	-504.60	-156.74	-2.7529	1.8220	2.4113	1790.84
310	569.80	-483.49	-132.49	-2.6734	1.8505	2.4388	1766.37
320	564.73	-462.11	-107.96	-2.5955	1.8803	2.4676	1742.75
330	559.74	-440.44	-83.132	-2.5191	1.9112	2.4973	1719.96
340	554.82	-418.49	-58.006	-2.4441	1.9432	2.5279	1698.00
350	549.96	-396.23	-32.571	-2.3704	1.9760	2.5593	1676.85
360	545.18	-373.67	-6.8178	-2.2978	2.0096	2.5913	1656.49
370	540.46	-350.80	19.258	-2.2264	2.0438	2.6239	1636.91
380	535.81	-327.61	45.661	-2.1560	2.0785	2.6568	1618.08
390	531.22	-304.09	72.395	-2.0865	2.1136	2.6901	1599.98
400	526.70	-280.26	99.464	-2.0180	2.1490	2.7236	1582.60
425	515.67	-219.24	168.61	-1.8504	2.2384	2.8079	1542.13
450	505.02	-156.17	239.86	-1.6875	2.3281	2.8921	1505.62
475	494.74	-91.049	313.20	-1.5289	2.4174	2.9755	1472.72
500	484.82	-23.906	388.62	-1.3742	2.5057	3.0576	1443.10
525	475.24	45.232	466.07	-1.2230	2.5925	3.1382	1416.43
550	466.00	116.33	545.51	-1.0752	2.6777	3.2168	1392.44
575	457.08	189.34	626.90	-0.930 53	2.7610	3.2936	1370.86
600	448.47	264.22	710.17	-0.788 77	2.8424	3.3683	1351.44
625	440.17	340.92	795.30	-0.649 78	2.9218	3.4411	1333.98
650	432.15	419.41	882.21	-0.513 44	2.9992	3.5118	1318.28
675	424.41	499.63	970.87	-0.379 61	3.0746	3.5806	1304.17
400 MPa							
141.42 ^a	710.01	-825.38	-262.01	-4.6994	1.7552	2.2026	2663.73
145	708.11	-819.00	-254.12	-4.6444	1.7543	2.2047	2652.58
150	705.49	-810.07	-243.09	-4.5696	1.7531	2.2075	2637.26
155	702.89	-801.12	-232.05	-4.4971	1.7521	2.2100	2622.24
160	700.32	-792.16	-220.99	-4.4269	1.7513	2.2124	2607.52
165	697.77	-783.18	-209.92	-4.3588	1.7508	2.2147	2593.09
170	695.24	-774.18	-198.84	-4.2927	1.7505	2.2171	2578.93
175	692.74	-765.17	-187.75	-4.2284	1.7506	2.2196	2565.02
180	690.26	-756.14	-176.65	-4.1658	1.7510	2.2222	2551.36

TABLE 30. Thermodynamic properties of ethane in the single-phase region—Continued

<i>T</i> (K)	<i>ρ</i> (kg m ⁻³)	<i>u</i> (kJ kg ⁻¹)	<i>h</i> (kJ kg ⁻¹)	<i>s</i> (kJ kg ⁻¹ K ⁻¹)	<i>c_v</i> (kJ kg ⁻¹ K ⁻¹)	<i>c_p</i> (kJ kg ⁻¹ K ⁻¹)	<i>w</i> (m s ⁻¹)
400 MPa							
185	687.81	-747.09	-165.53	-4.1049	1.7519	2.2251	2537.92
190	685.38	-738.01	-154.40	-4.0455	1.7533	2.2283	2524.70
195	682.97	-728.92	-143.25	-3.9876	1.7552	2.2318	2511.68
200	680.58	-719.81	-132.08	-3.9310	1.7576	2.2357	2498.85
210	675.88	-701.50	-109.68	-3.8217	1.7641	2.2448	2473.73
220	671.26	-683.07	-87.174	-3.7171	1.7729	2.2558	2449.26
230	666.72	-664.51	-64.553	-3.6165	1.7840	2.2687	2425.41
240	662.25	-645.79	-41.793	-3.5196	1.7974	2.2837	2402.12
250	657.87	-626.90	-18.873	-3.4261	1.8132	2.3006	2379.39
260	653.56	-607.81	4.2260	-3.3355	1.8311	2.3195	2357.19
270	649.31	-588.51	27.523	-3.2476	1.8511	2.3402	2335.52
280	645.14	-568.98	51.036	-3.1621	1.8730	2.3627	2314.37
290	641.03	-549.21	74.783	-3.0787	1.8967	2.3868	2293.76
300	636.99	-529.18	98.778	-2.9974	1.9220	2.4124	2273.66
310	633.01	-508.87	123.04	-2.9178	1.9489	2.4394	2254.10
320	629.08	-488.28	147.57	-2.8400	1.9770	2.4675	2235.06
330	625.22	-467.39	172.39	-2.7636	2.0064	2.4968	2216.55
340	621.41	-446.19	197.51	-2.6886	2.0368	2.5270	2198.57
350	617.66	-424.67	222.93	-2.6149	2.0681	2.5580	2181.11
360	613.96	-402.84	248.67	-2.5424	2.1002	2.5897	2164.16
370	610.31	-380.68	274.73	-2.4710	2.1329	2.6219	2147.73
380	606.71	-358.18	301.11	-2.4007	2.1661	2.6547	2131.79
390	603.17	-335.35	327.82	-2.3313	2.1998	2.6878	2116.35
400	599.67	-312.17	354.87	-2.2628	2.2339	2.7212	2101.39
425	591.12	-252.73	423.95	-2.0953	2.3200	2.8055	2066.02
450	582.85	-191.14	495.14	-1.9325	2.4066	2.8901	2033.39
475	574.83	-127.40	568.45	-1.7740	2.4930	2.9742	2003.29
500	567.07	-61.537	643.84	-1.6194	2.5785	3.0572	1975.53
525	559.54	6.4235	721.30	-1.4682	2.6627	3.1388	1949.92
550	552.23	76.438	800.77	-1.3204	2.7455	3.2187	1926.26
575	545.14	148.46	882.22	-1.1755	2.8265	3.2969	1904.40
600	538.25	222.45	965.60	-1.0336	2.9057	3.3732	1884.18
625	531.55	298.35	1050.86	-0.89440	2.9831	3.4475	1865.46
650	525.04	376.12	1137.96	-0.75776	3.0586	3.5199	1848.12
675	518.71	455.70	1226.84	-0.62359	3.1322	3.5904	1832.05
600 MPa							
160.77 ^a	732.73	-788.72	30.137	-4.6003	1.8345	2.2282	2885.11
165	730.88	-781.36	39.568	-4.5423	1.8340	2.2309	2875.15
170	728.71	-772.64	50.730	-4.4757	1.8336	2.2339	2863.60
175	726.57	-763.89	61.907	-4.4109	1.8334	2.2370	2852.27
180	724.44	-755.12	73.100	-4.3478	1.8336	2.2402	2841.14
185	722.33	-746.33	84.309	-4.2864	1.8341	2.2435	2830.20
190	720.24	-737.52	95.535	-4.2265	1.8351	2.2470	2819.43
195	718.17	-728.68	106.78	-4.1681	1.8365	2.2509	2808.81
200	716.12	-719.81	118.04	-4.1111	1.8384	2.2551	2798.34
210	712.06	-701.98	140.64	-4.0008	1.8439	2.2646	2777.79
220	708.07	-684.03	163.34	-3.8952	1.8516	2.2758	2757.70
230	704.15	-665.92	186.17	-3.7938	1.8616	2.2890	2738.04
240	700.30	-647.65	209.13	-3.6961	1.8739	2.3040	2718.75
250	696.51	-629.19	232.25	-3.6017	1.8885	2.3210	2699.83
260	692.77	-610.53	255.55	-3.5103	1.9053	2.3398	2681.25
270	689.10	-591.64	279.05	-3.4216	1.9242	2.3605	2663.02
280	685.49	-572.52	302.77	-3.3353	1.9450	2.3829	2645.13
290	681.93	-553.14	326.72	-3.2513	1.9676	2.4069	2627.59
300	678.42	-533.49	350.91	-3.1693	1.9919	2.4323	2610.41
310	674.97	-513.56	375.37	-3.0891	2.0177	2.4591	2593.59

TABLE 30. Thermodynamic properties of ethane in the single-phase region—Continued

<i>T</i> (K)	<i>ρ</i> (kg m ⁻³)	<i>u</i> (kJ kg ⁻¹)	<i>h</i> (kJ kg ⁻¹)	<i>s</i> (kJ kg ⁻¹ K ⁻¹)	<i>c_v</i> (kJ kg ⁻¹ K ⁻¹)	<i>c_p</i> (kJ kg ⁻¹ K ⁻¹)	<i>w</i> (m s ⁻¹)
600 MPa							
320	671.56	-493.34	400.10	-3.0106	2.0448	2.4872	2577.14
330	668.21	-472.81	425.12	-2.9336	2.0732	2.5162	2561.06
340	664.90	-451.96	450.43	-2.8580	2.1026	2.5463	2545.37
350	661.64	-430.79	476.04	-2.7838	2.1329	2.5771	2530.05
360	658.43	-409.29	501.97	-2.7108	2.1641	2.6087	2515.12
370	655.25	-387.46	528.22	-2.6388	2.1959	2.6408	2500.57
380	652.12	-365.28	554.79	-2.5680	2.2283	2.6734	2486.39
390	649.03	-342.76	581.69	-2.4981	2.2611	2.7064	2472.60
400	645.99	-319.90	608.92	-2.4292	2.2943	2.7397	2459.17
425	638.53	-261.20	678.46	-2.2606	2.3784	2.8237	2427.19
450	631.31	-200.30	750.11	-2.0968	2.4631	2.9081	2397.38
475	624.30	-137.22	823.86	-1.9373	2.5476	2.9920	2369.60
500	617.50	-71.966	899.70	-1.7817	2.6315	3.0749	2343.71
525	610.89	-4.5852	977.59	-1.6297	2.7141	3.1565	2319.57
550	604.46	64.886	1057.51	-1.4810	2.7953	3.2365	2297.04
575	598.20	136.40	1139.41	-1.3354	2.8749	3.3148	2275.99
600	592.11	209.91	1223.23	-1.1927	2.9528	3.3912	2256.32
625	586.18	285.37	1308.95	-1.0528	3.0289	3.4657	2237.90
650	580.40	362.73	1396.50	-0.915 41	3.1031	3.5383	2220.65
675	574.76	441.94	1485.85	-0.780 54	3.1756	3.6091	2204.48
800 MPa							
177.75 ^a	752.83	-750.21	312.44	-4.5228	1.8937	2.2530	3078.58
180	751.98	-746.34	317.52	-4.4944	1.8938	2.2548	3074.37
185	750.10	-737.73	328.80	-4.4326	1.8943	2.2588	3065.16
190	748.23	-729.09	340.11	-4.3723	1.8952	2.2629	3056.08
195	746.37	-720.42	351.43	-4.3135	1.8965	2.2673	3047.12
200	744.54	-711.72	362.78	-4.2560	1.8982	2.2720	3038.28
210	740.90	-694.22	385.55	-4.1449	1.9032	2.2824	3020.89
220	737.32	-676.58	408.43	-4.0385	1.9104	2.2944	3003.83
230	733.79	-658.78	431.44	-3.9362	1.9199	2.3080	2987.06
240	730.32	-640.81	454.60	-3.8376	1.9316	2.3235	2970.55
250	726.90	-622.64	477.92	-3.7424	1.9456	2.3409	2954.27
260	723.53	-604.27	501.42	-3.6502	1.9617	2.3600	2938.21
270	720.21	-585.66	525.13	-3.5608	1.9799	2.3809	2922.37
280	716.94	-566.80	549.05	-3.4738	2.0000	2.4035	2906.77
290	713.72	-547.68	573.20	-3.3890	2.0220	2.4276	2891.39
300	710.54	-528.29	597.61	-3.3063	2.0456	2.4532	2876.26
310	707.41	-508.61	622.27	-3.2254	2.0707	2.4801	2861.39
320	704.33	-488.63	647.21	-3.1463	2.0972	2.5081	2846.78
330	701.28	-468.33	672.44	-3.0686	2.1249	2.5372	2832.45
340	698.28	-447.72	697.96	-2.9924	2.1536	2.5672	2818.40
350	695.31	-426.78	723.78	-2.9176	2.1833	2.5981	2804.64
360	692.39	-405.50	749.92	-2.8440	2.2139	2.6296	2791.17
370	689.50	-383.88	776.38	-2.7715	2.2450	2.6617	2778.01
380	686.65	-361.91	803.16	-2.7001	2.2768	2.6942	2765.15
390	683.84	-339.60	830.26	-2.6296	2.3091	2.7272	2752.58
400	681.06	-316.93	857.70	-2.5602	2.3417	2.7604	2740.32
425	674.26	-258.72	927.76	-2.3903	2.4243	2.8442	2710.97
450	667.67	-198.28	999.92	-2.2254	2.5077	2.9284	2683.41
475	661.26	-135.63	1074.18	-2.0648	2.5910	3.0122	2657.56
500	655.03	-70.793	1150.52	-1.9082	2.6736	3.0950	2633.31
525	648.98	-3.7999	1228.91	-1.7552	2.7551	3.1764	2610.56
550	643.08	65.304	1309.32	-1.6056	2.8353	3.2563	2589.20

TABLE 30. Thermodynamic properties of ethane in the single-phase region—Continued

<i>T</i> (K)	<i>ρ</i> (kg m ⁻³)	<i>u</i> (kJ kg ⁻¹)	<i>h</i> (kJ kg ⁻¹)	<i>s</i> (kJ kg ⁻¹ K ⁻¹)	<i>c_v</i> (kJ kg ⁻¹ K ⁻¹)	<i>c_p</i> (kJ kg ⁻¹ K ⁻¹)	<i>w</i> (m s ⁻¹)
800 MPa							
575	637.33	136.47	1391.71	-1.4591	2.9138	3.3344	2569.13
600	631.73	209.66	1476.03	-1.3156	2.9907	3.4107	2550.24
625	626.26	284.81	1562.23	-1.1748	3.0659	3.4852	2532.46
650	620.93	361.88	1650.27	-1.0367	3.1393	3.5578	2515.69
675	615.72	440.81	1740.11	-0.90111	3.2109	3.6285	2499.88
900 MPa							
185.55 ^a	762.11	-730.50	450.43	-4.4899	1.9186	2.2651	3167.17
190	760.53	-722.87	460.52	-4.4362	1.9195	2.2692	3159.71
195	758.76	-714.27	471.88	-4.3772	1.9208	2.2739	3151.42
200	757.00	-705.64	483.26	-4.3195	1.9225	2.2789	3143.24
210	753.53	-688.28	506.10	-4.2081	1.9275	2.2898	3127.12
220	750.10	-670.77	529.06	-4.1013	1.9347	2.3023	3111.30
230	746.73	-653.11	552.15	-3.9986	1.9440	2.3163	3095.71
240	743.40	-635.26	575.40	-3.8997	1.9556	2.3322	3080.32
250	740.12	-617.21	598.80	-3.8042	1.9693	2.3498	3065.11
260	736.89	-598.95	622.40	-3.7116	1.9853	2.3692	3050.09
270	733.71	-580.45	646.19	-3.6218	2.0033	2.3903	3035.23
280	730.57	-561.71	670.21	-3.5345	2.0232	2.4130	3020.56
290	727.48	-542.70	694.46	-3.4494	2.0449	2.4373	3006.08
300	724.42	-523.41	718.96	-3.3663	2.0683	2.4630	2991.80
310	721.41	-503.83	743.72	-3.2851	2.0932	2.4899	2977.73
320	718.45	-483.94	768.76	-3.2056	2.1194	2.5180	2963.88
330	715.52	-463.75	794.09	-3.1277	2.1469	2.5472	2950.27
340	712.63	-443.23	819.71	-3.0512	2.1754	2.5773	2936.91
350	709.77	-422.38	845.63	-2.9761	2.2049	2.6081	2923.80
360	706.96	-401.19	871.87	-2.9022	2.2352	2.6397	2910.95
370	704.18	-379.66	898.43	-2.8294	2.2661	2.6718	2898.38
380	701.43	-357.78	925.31	-2.7577	2.2977	2.7043	2886.07
390	698.72	-335.55	952.52	-2.6871	2.3297	2.7373	2874.03
400	696.04	-312.97	980.06	-2.6173	2.3621	2.7705	2862.27
425	689.49	-254.95	1050.36	-2.4469	2.4442	2.8543	2834.04
450	683.13	-194.70	1122.77	-2.2813	2.5271	2.9385	2807.48
475	676.94	-132.22	1197.28	-2.1202	2.6099	3.0222	2782.49
500	670.93	-67.552	1273.87	-1.9631	2.6920	3.1049	2759.00
525	665.07	-0.71790	1352.52	-1.8096	2.7730	3.1863	2736.90
550	659.37	68.236	1433.17	-1.6595	2.8527	3.2661	2716.10
575	653.81	139.26	1515.80	-1.5126	2.9309	3.3441	2696.52
600	648.39	212.31	1600.36	-1.3687	3.0074	3.4204	2678.05
625	643.10	287.33	1686.81	-1.2276	3.0821	3.4948	2660.62
650	637.93	364.28	1775.09	-1.0891	3.1552	3.5673	2644.15
675	632.88	443.09	1865.16	-0.95311	3.2264	3.6380	2628.58

^aTemperature on the melting curve.^bSaturated liquid.^cSaturated vapor.

10. References

- Abdulagatov, I. M., S. B. Kiselev, L. N. Levina, Z. R. Zakaryaev, and O. N. Mamchenkova, Int. J. Thermophys. **17**, 423 (1996).
- Ambrose, D. and C. Tsonopoulos, J. Chem. Eng. Data **40**, 531 (1995).
- Atack, D. and W. G. Schneider, J. Phys. Colloid Chem. **54**, 1323 (1950).
- Atake, T. and H. Chihara, Chem. Lett. **1976**, 683 (1976).
- Barclay, D. A., J. L. Flebbe, and D. B. Manley, J. Chem. Eng. Data **27**, 135 (1982).
- Beattie, J. A., C. Hadlock, and N. Poffenberger, J. Chem. Phys. **3**, 93 (1935).
- Beattie, J. A., G.-J. Su, and G. L. Simard, J. Am. Chem. Soc. **61**, 924 (1939a).
- Beattie, J. A., G.-J. Su, and G. L. Simard, J. Am. Chem. Soc. **61**, 926 (1939b).
- Bedford, R. E. and C. G. M. Kirby, Metrologia **5**, 83 (1969).
- Bedford, R. E., G. Bonnier, H. Maas, and F. Pavese, Metrologia **20**, 145 (1984).
- Bell, T. N., C. M. Bignell, and P. J. Dunlop, Physica A **181**, 221 (1992).
- Bender, R., Dissertation, Universität Karlsruhe, Germany, 1982.
- Berestov, A. T., M. S. Giterman, and N. G. Shmakov, Zh. Eksp. Teor. Fiz. **64**, 2232 (1973); [Sov. Phys.-JETP **37**, 1128 (1973)].
- Besserer, G. J. and D. B. Robinson, J. Chem. Eng. Data **18**, 137 (1973).
- Bier, K., J. Kunze, G. Maurer, and H. Sand, J. Chem. Eng. Data **21**, 5 (1976a).

- Bier, K., J. Kunze, and G. Maurer, *J. Chem. Thermodyn.* **8**, 857 (1976b).
 Boyes, S. J., Ph.D. thesis, University of London, U.K., 1992.
 Brachthäuser, K., R. Kleinrahm, H. W. Lösch, and W. Wagner, *Fortschr.-Ber. VDI*, Reihe 8, Nr. 371, VDI-Verlag, Düsseldorf, 1993.
- Brown, T. S., A. J. Kidney, and E. D. Sloan, *Fluid Phase Equilib.* **40**, 169 (1988).
 Brunner, E., *J. Chem. Thermodyn.* **19**, 823 (1987).
 Brunner, E., *J. Chem. Thermodyn.* **20**, 273 (1988).
 Büchner, K., G. Maurer, and E. Bender, *Cryogenics* **21**, 157 (1981).
 Bulavin, L. A., Yu. M. Ostanevich, A. P. Simkina, and A. V. Stelkov, *Ukr. Fiz. Zh. (Ukr. Ed.)* **16**, 90 (1971).
 Bulavin, L. A. and Yu. L. Shimanskii, *Pis'ma Zh. Eksp. Teor. Fiz.* **29**, 482 (1979).
 Burnett, L. J. and B. H. Muller, *J. Chem. Eng. Data* **15**, 154 (1970).
 Burrell, G. A. and G. W. Jones, Bureau of Mines, Rep. of Investigation, No. 2276, 1921.
 Burrell, G. A. and I. W. Robertson, *J. Am. Chem. Soc.* **37**, 1893 (1915).
 Burton, M. and D. Balzarini, *Can. J. Phys.* **52**, 52 (1974).
 Byun, H.-S., T. P. DiNoia, and M. A. McHugh, *J. Chem. Eng. Data* **45**, 810 (2000).
 Cardoso, E. and R. Bell, *J. Chim. Phys.* **10**, 497 (1912).
 Carruth, G. F. and R. Kobayashi, *J. Chem. Eng.* **18**, 115 (1973).
 Chao, J., R. C. Wilhout, and B. J. Zwolinski, *J. Phys. Chem. Ref. Data* **2**, 427 (1973).
 Chashkin, Yu. R., V. A. Smirnov, and A. V. Voronel, *Teplofiz. Svoistva Veshchestv Mater.* **21**, 139 (1970).
 Chui, C.-H. and F. B. Canfield, *Trans. Faraday Soc.* **67**, 2933 (1971).
 Claus, P., R. Kleinrahm, and W. Wagner, *J. Chem. Thermodyn.* **35**, 159 (2003).
 Clusius, K. and K. Weigand, *Z. Phys. Chem. Abt. B* **46**, 1 (1940).
 Colgate, S. O., A. Sivaraman, and C. Dejsupa, *Fluid Phase Equilib.* **76**, 175 (1992).
 Coplen, T. B., *J. Phys. Chem. Ref. Data* **30**, 701 (2001).
 Dailey, B. P. and W. A. Felsing, *J. Am. Chem. Soc.* **65**, 42 (1943).
 Dana, L. I., A. C. Jenkins, J. N. Burdick, and R. C. Timm, *Ref. Eng.* **12**, 387 (1926).
 Dewar, J., *Philos. Mag.* **18**, 210 (1884).
 Djordjevich, L. and R. A. Budenholzer, *J. Chem. Eng. Data* **15**, 10 (1970).
 Douslin, D. R. and R. H. Harrison, *J. Chem. Thermodyn.* **5**, 491 (1973).
 Dymond, J. H. and E. B. Smith, *The Virial Coefficients of Pure Gases: A Critical Compilation* (Clarendon, Oxford, 1980).
 Eggers, D. F. Jr., *J. Phys. Chem.* **79**, 2116 (1975).
 Ernst, G. and U. E. Hochberg, *J. Chem. Thermodyn.* **21**, 407 (1989).
 Esper, G., W. Lemming, W. Beckermann, and F. Kohler, *Fluid Phase Equilib.* **105**, 173 (1995).
 Estrada-Alexanders, A. F. and J. P. M. Trusler, *J. Chem. Thermodyn.* **29**, 991 (1997).
 Eucken, A. and F. Hauck, *Z. Phys. Chem.* **134**, 161 (1928).
 Eucken, A. and A. Parts, *Z. Phys. Chem.* **20**, 184 (1933).
 Fredenslund, A. and J. Mollerup, *J. Chem. Soc. Faraday Trans. I*, 1653 (1974).
 Friend, D. G., H. Ingham, and J. F. Ely, *J. Phys. Chem. Ref. Data* **20**, 275 (1991).
 Funke, M., R. Kleinrahm, and W. Wagner, *J. Chem. Thermodyn.* **34**, 2001 (2002a).
 Funke, M., R. Kleinrahm, and W. Wagner, *J. Chem. Thermodyn.* **34**, 2017 (2002b).
 Furtado, A., Ph.D. thesis, University of Michigan, Ann Arbor, Michigan, 1973.
 Geijsel, J. I., J. A. Schouten, and N. J. Trappeniers, "The phase diagram of ethane under high pressure," in *High Pressure Science & Technology*, Vol. 2, edited by B. Vodar and Ph. Marteau (Pergamon, Oxford, 1979), p. 645.
 Golovskii, Y. A., E. P. Mitsevich, and V. A. Tsymarnyy, VNII Gazprom Depos. No. 39M, 1978.
 Goodwin, R. D., H. M. Roder, and G. C. Strat, *Thermophysical Properties of Ethane from 90 to 600 K at Pressures to 700 bar*, NBS Technical Note 684 (NBS Boulder, 1976).
 Grini, P. G., Dr.-Ing. thesis, Norwegian Institute of Technology, Trondheim, Norway, 1994.
 Grini, P. G., H. S. Mæhlum, E. Brendeng, and G. A. Owren, *J. Chem. Thermodyn.* **28**, 667 (1996).
 Gunn, R. J., J. W. Eldridge, V. C. Okay, and T. J. Lee, *AIChE J.* **20**, 357 (1974).
 Gunn, R. D., M.Sc. thesis, University of California, Berkeley, California, 1958.
 Guo, X.-Y., R. Kleinrahm, and W. Wagner, Research Report, Lehrstuhl für Thermodynamik, Ruhr-Universität Bochum, 1992.
 Gurvich, L. V., I. V. Veyts, and C. B. Alcock, *Thermodynamic Properties of Individual Substances* 4th ed., Vol. 2 (Hemisphere, Washington, 1991).
 Haase, R. and W. Tillmann, *Z. Phys. Chem.* **186**, 99 (1994).
 Händel, G., R. Kleinrahm, and W. Wagner, *J. Chem. Thermodyn.* **24**, 685 (1992).
 Hahn, R., K. Schäfer, and B. Schramm, *Ber. Bunsenges. Phys. Chem.* **78**, 287 (1974).
 Hainlen, A., *Justus Liebigs Ann. Chem.* **282**, 229 (1894).
 Hamann, S. D. and W. J. McManamey, *Trans. Faraday Soc.* **49**, 149 (1953).
 Haynes, W. M. and M. J. Hiza, *J. Chem. Thermodyn.* **9**, 179 (1977).
 Heuse, W., *Ann. Phys.* **59**, 86 (1919).
 Hirschfelder, J. O., F. T. McClure, and I. F. Weeks, *J. Chem. Phys.* **10**, 201 (1942).
 Holcomb, C. D., J. W. Magee, and W. M. Haynes, Research Report RR-147, Gas Processors Association, Tulsa, 1995.
 Holste, J. C., J. G. Young, P. T. Eubank, and K. R. Hall, *AIChE J.* **28**, 807 (1982).
 Hoover, A. E., L. Nagata, T. W. Leland, and R. Kobayashi, *J. Chem. Phys.* **48**, 2633 (1968).
 Hou, H., J. C. Holste, and K. R. Hall, *J. Chem. Eng. Data* **41**, 344 (1996).
 Huff, J. A. and T. M. Reed, *J. Chem. Eng. Data* **8**, 306 (1963).
 Jaeschke, M. and A. E. Humphreys (private communication). Data published in extracts in *GERG Technical Monograph 4* (VDI-Verlag, Düsseldorf, 1990).
 Jensen, R. H. and F. Kurata, *J. Petrol. Tech.* **21**, 683 (1969).
 Kahre, L. C., *J. Chem. Eng. Data* **18**, 267 (1973).
 Kay, W. B., *Ind. Eng. Chem.* **30**, 459 (1938).
 Kay, W. B., *J. Phys. Chem.* **68**, 827 (1964).
 Kay, W. B. and R. E. Albert, *Ind. Eng. Chem.* **48**, 422 (1956).
 Kay, W. B. and D. B. Brice, *Ind. Eng. Chem.* **45**, 615 (1953).
 Kay, W. B. and T. D. Nevens, *Chem. Eng. Prog. Symp. Ser.* **48**, 108 (1952).
 Kerl, K. and H. Häusler, *Ber. Bunsenges. Phys. Chem.* **88**, 992 (1984).
 Khazanova, N. E. and E. E. Sominskaya, *J. Phys. Chem.* **45**, 88 (1971).
 Khodeeva, S. M., Russ. *J. Phys. Chem. (Engl. Transl.)* **40**, 1061 (1966).
 Kistiakowski, G. B. and W. W. Rice, *J. Chem. Phys.* **7**, 281 (1939).
 Kleinrahm, R. and W. Wagner, *J. Chem. Thermodyn.* **18**, 739 (1986).
 Klimeck, R. (private communication, 2000).
 Klosek, J. and C. McKinley, C., *Densities of liquefied natural gas and of low molecular weight hydrocarbons*, Proc. 1st Int. Conference of LNG, Chicago, 1968.
 Kuenen, J. P. and W. G. Robson, *Philos. Mag.* **6**, 622 (1902a).
 Kuenen, J. P. and W. G. Robson, *Philos. Mag.* **6**, 149 (1902b).
 Lambert, J. D., G. A. H. Roberts, J. S. Rowlinson, and V. J. Wilkinson, *Proc. R. Soc. A* **196**, 113 (1949).
 Lammers, J. N. J. J., P. H. G. van Kasteren, G. F. Kroon, and H. Zeldernrust, *Enthalpy measurements of natural gas components and mixed refrigerants with a flow calorimeter*, Proc. 57th Ann. Conf. Gas Proc. Assoc., 1978, p. 18.
 Lau, W.-W. R., Ph.D. thesis, Texas A&M University, Texas, 1986.
 Lau, W.-W. R., C.-A. Hwang, J. C. Holste, K. R. Hall, B. E. Gammon, and K. N. Marsh, *J. Chem. Eng. Data* **42**, 900 (1997).
 Leadbetter, A. J., D. J. Taylor, and B. Vincent, *Can. J. Chem.* **42**, 2930 (1964).
 Lemming, W., *Fortschr.-Ber. VDI*, Reihe 19, Nr. 32, VDI-Verlag Düsseldorf, 1989.
 Lichtenhaller, R. N. and K. Schäfer, *Ber. Bunsenges. Phys. Chem.* **73**, 42 (1969).
 Loomis, A. G. and J. E. Walters, *J. Am. Chem. Soc.* **48**, 2051 (1926).
 Lu, H., D. M. Newitt, and M. Ruhemann, *Proc. R. Soc. London A* **178**, 506 (1941).
 Luo, C. C. and R. C. Miller, *Cryogenics* **21**, 85 (1981).
 Maass, O. and C. H. Wright, *J. Am. Chem. Soc.* **43**, 1098 (1921).
 Mansoorian, H., K. R. Hall, J. C. Holste, and P. T. Eubank, *J. Chem. Thermodyn.* **13**, 1001 (1981).
 Mason, S. G., S. N. Naldrett, and O. Maass, *Can. J. Res.* **18**, 103 (1940).
 Mason, E. A. and T. H. Spurling, "The virial equation of state," in *The Int.*

- Enc. of Phys. Chem. and Chem. Phys.* (Pergamon, Oxford, 1969).
- McClune, C. R., *Cryogenics* **16**, 289 (1976).
- Michels, A. and W. Nederbragt, *Physica VI*, 656 (1939).
- Michels, A., W. van Straaten, and J. Dawson, *Physica XX*, 17 (1954).
- Miniovich, V. M. and G. A. Sorina, *Russ. J. Phys. Chem.* **45**, 306 (1971).
- Miyazaki, T., A. V. Hejmadi, and J. E. Powers, *J. Chem. Thermodyn.* **12**, 105 (1980).
- Mohr, P. J. and B. N. Taylor, *J. Phys. Chem. Ref. Data* **28**, 1713 (1999).
- Morrison, G. and J. M. Kincaid, *AIChE J.* **30**, 257 (1984).
- Murray, F. E. and C. G. Mason, *Can. J. Chem.* **30**, 550 (1952).
- Noury, J., *Comptes Rendus* **234**, 303 (1952).
- Ohgaki, K. and T. Katayama, *Fluid Phase Equilib.* **1**, 27 (1977).
- Olszewski, K., *Philos. Mag.* **39**, 188 (1895).
- Orrit, J. E. and J. M. Laupretre, *Adv. Cryog. Eng.* **23**, 573 (1978).
- Pal, A. K., G. A. Pope, Y. Arai, N. F. Carnahan, and R. Kobayashi, *J. Chem. Eng. Data* **21**, 394 (1976).
- Palmer, H. B., *J. Chem. Phys.* **22**, 625 (1954).
- Pamidimukkala, K. M., D. Rogers, and G. B. Skinner, *J. Phys. Chem. Ref. Data* **11**, 83 (1982).
- Pavese, F., *J. Chem. Thermodyn.* **10**, 369 (1978).
- Parrish, W. R., *Fluid Phase Equilib.* **18**, 279 (1984).
- Pestak, M. W., R. E. Goldstein, M. H. W. Chan, J. R. de Bruyn, D. A. Balzarini, and N. W. Ashcroft, *Phys. Rev. B* **36**, 599 (1987).
- Poole, G. R. and R. A. Aziz, *Can. J. Phys.* **50**, 721 (1972).
- Pope, G. A., Ph.D. thesis, Rice University, Houston, 1972.
- Porter, F., *J. Am. Chem. Soc.* **48**, 2055 (1926).
- Preston-Thomas, H., *Metrologia* **27**, 3 (1990).
- Prins, A., *Proc. Acad. Sci. Amsterdam* **17**, 1095 (1915).
- Quint, N., *Z. Phys. Chem.* **39**, 14 (1902).
- Reamer, H. H., R. H. Olds, B. H. Sage, and W. N. Lacey, *Ind. Eng. Chem.* **36**, 956 (1944).
- Regnier, J., *J. Chim. Phys. Phys.-Chim. Biol.* **69**, 942 (1972).
- Rigby, M., J. H. Dymond, and E. B. Smith, "Second virial coefficients," in *The Virial Coefficients of Pure Gases: A Critical Compilation*, edited by J. H. Dymond and E. B. Smith (Clarendon, Oxford, 1980).
- Roder, H. M., *J. Chem. Phys.* **65**, 1371 (1976a).
- Roder, H. M., *J. Res. NBS*, **80A**, 739 (1976b).
- Rodosevich, J. B. and R. C. Miller, *AIChE J.* **19**, 729 (1973).
- Rossini, F. D., K. S. Pitzer, R. L. Arnett, R. M. Braun, and G. C. Pimentel, *Selected Values of Physical and Thermodynamic Properties of Hydrocarbons and Related Compounds* (American Petroleum Institute, Carnegie Press, Pittsburgh, 1953).
- Rusby, R. L., *J. Chem. Thermodyn.* **23**, 1153 (1991).
- Sage, B. H., D. C. Webster, and W. N. Lacey, *Ind. Eng. Chem.* **29**, 658 (1937).
- Schäfer, K. and W. Auer, *Werte der Thermodynamischen Funktionen bei Standarddrücken in Abhängigkeit von der Temperatur für Ausgewählte Stoffe*, Landolt-Börnstein (Springer, Berlin, 1961), Vol. 2.
- Schäfer, K., B. Schramm, and J. S. Urieta Navarro, *Z. Phys. Chem.* **93**, 203 (1974).
- Schmidt, E. and W. Thomas, *Fortsch. Geb. Ingenieurwes.* **20B**, 161 (1954).
- Schmidt, E. and W. Wagner, *Fluid Phase Equilib.* **19**, 175 (1985).
- Schutte, W. H. M., K. O. Prins, and N. J. Trappeniers, "A high pressure NMR investigation of phase transition in solid ethane," in *Magnetic Resonance and Related Phenomena*, edited by E. Kundla, Proceedings of the XXth Congress Ampère, Tallinn, 1978 (Springer, Berlin, 1979).
- Setzmann, U. and W. Wagner, *Int. J. Thermophys.* **10**, 1103 (1989).
- Setzmann, U. and W. Wagner, *J. Phys. Chem. Ref. Data* **20**, 1061 (1991).
- Shinsaka, K., N. Gee, and G. R. Freeman, *J. Chem. Thermodyn.* **17**, 1111 (1985).
- Shmakov, N. G., *Teplofiz. Svoistva Veshestv Material. Moskau GSSSD* **7**, 155 (1973).
- Sliwinski, P., *Z. Phys. Chem. Neue Folge* **63**, 263 (1969).
- Span, R., *Multiparameter Equations of State—An Accurate Source of Thermodynamic Property Data* (Springer, Berlin, 2000).
- Span, R. and W. Wagner, *J. Phys. Chem. Ref. Data* **25**, 1509 (1996).
- Span, R., E. W. Lemmon, R. T. Jacobsen, W. Wagner, and A. Yokozeki, *J. Phys. Chem. Ref. Data* **29**, 1361 (2000).
- Span, R. and W. Wagner, *Int. J. Thermophys.* **18**, 1415 (1997).
- Span, R. and W. Wagner, *Int. J. Thermophys.* **24**, 1 (2003a).
- Span, R. and W. Wagner, *Int. J. Thermophys.* **24**, 41 (2003b).
- Straty, G. C. and R. Tsumura, *J. Chem. Phys.* **64**, 859 (1976a).
- Straty, G. C. and R. Tsumura, *J. Res. NBS* **80A**, 35 (1976b).
- Strein, K., R. N. Lichtenhaler, B. Schramm, and K. Schäfer, *Ber. Bunsenges. Phys. Chem.* **75**, 1308 (1971).
- Strumpf, H. J., A. F. Collings, and C. J. Pings, *J. Chem. Phys.* **60**, 3109 (1974).
- Sychev, V. V., A. A. Vasserman, A. D. Kozlov, V. A. Zagoruchenko, G. A. Spiridonov, and V. A. Tsymarny, *Thermodynamic Properties of Ethane* (Hemisphere, Washington, D.C., 1987).
- Tanneberger, H., *Z. Phys.* **153**, 445 (1959).
- Tegeler, C., R. Span, and W. Wagner, *Fortschr.-Ber. VDI*, Reihe 3, Nr. 480, VDI-Verlag, Düsseldorf, 1997.
- Teja, A. S. and A. Singh, *Cryogenics* **17**, 591 (1977).
- Terres, E., W. Jahn, and H. Reissmann, *Brennstoff-Chemie* **38**, 129 (1957).
- Thompson, H. W., *Trans. Faraday Soc.* **37**, 344 (1941).
- Tickner, A. W., F. P. Lossing, *J. Phys. Colloid Chem.* **55**, 733 (1951).
- Tomlinson, J. R., *Tech. Pub. TP-1*, Natural Gas Processors Assoc., Tulsa, 1971.
- Trusler, J. P. M., *Physical Acoustics and Metrology of Fluids* (Adam Hilger, Bristol, 1991).
- Trusler, J. P. M. and M. F. Costa Gomez, Research report for the GERG-project "Fundamental equations for calorific properties," London, 1996.
- Tsiklis, D. S. and V. M. Prokhorov, *Zh. Fiz. Khim.* **41**, 2195 (1967).
- Tsiklis, D. S., A. I. Semenova, S. S. Tsimermann, and E. A. Emel'yanova, *Russ. J. Phys. Chem.* **46**, 1677 (1972).
- Tsumura, R. and G. C. Straty, *Cryogenics* **17**, 195 (1977).
- van der Putten, L., J. A. Schouten, and N. J. Trappeniers, *High Temp.-High Press.* **17**, 533 (1985).
- Vangeel, E., private communication with NBS, Boulder. Data published in Goodwin *et al.* (1976).
- Van Hook, W. A., *J. Chem. Phys.* **44**, 234 (1966).
- van Kasteren, P. H. G. and H. Zeldnerust, *Ind. Eng. Chem. Fundam.* **18**, 339 (1979).
- Wagner, W., *Cryogenics* **12**, 214 (1972).
- Wagner, W., K. Brachthäuser, R. Kleinrahm, and H. W. Lösch, *Int. J. Thermophys.* **16**, 399 (1995).
- Wagner, W. and A. Prüß, *J. Phys. Chem. Ref. Data* **31**, 387 (2002).
- Wagner, W. and R. Kleinrahm, *Metrologia* **41**, S24 (2004).
- Wallace, C. B., L. H. Silberberg, and J. J. McKetta, *Hydrocarbon Processes* **43**, 177 (1964).
- Weber, L. A., *Int. J. Thermophys.* **13**, 1011 (1992).
- Whiteway, S. G. and S. G. Mason, *Can. J. Chem.* **31**, 569 (1953).
- Wiebe, R., K. H. Hubbard, and M. J. Brevoort, *J. Am. Chem. Soc.* **52**, 611 (1930).
- Wieldraaijer, H., J. A. Schouten, and N. J. Trappeniers, *High Temp.-High Press.* **15**, 87 (1983).
- Witt, R. K. and J. D. Kemp, *J. Am. Chem. Soc.* **59**, 273 (1937).
- Young, J. G., M.Sc. thesis, Texas A&M University, Texas, 1978.
- Younglove, B. A. and J. F. Ely, *J. Phys. Chem. Ref. Data* **16**, 577 (1987).